TÉCNICO LISBOA

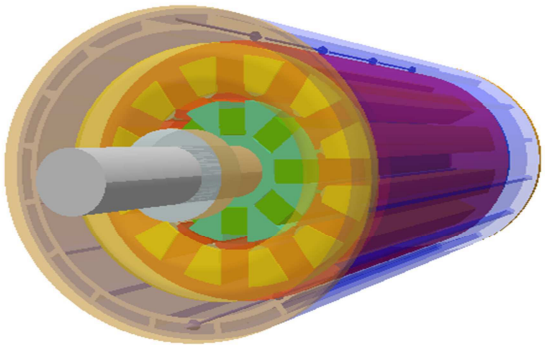

Virtual Prototyping of a Brushless Permanent Magnet AC Motor - Electromagnetic and Thermal Design using CAD Software

Bruno Ricardo da Fonseca Marques

Thesis to obtain the Master of Science Degree in

Electrical and Computer Engineering

Examination Committee

Chairperson: Prof. Dr. Paulo José da Costa Branco

Members of the Committee: Prof. Dr. Elmano da Fonseca Margato

Members of the Committee: Prof. Dr. Moisés Simões Piedade

Supervisor: Prof. Dr. Gil Domingos Marques

Co-Supervisor: Prof. Dr. Duarte de Mesquita e Sousa

November 2012

"*Learn from yesterday, live for today, hope for tomorrow. The important thing is not to stop questioning*."

Albert Einstein

Acknowledgements

This is the hardest chapter to write because such work made it possible to establish many contacts around the world, and learn many things with each person I met. It's very difficult to be fair and mention all of them. I will not list the people in a preference order but rather in a logical sequence, which begins with the situation that motivated me for electric machines study, passing then through companies and engineers that helped me. In the end I will refer all the friends and companions that supported me and believed in my potential.

To Mr. Faísca, train driver of IC 515, and the reviser Mr. Pedro, for the unique opportunity of taking contact with a locomotive in a trip between Nelas and Lisbon. This journey inspired me to railroad passion and was my first contact with machines in a traction application.

To INDIELEC© (SPAIN), personally represented by Eng. Juanjo Martinez and mainly to Dr. Vicente Aucejo, for all support and attention regarding the distribution of **SPEED** and MOTOR-CAD software. I have to say that without Vicente it wouldn't have been possible to do this work. He was always very diligent and available to help in the licensing issues. Many thanks for it!

To MOTOR DESIGN LTD© (England), personally represented by Dr. Dave Staton, Dr. Mircea Popescu, Eng. Douglas Hawkins and Eng. James Goss, for all the help given with MOTOR CAD software and the kindness to evaluate a copy of MOTOR LAB software. Dougie Hawkins, was always very receptive to clarify my questions carefully. Grateful to Dave and Mircea for all the advices and interest demonstrated in this work. To James for the effort to adjust MOTOR LAB software to my application and support it every moment.

To SPIN© (Italy), personally represented by Dr. Alessandro Tassi, Eng. Giuseppe Zanocchi and Eng. Luca Gregorio, for all the kindness taken when I went to Italy to the training course of **BPM** machines design and thermal analysis. All the training and support was essential to launch my project and learn more about machine design using **CAD** tools, as **SPEED** and MOTOR CAD software.

To QUALICAD© (Portugal), personally represented by Miss Ana Moreira and Mr. João Santos, for all the technical support with AutoCAD® software. This was crucial to achieve the final machine sketch and **2D** drawing.

To CEDRAT© (France), personally represented by Mr. Julien Salinas and Miss Christiane Ribard, for the support and to make possible a trial evaluation of FLUX and PORTUNUS software. Mainly FLUX because was very important to achieve the base **FEA** knowledge to make the necessary approach to this work.

To CD-ADAPCO© (USA), personally represented by Dr. Markus Anders and Dr. T.J.Miller, for all the support and advices given with **SPEED** software, very useful in the initial phase.

To VACCUMCHMELZE© (SPAIN), personally represented by Mr. Jose Gato and Mr. Oscar Garcia, for all the precious information about the iron cobalt alloys and availability to discuss sponsorships schemes to the formula student team.

To all the people and companies that came across in CWIEME 2012 at Berlin, with special focus to VAC©, HPMG©, KIENLE SPIESS©, ELANTAS©, SINTEX©, O.S.R©, COGENT©, CUNEXT©. They helped me to understand more about the industrial procedures and manufacturing processes, so important to implement this constrains in the machine design.

To TIANJIN NIBBOH MAGNETS© (China), personally represented by my friend Miss Yogi Wang and Mr. Li Wang. They were very important during the first approach of my design, always very sympathetic with the setbacks of the project. Most of the knowledge acquired about the manufacturing issues of rare earth magnets I owe to Yogi, so many thanks for that.

To WUHAN MAIKE© (China), personally represented by Miss Celine, for all the learning about silicon iron and the manufacturing constrains in the grain oriented and non-grain oriented steel.

To PEÇO LOPES© (Portugal), personally represented by Mr. Lopes and his wife, for all the kindness evaluating the budgets of steel and stacking process during the first phase of project.

To FERNANDO A LEMOS© (Portugal), personally represented by Mr. Nuno Santos, for the availability to do the machine winding and all useful explanations about the processes involved, always providing their facilities for what was needed.

To emeritus professor Tapani Jokinen, from Aalto University in Finland, for all the advices and ideas shared.

To TELEPERFORMANCE© (Portugal), personally represented by Mr. Daniel Pelado and Mr. Francisco Ferreira, mainly in the understanding of my personal situation as a working student. It's never easy to manage such situation in a big company as VODAFONE PT.

To all my colleagues of *Projecto FST Novabase* for all the help during this process of machine design. Always believing in my entrepreneur capacity to bring the necessary *know-how* to achieve the machine that team purpose: Jessica Costa, Miguel Figueiroa, Pedro Oliveira, Bruno Santos, Miguel Guedes, Miguel Silva, João Duarte and David Tempero.

To all the persons and students that came across in FS2012 at Silverstone, so important with all the ideas shared, especially with TU Delft and AMZ teams.

To my colleagues inside the IST, supporting and helping to solve the many bureaucratic processes inside the university, that could have been more severe if it wasn´t for their help: Rafael Ortega, Jaime Ribeiro and Maria Barradas.

To all my friends, starting with my great love, Filipa Pinto, so important in the support at the difficult moments and always comprehensive when I have to work and don´t give her the necessary and deserved attention. To Sandra Santos and her cousin Helena for making their house available which allowed me to take a rest and work in some difficult times. To my mother, Alice Marques, for the financial support during the project. To my grandfather, Hernani Fonseca, for believing always in my potential. To my sister Ana Marques for reviewing the thesis and to all friends that cross my way during this journey: Isabel Ana, Vasco Sani, Vasco Gonçalves, Fabio Cardoso, Magda Troeira, Isabel Paulo, Franco Bortot, Luis Morais, Jorge Garcia, Lisandra Lopes and Telma Rendeiro.

To my advisor, Dr. Gil Marques, for given me the idea to assist the presentation webinar of MOTOR CAD software, which was a turning point in my project. My entire journey starts here, and thereafter the learning process never ends.

The most significant words are for the two persons that represent everything I am, they were more than a family along these years. To Teresinha for all the faith and pure friendship and to Nina, an exemplar human being, so strong and determined. This work is a tribute for her unique way of life, only ended when reaching the age of 97.

Resumo

Este trabalho tem como objectivo descrever o projecto electromagnético e térmico do motor síncrono de ímanes permanentes a ser aplicado ao carro FST05e do Projecto FST Novabase. Trata-se dum veículo eléctrico destinado a participar nas provas de *Formula Student*.

O desafio passa por alcançar uma máquina com elevada densidade de potência, cumprindo com os objectivos da equipa nas provas em competição que mais exigem do motor: Aceleração, *Autocross*, *Endurance* e *Fuel Economy*. No final pretende-se um motor leve, com baixo momento de inércia e com o menor custo possível.

Estas exigências levaram à utilização de ferramentas de *software* **CAD** que permitissem um projecto electromagnético e térmico integrado para alcançar os requisitos de potência exigidos pela equipa, tendo em vista os limites de peso. O projecto electromagnético foi desenvolvido com o módulo **PC-BDC** do *software* **SPEED** e o projecto térmico com o *software* MOTOR-CAD da Motor Design Ltd©. Para análise **FEA** foi usado o módulo **PC-FEA** do *software* **SPEED**.

O trabalho descreve o projecto electromagnético e térmico da máquina do ponto de vista da utilização de modelos analíticos de parâmetros concentrados e da utilização de modelos numéricos através de **FEA**. São verificados os regimes de funcionamento cíclico nas provas descritas na competição. São estudadas as curvas de performance, os limites térmicos e os mapas de eficiência usando o *software* MOTOR LAB.

Os resultados obtidos ultrapassam as expectativas da equipa.

Palavras-Chave: Maquinas AC Imanes; Máquinas Fluxo Radial; Máquinas Elevada Densidade Potência; Análise Térmica Máquinas; SPEED PC-BDC

Abstract

This work's aim is to describe the electromagnetic and thermal design of a brushless permanent magnet **AC** motor to be applied on a formula student prototype car, FST05e, from *Projecto FST Novabase*. It´s a Battery Electric Vehicle (**BEV**) designed to participate in Formula Student events.

The challenge is to create a machine with high power density and fulfill the team goals. In all trials of competition the motor is pushed to the limits, testing acceleration, autocross, endurance, and fuel economy. The main project goal is to achieve a lightweight motor with a reduced moment of inertia, as well as keeping it cost efficient.

In an iterative way to achieve the power required with less weight, it was used **CAD** software to make the machine's electromagnetic and thermal design. The first one was developed with **PC-BDC** software from **SPEED** while the second one was developed with MOTOR CAD software from Motor Design Ltd©. To do **FEA**, **PC-FEA** software from **SPEED** was used.

This work describes the electromagnetic and thermal design process, both with the use of analytical formulations, based on lumped circuit models, and numerical analysis using **FEA**. The duty cycles for all trials in competition are analyzed to verify the thermal machine behavior. Performance charts, thermal limits and efficiency maps of the machine are also studied using MOTOR LAB software.

At the end, the design obtained exceeds even the team expectations.

Keywords: PM AC Machine; Design PM Machine; Radial Flux PM Machine; Thermal Analysis PM Machine; SPEED PC-BDC

Contents

List of Tables

List of Figures

List of Abbreviations

2D	Two Dimensions
3D	Three Dimensions
AC	Alternate Current
Ag	Silver
AlNiCo	Aluminum – Nickel – Cobalt
BCS	Best Configuration Searcher
BEV	Battery Electric Vehicle
BPM	Brushless Permanent Magnet
CAD	Computer-Aided Design
CFD	Computer Fluid Dynamics
CLV	Conductor Location Vector
DBM	Data Base Manager
DC	Direct Current
DXF	Drawing eXchange Format
EM	ElectroMagnetic
EMF	Electro Motive Force
FEA	Finite Element Analysis
FEMM	Finite Element Method Magnetics
FOC	Field Oriented Control
G.C.D	Greatest Common Divisor
GDF	Geometry Description File
GoFER	Go Finite Element and Return
GoTAR	Go Thermal Analysis and Return
HP	Horse Power
IPM	Interior Permanent Magnet
I-Psi	*(i,ψ)* diagram
L.C.M	Least Common Multiple
Li-Poly	Lithium Polymer
Match FE	Matching **FEA**
MMF	Magneto Motive Force
MSI	Maxwell Surface Integral
MST	Maxwell Stress Tensor
NdFeB	Neodymium-Iron-Boron
PC-BDC	**BPM** SPEED's module
PC-FEA	**FEA** SPEED's module
PEN	Polyethylene Naphthalate
PETP	Polyethylene Terephthalate
PM	Permanent Magnet

PWM	Pulse Width Modulation
RMS	Root Mean Square
RPM	Rotation Per Minute
RYB	Red – Yellow – Blue
SmCo	Samarium-Cobalt
SMPM	Surface Mounted Permanent Magnet
SPEED	Scottish Power Electronics & Electrical Drives
TEFC	Totally Enclosed Fan Cooled
TENV	Totally Enclosed Non Ventilated
THD	Total Harmonic Distortion
TMG	Triangular Mesh Generator
VBA	Visual Basic for Applications
VPI	Vacuum Pressure Impregnation
VW	Virtual Work
Zn	Zinc

List of Variables

A	Vector potential
B	Iron flux density
BetaM	Magnet pole arc
Bg1	Peak of fundamental **Bgap** at open circuit
Bgap	Flux density distribution in air gap
Bm	Magnet flux density
Br	Remanence field in **PM**
Bt	Stator tooth flux density
Btooth	Flux density distribution in stator tooth
By	Stator yoke flux density
CapThk	End cap thickness
Cpp	Coils per pole
D	Stator bore diameter
Dtot	Total machine diameter
Eq1	**RMS** fundamental **EMF** per phase
Fpt	Fin pitch/thickness ratio
FrLgth	Frame axial length
FrThk	Frame radial thickness
fsp	Slotting passing frequency
Gap	Air gap length
Gr	Grashof number
h	Heat transfer coefficient
H	Iron field strength
Hc	Coercivity field strength in **PM**
Hm	Magnet field strength
Id1	**RMS** *d-axis* fundamental component of phase current
IG_ls	Interface Gap between liner and stator lamination
IG_sh	Interface Gap between stator lamination and housing
Inset	Magnet inset
Iph1	Fundamental component of phase current
Iq1	**RMS** *q-axis* fundamental component of phase current
Isp	Set point current
J	Current density
Jn	Nominal current density
k	Thermal conductivity
Ks1	Fundamental skew factor
Kw1	Fundamental winding factor
Ld	*d-axis* synchronous inductance

LDiff	Differential leakage inductance
Let	End turn length
LgthOEnd	Axial length between extremities of end turns
Lq	*q-axis* synchronous inductance
Lstk	Stator stack length
m	Number of phases
MagWid	Magnet width
Mlgth	Total motor length
MLT	Mean length of turns
Mw	Machine total weight (all components mounted)
η	Efficiency
Nc	Corner speed
Nsh	Number of strands
Nu	Nusselt number
NWFT	Exponent of friction and windage loss
p	Number of pole pairs
P	Pressure drop
PF	Fundamental power factor
Ph	Pressure drop across housing
Pmax	Maximum power
Pn	Nominal power
Ppch	Number of parallel paths in ducting system
Ppeak	Peak power
Ppth	Number of parallel paths in phase winding
Pr	Prandtl number
Psh	Shaft power
Pwjd	Total power dissipated by water jacket system
Q	Flow rate
R	Duct wall resistance
Rad1	Rotor radius
Rad3	Stator outer radius
RadSH	Shaft radius
Re	Reynolds number
ReC	Critical **Re**
RotJ	Moment of inertia
Rph20	Phase winding resistance at 20ºC
RPM0	Speed at **Wf0**
RPM1	Speed at **Wwf**
SD	Slot depth
SO	Slot opening

SOang	Angle of stator tooth tip
Sp	Coil pitch
Sph	Specific heat
t	Time
Tc	Turns per coil
Te	Average torque from *i-psi* diagram
Tei	Alignment torque
TGD	Radial depth of tooth tip
Tinl	Water jacket inlet temperature
Tlf	Insulation lifetime
Tlim	Time limit to maintain **Ppeak**
TMag	Magnet temperature
Tmax	Maximum torque
Tpeak	Peak torque
Tph	Turns in series per phase
TRV	Torque per unit of rotor volume
Tsh	Shaft torque
Ttot	Total torque
TWav	Winding average temperature
TWhs	Winding hot spot temperature
Twjo	Water jacket outlet fluid temperature
TWS	Stator tooth width
v	Linear velocity
V0	Zero sequence voltage
V1	Positive sequence voltage
V2	Negative sequence voltage
Vf	Fluid velocity
Vll1	**RMS** fundamental line voltage (inverter terminals)
Vph1	Fundamental component of phase voltage
Vrot	Rotor volume
Vs	**DC** battery voltage
W	Average energy conversion per cycle
WCu	Copper loss
Wf0	Friction and windage loss at **RPM0**
WFe	Iron loss
WireDia	Bare wire diameter
WMag	Magnet loss
Wt_FeR	Iron weight in the rotor
Wt_RSS	Rotor weight as solid steel
Wt_Tot	Total weight (iron, copper and magnets)

WTot	Total loss
Wwf	Friction and windage loss at **RPM1**
Xd	*d-axis* synchronous reactance
Xq	*q-axis* synchronous reactance
γ	Phase angle between **Iph1** and **Eq1**
δ	Load angle
λ	Skin depth
μr	Iron relative permeability
ρ	Density
σ	Conductivity
Φ1	Fundamental air gap flux per pole
ψ1d	Fundamental component of **PM** flux-linkage
ψd1	Fundamental *d-axis* flux linkage
ψq1	Fundamental *q-axis* flux linkage
ω	Fundamental angular frequency

1. Introduction

In passage from the XIX to the XX century most of vehicles were electric. This was the natural consequence of their superior reliability and cleanliness when compared with the cars engaged with internal combustion engines. However, since the last ones became more reliable and with lower cost, their usage increased a lot which turned the disadvantages of electric cars more evident, resulting in the oblivion of these vehicles for almost a century.

Figure 1.1 – Lead Wedge Autolite car, 1968 (Jerry Kugel and Danny Eames) [5].

At present times the current increase of fuel price, the environment issues and technological evolution of electrical motoring techniques since the last decades, created a “new life” concerning electrical mobility. The past limitations are still the same, although some solutions are appearing and result in a natural mitigation of those problems. The electrical energy storage has little capacity and is expensive, besides their significant weight, volume and reduced longevity. To these issues, is also important add the excessive slowness in the charging system and the fear of some people to use a vehicle that is moved by electrical energy.

Times are changing and the electric vehicles have advantages due to the less environment impact. This reason is pushing them to a constant progression in the market and in some countries government is giving incentives to its purchase. On the other hand, due to the lowest price of electrical energy, the operation of an electric car could encipher at 1€/100 km [5], ten times less than a conventional combustion engine vehicle.

Recently electric sports cars have appeared with high performance standards, which is possible due to electrical motors with high power densities and mainly with high torque per unit of rotor volume (**TRV**). Despite of their huge price and low autonomy, this kind of car is growing on popularity with wealthy people that have at same time environmental concerns. This phenomenon is the source of a niche market arising.

Next figure shows the typical architecture of a battery electric vehicle (**BEV**) consisting in an electric motor, an energy storage unit and a power converter which transfers the energy stored to the machine [1].

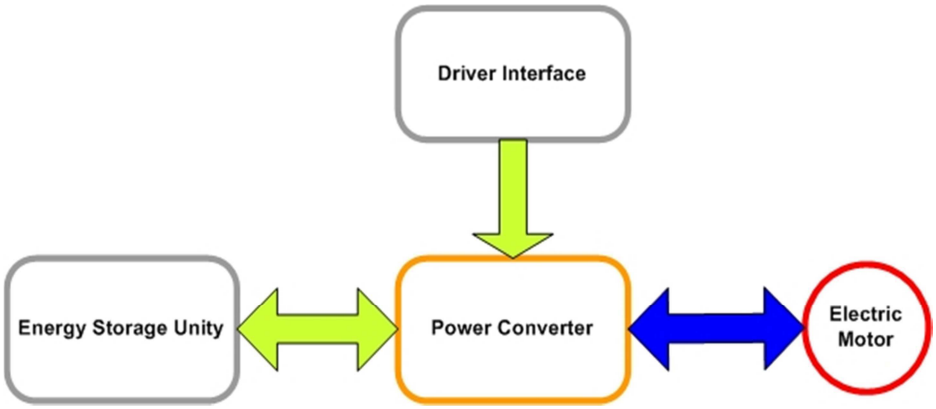

Figure 1.2 – Typical BEV propulsion.

This work is focused in electric motor part, in design aspects that allow the machine to achieve highest performances. The motor is the heart and the force of any car.

The electric motors are more efficient than combustion engines, which allow the increase of the vehicle autonomy and so reducing the batteries number. On the other hand, machines with higher power density turn possible the reducing of car's weight. The materials evolution, mainly the permanent magnets (**PM**), opened a new window for motors miniaturization and their use was very well succeeded in the past years. However, these rare earth materials have a very costly holding, forcing inclusive EUA to cease their exploitation. Actually the big provider is China which recently limited their exportation by politic reasons.

The electric motors research doesn't stop. There are many technologies under development like switched reluctance and doubly salient permanent magnet machines [5].

1.1. Permanent Magnet Machines Evolution

The **PM** synchronous machine was known in the early 1950's [8]. Although most **PM** machines at that time were generators, motors were also manufactured [11] and classical *dq* theory was used to analyze them. The motors were "line-start", a combination between an induction rotor machine and magnets, supplied from the **AC** mains without electronics. In the early 1970's, the discovery of high energy **Sm-Co** magnets gave new impetus to the development of **PM AC** motors. Lower energy ferrite magnets were already used in **DC** brush type motors and improvements in these magnets also encouraged new work in **AC** line start machines, notably by Brown Boveri: Isosyn motor (1978) and Reliance Electric (1979). Some of these motors were used with inverters, but they were still "line-start" motors without shaft position sensing.

Figure 1.3 – Line-start PM motor: 2 poles, 2.5 HP (Smith Corporation) [4].

The brushless **DC** motor emerged at the mid 70's, notably from Papst. Although similar to the **AC** brushless permanent magnet (**BPM**) machine, the method of driving it was different.

Nowadays the improvements in soft iron material have also contributed significantly in the development of **BPM** machines. Reduced losses in electrical lamination steels have been achieved through metallurgical and process development, including thin gauges, improved chemical composition, heat-treatment and improved core-plate insulation. **BPM** motors are often designed for high power densities, working in small spaces. To achieve this, the use of high quality steels can be as important as the magnets themselves.

1.2. Formula Student

This competition is organized by Society of Automotive Engineers (SAE) and other engineers societies (IMechE, VDI, others) [1]. It occurs every year in different countries as individual events, each one with its own character and challenges. Formula Student boosts university students from around the world to design and build a single-seat racing car, which is then put to the test at various circuits in different competitions: Acceleration; Autocross, Endurance and Fuel Economy. Students work together on the car, developing their creativity, technical abilities, teamwork and communications skills, as well as learning how to deliver projects to budget and deadlines. This work focus mainly four dynamic events, all designed to test different aspects of the car's performance [3], [22]:

- **Acceleration**: This event focuses on the car's powertrain performance, drivability and on the suspension's ability to provide maximum type grip. The first place wins **75 points**.
- **Autocross**: This tests the car's maneuverability and handling qualities on 800m course. To do it well, cars have to be quick as well as nimble around the corners. The first place wins **150 points**.
- **Endurance**: The biggest test of the teams is the 22 km endurance race where cars have to prove their reliability. There is also a mandatory stop, driver change and hot restart that really

tests reliability and team's ability to efficiently make changes to pedal positions, seats, etc. The first place wins **300 points**.

- **Fuel economy**: The objective is to achieve the best fuel efficiency possible, quantified in 125 grams of CO_2 per km during the endurance trial. When this goal is accomplished, the team wins **100 points**.

This work is directed to a particular prototype vehicle, built at Instituto Superior Técnico by *Projecto FST Novabase*, to participate in Formula Student competitions. The next picture shows FST04e prototype, the first in the gender in Portugal, although the project is being directed to FST05e:

Figure 1.4 – FST04e in charging area (FSUK12).

Developing a project for a Formula Student prototype sets certain requirements in terms of both system capabilities and project management. It has to be able to sustain a harsh environment, namely vibrations, heat, liquids, electromagnetic interface and has to be also lightweight and user-friendly.

1.3. Team Requirements

A list regarding the team requirements for the machine will be presented, sorted by the different categories that have to be considered in the project.

1.3.1. Dimensions and others related

1) Total ideal diameter: 12 cm.
2) Total ideal axial length without shaft: 20 cm.
3) No flange or foot mounting.
4) Less moment of inertia than axial flux machine used on FST04e, Agni 95R [16].
5) Shaft dimensions in the same order of Agni 95R: internal hub with 3 cm diameter.
6) Total weight: maximum of 10 kg.

1.3.2. Speed and power envelope

1) Peak power, **Ppeak,** of 42.5 kW at 6000 **RPM**. The maximum power allowed in competition is 85 kW, so for each motor this is the limit.
2) Field weakening can be used to explore superior velocities at constant power, until a maximum around 9000 **RPM**.

1.3.3. Drive

1) *Sinewave* current control. The objective is to set up the bridge with another thesis developed inside the project by Mr José Santos, about space vector modulation.
2) Nominal DC battery voltage is 533V. It's composed by 288 Lithium Polymer (**Li-Poly**) cells.

1.3.4. Cooling system

1) If water jacket is needed, the pump flow rate to be considered is 50 cm^3/s.
2) The cooling has to be good enough to machine handle all the requirements at the 4 main trials described in last section.

1.3.5. Cost

1) Since this is a high performance prototype the final cost is normally high, however the best and more economical choice has to be made.

1.4. Thesis's Structure

This work is divided in 7 chapters.

In chapter 2 the first approach to this project will be introduced in order to focus the results obtained and the essential topics that justify the change in framework.

In chapter 3, **CAD** software solutions will be described in more detail. The focus will be on the models inside it to give some contrast to previous work. The interaction between the tools that permit the iterative electromagnetic and thermal design will be presented.

In chapter 4, the **EM** project of MM03_V3 prototype will be described. This includes an explanation of the design options; preliminary results obtained during the design process and suggestions about construction issues.

In chapter 5, the thermal design of MM03_V3 prototype will be described. This includes the main options to define the cooling system and materials; final results integrated with **EM** project and suggestions about construction details.

In chapter 6 performance results will be presented, which include: duty cycle analysis for all the competition trials; efficiency maps; thermal maps and thermal limit envelope at steady state and transient operation.

In chapter 7 the main work conclusions and also some improvement points in the design, including reference to future work, will be presented.

2. First Design

The electric machine used in FST04e is the Agni 95R from Agni Motors [16]. It's a **PM** axial flux machine and the main characteristics can be consulted in the following table.

Overall Characteristics	Values
Pn	**15 kW**
Jn	**6 A/mm^2**
Ppeak	**30 kW**
Tlim	**30 sec**
Rotor diameter	**19 cm**
Motor length	**13.7 cm**
Total weight	**11 kg**
Inertia moment	**0.0238 kg.m^2**

Table 2.1 – Overall characteristics of Agni 95R.

In propulsion system flowchart exposed in section 1, the electric motor part is composed by two of these motors connected to the same sprocket, electrically in series. A cooling system to the machine was developed to avoid the overheating that was detected in tests at rated power. It was decided to put a fan that blows air into the machine's housing and end cap vents. Such forced convection cooling is a mix between a through ventilation and totally enclosed fan cooled (**TEFC**) model.

In the first step of design, this machine was viewed as a first reference in the results point of view.

2.1. Machine Type

Since it's necessary to define one machine type and topology, the first thing to look at is the advantages and disadvantages of current motor. As being a **DC** machine, the control is simpler to implement and the axial flux type has low values in the length, which allows a better exploring of car rear space. However the brushes weariness and the high moment of inertia indicates that there must be some changes, passing to a brushless machine type and leaving the axial flux machines due to typical high rotor diameter. At this time the brushless radial flux machine represents a better option as it can avoid especially high rotor diameter that increases the moment of inertia in a square relation. Moreover, there is more freedom to explore the axial length on the new FST05e, so there's no special need to have a small dimension on it.

Assuming these considerations, the decision was to choose between a brushless **DC** or **AC** machine. As the main goal is to attain a high power density machine, the best is selecting the one that produces more torque at same conditions. Deciding by a 3-phase machine is a good approach as the torque is proportional to the phase number. Nevertheless there are two possibilities: synchronous or asynchronous motor.

For this application the asynchronous machine has some points in disfavor: more rotor copper loss comparing to **BPM** machine and more weight in the rotor because cooper has bigger specific

gravity; more cooling power to the same torque due to the previous explanation, which tends to result in a less thermally utilized machine with the same active parts; less torque for the same active parts, resulting in a less compacting design and shorter accelerating times for the same moment of inertia [23]. Besides that, synchronous machine has a torque-speed profile more or less constant until the corner speed, which gives more acceleration capability in a wide speed range. This issue is important in the dynamic point of view on a race car. The powerful magnets available today, like **NdFeB** or **Sm-Co**, allows higher air gap flux densities which permit to attain the same air gap field with less material, so less rotor weight. The high magnet cost and the demagnetization withstand is also important and can be a disadvantage, however it can be mitigated if a good electromagnetic (**EM**) design is made. This discussion turn **BPM AC** machine the preferred topology to electric vehicle traction, due to their inherent high efficiencies and excellent power densities.

For this kind of machines concerning the rotor position there are two possibilities: interior rotor or exterior rotor. In the geometric point of view, the exterior rotor has a bigger rotor radius because it is the exterior part of the motor. So the moment of inertia is bigger than with interior rotor machine. The formula student team AMZ [25] is using this kind of topology now, however they will change soon to an interior rotor and possibly these considerations can justify it.

Deciding for an interior rotor machine and maintaining a classic stator, is important to check what kind of topology is chosen taking into account the saliency: salient pole or non-salient pole machine.

Surface mounted permanent magnet (**SMPM**) machine is the classic non-salient pole. Despite of its simplicity and lower construction cost compared to other **BPM** machines, the magnets are very exposed to demagnetization fields and losses, as they are on the surface. Furthermore, the magnets are subject to centrifugal forces that can cause their detachment from the rotor. Sometimes this implies the use of a rotor sleeve to sustain the magnet or to give a seal when a wet rotor cooling strategy is used. Moreover, due to the typically low inductance, a relatively high chopping frequency is needed to minimize the current ripple which is bad to the commutation losses. In the weight point of view, this kind of machines generally has a large rotor yoke with massive iron, increasing the weight. Therefore the best is somehow to have the magnets protected in the rotor iron, and at the same time with the less iron possible.

Analyzing interior permanent magnet (**IPM**) machines, there are many topologies. The general advantage is the possibility to concentrate the flux generated by the permanent magnets in the rotor and thus achieve high air gap flux densities, which is good for torque production. Moreover, the magnets are well protected against demagnetization and mechanical stress. It's common to find saliency in these machines because typically *d-axis* synchronous inductance (**Ld**) is inferior to *q-axis* synchronous inductance (**Lq**), which means that reluctance torque can be used, by phasing advance the current. Since team needs high **TRV**, it could be interesting to explore this topic comparing with **SMPM** where this is less possible. Regarding the use of field weakening, since the team is not too much interested in exploring high speeds, above 6000 **RPM**, it could be assumed that it's not necessary a high saliency in the machine. The challenge passes to find an **IPM** geometry where the saliency could be more or less manipulated, and at the same time with a non-massive rotor

iron and with no iron bridges. This feature causes the permanent magnet flux leakage through the bridges and sometimes its saturation, instead of crossing the air gap and contributes to the torque.

The best geometry to attain all this goals is the spoke type. It was developed to increase the air gap flux density by the flux concentration principle, and has also known some applications as generator and servo-motor [4]. The following picture illustrates the machine:

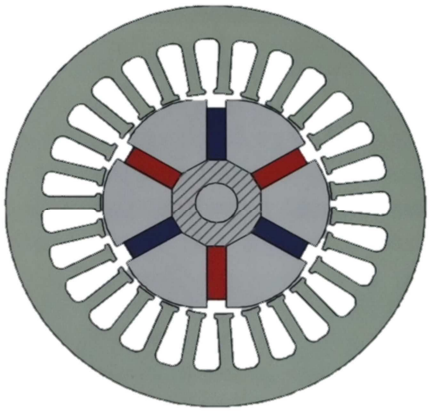

Figure 2.1 – Spoke rotor IPM machine [4].

The only limitation in this geometry is the material on the shaft. In this topology a non-ferromagnetic material must be used or a large portion of the flux generated by the permanent magnets would leak through. However this is not a severe problem because there are many materials available in the market to fulfill these requirements at low price. The magnets inset in the pole piece protect them against the slot effects on the air gap flux distribution, one cause of the magnet losses. Then, the iron polar piece can be manipulated to increase or decrease the saliency and the rotor weight. It is interesting to check here the optimum relation between weight, saliency and air gap flux density that naturally depends on the magnet length when the polar piece arc is changed. The inner shaft and the hub are considered as an entire piece in the design.

In a salient pole machine like the one showed, the basic theory to analyze its behavior is the phasor diagram of classical synchronous machine, so the controllers may be based on vector principles. Since that is a requirement to a *sinewave* drive, it's possible to use phasor diagram to analyze the machine and apply field oriented control (**FOC**) principles. These allow the achieving of a good performance and low torque ripple, but to guarantee it **EMF** should be as sinusoidal as possible. Another good property of salient pole machines is the inductance variation with rotor position, making possible to estimate it without sensors. Some work has been done also with non-salient pole machines to attain the same goal [38].

2.2. Design Procedures

To initiate the first design process, initial assumptions were taken, and then an optimization process was applied.

2.2.1. Initial Assumptions

First, it's necessary to choose the number of machine poles. Once the team always refers the interest in the base speed of 6000 **RPM**, the first approach was choosing a good frequency to easily find low loss iron. Based on the recent aerospace applications, it's common to find 400 Hz as an operating frequency of much equipment. So as field rotates synchronously with the rotor, we can get 8 poles to this machine.

To define the materials the approach was simple too. If the machine has permanent magnets, the choice goes for using the strongest magnets, based on **NdFeB** rare earth material. Within the iron the option was to use the typical silicon iron already employed in standard machines, with oriented grain. It has less losses comparing with non-oriented, but low permeability. The initial analytical modulation consider the iron **BH** curve as a linear one, in other words, only the linear permeability was used to do the basic calculations. More information about application of grain oriented electrical steels in motors can be consulted [58].

To the winding, the most simple option was used, a concentric distribution with 24 slots, given 3 slots/pole. This simple model not considers coil span (**Sp**).

In order to compare the results with Agni 95R, it was necessary to develop the calculations to the same power and current density. First, let us assume that the machine will not be saturated at the rated power. Analyzing the following table it's possible to have a rough estimative about the current densities limits as function of the cooling system.

Condition	A/mm²	A/in²
Totally enclosed	1.5—5	1000—3000
Air-over, fan-cooled	5—10	3000—6000
Liquid cooled	10—30	6000—20000

Figure 2.2 – Current densities for different cooling systems [8].

It's possible to check that 6 A/mm^2 is typical with a through ventilation machine like Agni 95R. So it's assumed the same current density in the new machine project, on the grounds that the same cooling system is available. Then it's possible to compare results and see what the best machine is.

2.2.2. Optimization Process

The next flowchart describes the idea under the optimization process taken. The objective function is the machine weight, which has to be minimized. The nominal power and current density requirements of Agni 95R have to be fulfill, as well as the constrains that guarantee the mechanical and magnetic behaviors, expressed as a function of the design variables.

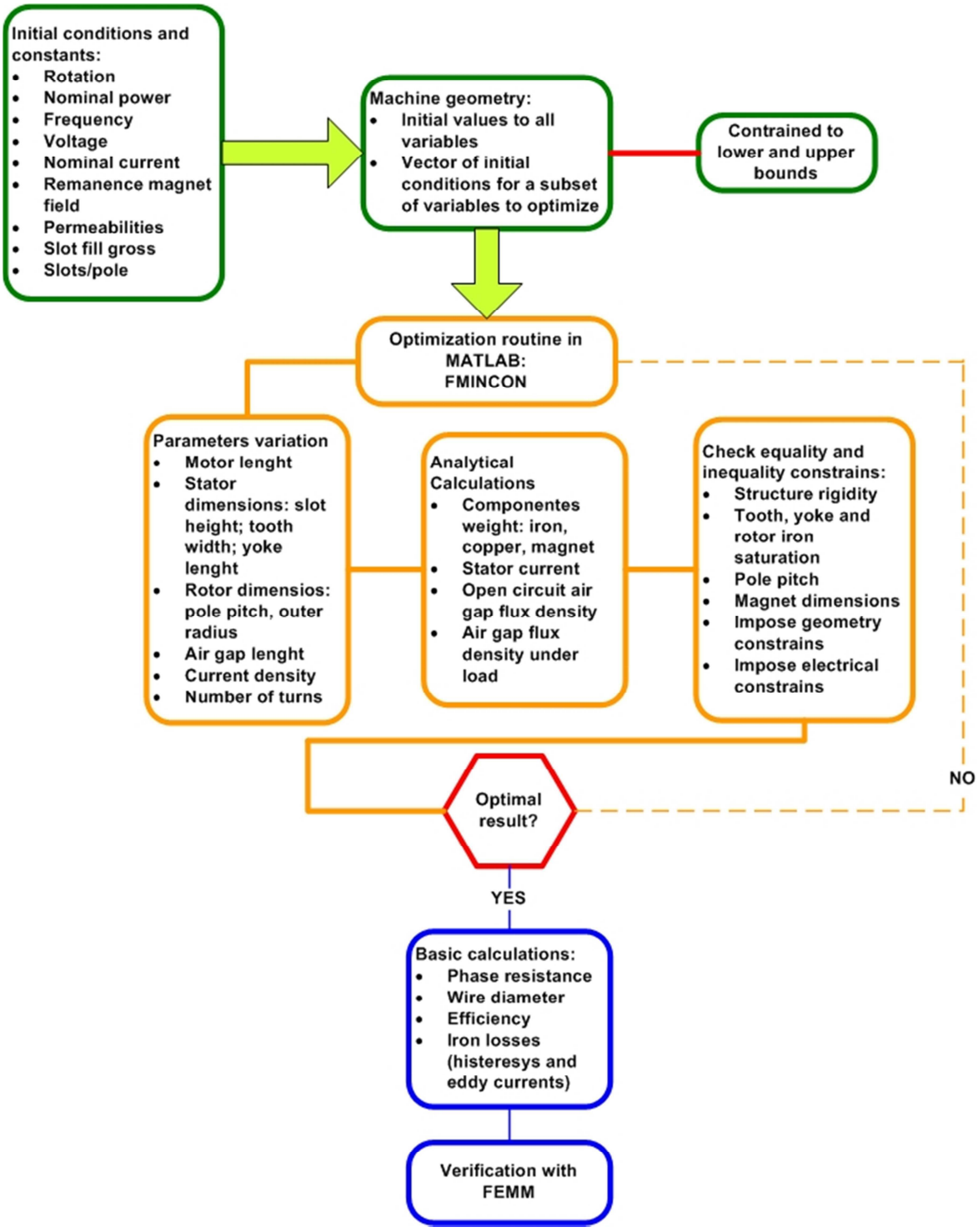

Figure 2.3 – Optimization process.

This procedure is similar to the one studied in the referred work for low speed drives [2]. Regarding the analytical calculations, the air gap flux density was deduced like exposed in [2] as well as the inequality, equality constrains and variables range. The carter coefficient, the effective air gap and other parameters calculation as the copper area and phase resistance were calculated as exposed in [26], [27]. The constants used in the materials were taken based in internet research, as can be consulted in [28], [29].

2.3. Results & Conclusions

The following table summarizes the important results obtained with the previous approach.

Results	Values
Gap	**0.9 mm**
Slot height	**2.2 cm**
Slot width	**0.48 cm**
Tooth width	**0.85 cm**
Stator yoke	**1.1 cm**
Magnet width	**0.1 cm**
Length	**12 cm**
Current Density	**6 A/mm^2**
Rotor Diameter	**10.2 cm**
Total diameter	**17 cm**
Weight	**10.4 kg**
Shaft weight	**2.8 kg**
Slot fill gross	**60 %**

Table 2.2 – Optimization design results.

When comparing this table with table 2.1 it's easy to see that this machine is heavier and has little difference in rotor diameter. It's important to refer that this weight doesn't include other mechanical parts as housing, bearings and end caps. Therefore the weight will be higher than this 13.2 kg. Another important point is the slot fill obtained. As this machine considers a simple distributed winding with equal number of turns, means that end winding is overlapping. Considering constructive details, even with a machine wound, it's almost impossible to achieve a slot fill gross so high. If a more reliable approach is taken, like 45% for a hand wound, it means that phase resistance will increase to the same slot area. For equal rated power and current densities, the losses will increase which will give certainly a worse thermal performance than Agni 95R.

In conclusion this design doesn't fulfill the team goals. However it's important to establish more considerations about this process in order to take some conclusion to the future.

2.3.1. Geometry

The variables used in analytical model describe with few details the slots. The slot opening is not considered and the slot is modeled as a simple rectangular shape. This is a bad model, in one hand because is not considering the slotting effects on the air gap field and in other hand because this variable is important to avail the cogging torque. Moreover, no fringing effects on the air gap field distribution are considered, which is like assuming the air gap distribution as a *squarewave*. The slot opening depth is not modeled also and it can be of a major influence to the cogging, especially when the machine is heavily saturated.

The starting conditions vector doesn't represent a machine with real dimensions or a machine that is already constructed and tested. The optimization process can't be used to obtain a first iteration design, principally when the solution is not known and the starting conditions are also abstract. It's better to optimize a certain characteristic with a machine well designed and known.

2.3.2. Analytic Models

Some of the formulations taken are based in a work that investigates geometry variations in a non-salient pole generator, as a **SMPM**. In this kind of machines the analytical models work better than with interior magnets machines, due to magnetic symmetry. So it's risky to extrapolate such modulation to this problem.

These analytical linear models are based on superposition method. If it's considered that at **Ppeak** the machine will be very saturated, these kinds of models don't work due to iron saturation. To have a correct estimation with an analytical approach, the entire **BH** curve has to be modeled. In a salient pole machine finite element analyses (**FEA**) is crucial to check the saturation.

2.3.3. Iron Material

The iron data used in the algorithm is not given by the producers but instead taken from some references in the internet. When the aim of the project is to construct a machine, the initial virtual prototyping must include material data resulting by several tests. The iron loss curves, in order to estimate the coefficients of Steinmetz equation, are also important. Even with this procedure, it's difficult to determine the iron losses accurately as the iron properties change due to stress with manufacture and burs in interlamination insulation. Using **FEA** can help, but to obtain reliable results it's necessary good data and engineering judgment to quantify a correction factor to iron losses.

2.3.4. Winding

The winding is based in a very simple and classical model, however no winding factors were assumed when the **EMF** was calculated. In fact it was assumed that fundamental winding factor (**Kw1**) is equal to 1. So if slots/pole is 3, it means that coil **Sp** is also 3 to be consistent with the winding factor assumed. Being this a distributed winding, this kind of throw doesn't permit harmonic filtering because no short pitched is used. The **EMF** has the same waveshape of the air gap flux density, which is not sinusoidal, unless profiling of iron polar piece was considered to create a tapered air gap, but it was not the case. Since *sinewave* drive is required, it's necessary a *sinewave* **EMF** to avoid torque ripple.

Considering still the winding factors, if it's necessary skew to eliminate the cogging torque, the fundamental skew factor (**Ks1**) must be considered in **EMF** analytical calculations. However it doesn't and the effect is over predicting the **RMS** fundamental **EMF** per phase (**Eq1**) in the calculations because this decreases with skew factor.

The winding connection was not considered too. This is important to evaluate the best connection to reduce the torque ripple. If the connection is wye, automatically the 3rd harmonic of line-line **EMF** is eliminated, which has great impact on torque ripple profile. It's important to evaluate this effect and quantify the final result.

2.3.5. FEA Calculations

The **FEA** software used was **FEMM**, which is a free license application. Thinking in **Ppeak** working point as it is the most exigent to the machine, it's reasonable to accept that motor will be heavily saturated due to the high load applied related to its weight. Therefore this kind of analysis is essential to check **Xq** saturation, which reduces the torque. There is no way to analyze the torque production using analytical formulation when the machine is saturated because phasor diagram becomes inaccurate in these conditions. When **FEA** is used for this, it's very important to have control under the mesh generator to obtain reliable results, mainly if Maxwell stress tensor (**MST**) method is used. The **FEMM** mesh optimization algorithm is closed to the user and it's not possible to have control on program decisions.

As a typical magneto-static **2D** program it's not possible to perform classical **3D** calculations, whereby studying the skew effects. Neither a **2D** sliced skew model is available so it's impossible to check the skew that eliminates the cogging and filters the harmonic content of the air gap flux.

There is no way to get a good prediction of the cogging torque too. As an interior magnet machine doesn't have analytical formulations to calculate the cogging like with **SMPM**, only **FEA** could give some idea on it. To get a good prediction it's required to use more than one method and a good mesh to compare the results. The only torque computations are with **MST** which is clearly inadequate. At least a co-energy method is useful.

There isn't any transient solver to check rotor losses and see its relevance. As this interior magnet machine has not the magnets entirely buried within the rotor, it's possible to have some magnet losses that can't be negligible.

There is no way to check the iron losses using **FEA**. There is no internal computation using modified Steinmetz equations or Bertotti model, which turn more difficult the analytical losses calibration and avail security factors.

The thermal **FEA** available is very rudimentary which turns impossible to check the temperatures profile in the slot. The materials database doesn't support any introduction of insulation, liners or impregnation materials.

The script language turns difficult to compute complex geometries, different from linear machines. In an iterative process like this, where the geometry is always changing, it's not practical to use a **CAD** drawing in a **DXF** format for each machine obtained. Even if used MATLAB®, taking the advantage of Windows® Active X to do scripts and interact with **FEMM** to calibrate the open circuit **EMF**, the work will be so hard that it's impossible to do everything in useful time. The leakage of automated tools turns the task too much dificult for such complicated and exigent project, where everything is pushed to the limit.

2.3.6. Cooling System

To avail in more detail this important issue, it's better to look to **Ppeak**, since it is the main team requirement in terms of performance. It's possible to inset this machine in a certain cooling category, in terms of maximum **TRV**. As the team has the requirement to an ideal diameter of 12 cm, was considered half value to the rotor diameter and the rest to the air gap, stator and housing. Since peak

torque (**Tpeak**) is defined in **Ppeak** at 6000 **RPM**, the rotor stack volume may be calculated considering it as a smooth cylinder with the ideal length defined in section 1.3.

$$TRV = {Tmax}/{Vrot} = 119.6\ kN.m/m^3 \qquad (\mathbf{2.1})$$

Comparing with the following table, which rates the different cooling types with **TRV** value, is possible to have a rough estimative of the cooling strategy to use.

Class of machine	TRV kNm/m³	σ lbf/in²
Small totally-enclosed motors (Ferrite magnets)	7 - 14	0.5 - 1
Totally-enclosed motors (sintered Rare Earth or NdFeB magnets)	14 - 42	1 - 3
Totally-enclosed motors (Bonded NdFeB magnets)	20	1.5
Integral-hp industrial motors	7 - 30	0.5 - 2
High-performance servomotors	15 - 50	2 - 4
Aerospace machines	30 - 75	2 - 5
Large liquid-cooled machines (e.g. turbine-generators)	100 - 250	7 - 18

Figure 2.4 – Typical values for TRV [8].

This machine is well defined as a machine that needs an intensive liquid cooling strategy, using housing water jackets for example.

The previous modulation doesn't describe the machine's thermal behavior. In the analytical formulations described there are no equations to take into account all the necessary forced convection phenomena. The losses depend on temperature and the temperature on losses, so it's necessary to get a correct update of the phase resistance with the temperature increase. Moreover, in a permanent magnet machine that uses **NdFeB** magnets it's important to quantify the flux lost with temperature increase because the temperature coefficient of **Br** is negative. This effect reduces the torque and if it's not predicted, the final results will be much different from the constructed prototype, in the power density point of view. It's necessary also to have a good prediction of magnet temperature, at steady state or transient operation, to evaluate the demagnetization withstand and the best grade to choose.

The traditional methods to develop the cooling system, based on single parameters like current density or range in the heat transfer coefficients to a certain type of cooling, doesn't give the correct indication where to concentrate the effort to reduce the temperature. More is needed, as robust design analysis to check the main constrains in cooling system. Develop some scripts on MATLAB® with such heavy and complex formulations to describe the behavior of the equivalent thermal lumped circuit model of the machine is almost impossible to do in a feasible time. Besides that, it's necessary to have a more reliable idea of the materials to consider in the insulation system and the thermal class used, as it will define the exploration limit of the machine. Quantifying the sensitive points in the cooling, like interface gaps, bearing models, end space cooling, liner thickness and see its interference in the magnet and winding average and hot spot temperatures must be done.

3. SPEED & Motor CAD

Considering the last chapter analysis, it was necessary to change the project paradigm and look for another solution to attain the team goals. Regarding the problems related with geometry description, the best is using an interface that can model the machine in a vector format, like **DXF**. Herewith all the limitations describing the machine in slots and teeth, sometimes assumed to simplify the models, are no more an issue to worry.

The utilization of **CAD** tools to initiate the new project was a natural consequence. The choice passes to look to the more reliable tool and with well proven results in the market. After some research, was found **SPEED** software. It's a set of analytically based programs for the design of electric motors. Developed by **SPEED** laboratory at Glasgow University, it counts with hundreds of users worldwide and more than 20 years of continuously research, including feedback from users that really construct machines. Moreover, Glasgow University has been involved in motor design for the past 80 years, mainly due to Dr. Bernard Hague [31].

Regarding the thermal analysis, the process was easier because there is only one **CAD** package in the world dedicated to thermal analysis of electrical machines. Motor CAD was developed by Motor Design Ltd© and its first version was launched in 2001. Since then this software has been intensively used at the industry and users' feedbacks turn it reliable. Moreover, there are many tests in constructed prototypes which cooling system was developed using Motor CAD and final results were very good [24], [60], [62]. So this is the perfect tool to respond to the high demands of this project.

The next flowchart describes the loop procedure used in this new project phase. The specifications and possible solutions have been already discussed and decided. Despite of prototyping is out of this work bounds, it will be considered into a near future.

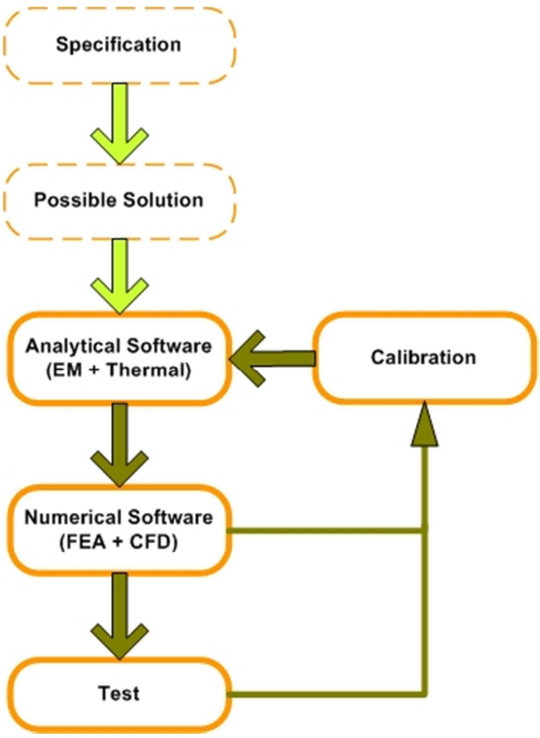

Figure 3.1 – Machine design process.

3.1. SPEED PC-BDC

SPEED software has several modules, each one to a certain kind of machines: induction, switched reluctance, **DC PM**, wound field universal and **BPM**. As the decision about the type of machine to use was already taken, the module used is that one dedicated to **BPM** machines design, or **PC-BDC** module.

The main models of this software will be exposed in order to give some contrast to the last procedure, understand better the differences and launch the new project.

3.1.1. EMF Calculation

The open circuit **EMF** waveform is a key basic property of a **PM** machine. For large air gap machines the best way is using a series expansion solution of Laplace/Poisson equation. The Rasmussen's method [8] can treat more complex magnetization patterns in simpler magnet shapes, while Hague-Boules method [8] can treat more complex magnet shapes. However as in this project it's necessary to guarantee high air gap flux density, this kind of calculations has no interest because large air gap will not be used. So the main methods to avail are BLV method or **Bgap** method [35] and tooth flux method or **Btooth** method [35].

The BLV method is based on the classical idea of a conductor with length *L* moving in a magnetic field of flux density *B* with velocity *V*. If conductors were filaments of vanishingly small cross-section area located in the air gap, as the rotor rotates the relative motion with velocity *V* generates **EMF**. It is a simple method but highly idealized as the stator surface is treated as smooth. This justifies the use of Carter's coefficient to formulate an effective air gap which models the effect of the slot openings on the bulk of the air gap. As a result a smooth or unslotted flux density distribution in the air gap (**Bgap**) is obtained, devoid of any modulation due to slot openings.

The tooth flux method is the direct application of Faraday's law, which states that **EMF** is equal to the rate of change of flux linkage. This method is preferred when coil **Sp** is small, as it calculates the **EMF** based on the flux that crosses one tooth, that's why it's called the tooth flux. It already accounts with flux leakage like zigzag, which means that tooth flux obtained is really the flux that links the coil with a certain number of turns (**TC**). If the winding has many coils, their **EMF** can simply be added together, taking into account the polarity of their connections and the respective phase of each coil, which is determined by its position relative to the magnet. If the coils span several teeth, the flux linking such a coil is the sum of the tooth fluxes for all the teeth spanned by the coil. In this case the pole-to-pole leakage flux is less significant, therefore the BLV method should give better result. However it's always possible to assemble the **EMF** of the entire winding when the flux waveform is known in a single-turn coil wound around one tooth. The coil list is required to define the slot positions of go and return conductors.

3.1.2. X Factors

The software **PC-BDC** is based on classical analytical calculation methods, which sometimes involve simplifications in order to achieve rapid calculation and good physical interpretation. To make allowances for this things that cannot be calculated accurately, there are various adjustment factors.

This principle of using calibrated design software is common in engineering because no calculation method is perfectly reliable or accurate and testing is the only way of being certain about a design. Since this work doesn't reflect yet the prototype phase, these factors can be used to adjust **FEA** results with the analytical ones, like depicted in figure 3.1. There are several types of adjustment factors and the most important in this design will be present:

- **XBrT** is the main means of adjusting the calculated value of the open-circuit flux produced by the magnet, including the **Bgap** distribution;
- **XBetaM** adjusts the width of **Bgap** distribution. Require **FEA**;
- **XFringe** adjusts the fringing effect in **Bgap** distribution. Require **FEA**;
- **XTTarc** adjust the total area of stator teeth through which the magnet flux passes in the lumped parameter magnetic equivalent circuit model. Require **FEA**;
- **XBtpk** adjusts the flux gathering arc which is used to integrate **Bgap** over the tooth arc. The tooth flux waveform (**Btooth)** is obtained as the rotor rotates**,** according to Simpson's rule [30]. Require **FEA**;
- **XTw** adjusts the effective tooth width in magnetic circuit calculations. Require **FEA**;
- **XCd** and **XCq** adjust the inductances **Ld** and **Lq**, especially in heavily saturated salient pole machine. Require **FEA**;
- **XLdiff** adjusts the harmonic leakage inductance. Require **FEA**;
- **XFe** adjusts the overall iron losses based on iron type and machine operation. Require some engineering judgment;

3.1.3. Magnetic Circuit

The most basic and important calculation in **BPM** is the determination of the flux produced by magnets. An important result of this is the operating point of magnets and the general saturation level of iron. It is also important to determine the distribution of flux around the air gap, because this determines in turn the waveform of the generated **EMF** which is also affected by the winding distribution. The most important magnetic circuit calculations in **BPM** to consider are based on equivalent circuit methods or pure analytical solution of Laplace/Poisson equations.

The following picture shows the magnetic circuit that is in the base of the nonlinear **PC-BDC** calculations. It is drawn for half of one Ampère's law contour, representing the **MMF** drops associated with one air gap. The magnet is represented by a Thévenin equivalent circuit in which *Fma* is the open circuit **MMF**. The flux densities in tooth (**Bt**) and yoke (**By**) are calculated from their permeance areas, and the associated **MMF** drops are obtained using the nonlinear **BH** curve of steel. Bridge leakage in interior magnet motors is modeled by the flux source *Φb*. The total magnetizing force in the magnet, **Hm**, can be calculated as the sum of all **MMF** divided by magnet length. The circuit is solved iteratively, and the basic result is the air gap flux, *Φg*. From this, the average flux density over the magnet pole arc can be calculated.

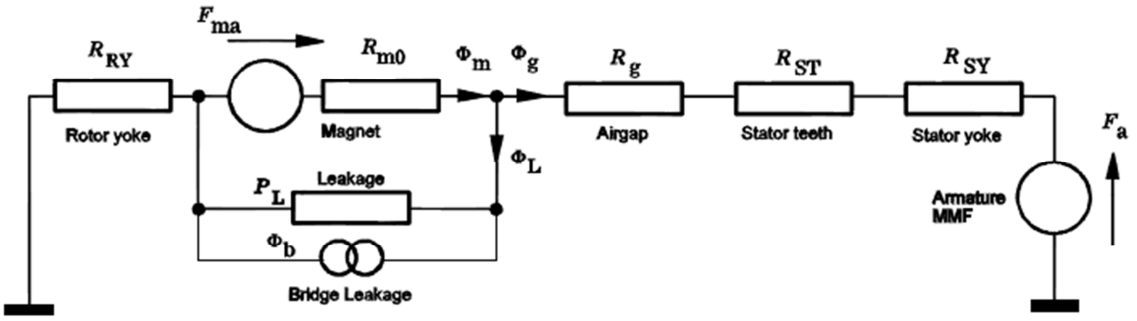

Figure 3.2 – Nonlinear magnetic circuit [8].

3.1.4. Fringing Function

The magnetic equivalent circuit method does not recognize the spatial distribution of flux. To maintain the simplicity and speed of the method it's possible to impose a distribution function of arbitrary shape, which can be corrected by comparison with test or **FEA**. Such a distribution function can be consulted in [8]. The following picture gives some illustration:

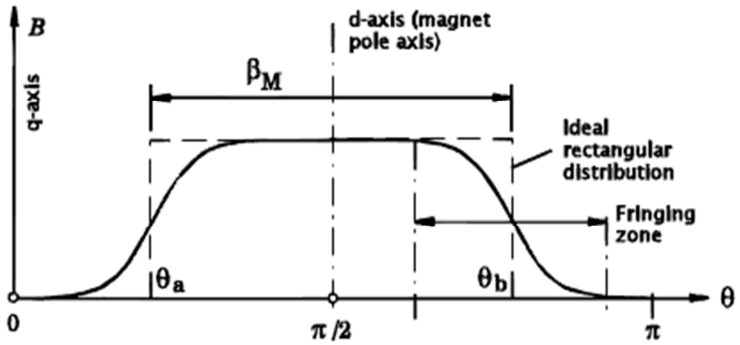

Figure 3.3 – Air gap flux density distribution [8].

This fringing function can be modified for skew and although it is approximate, is extremely fast in computation. Once the flux and its distribution are known, it's possible to calculate the fundamental space harmonic component and from this the fundamental air gap flux per pole (**Φ1**) and peak of fundamental **Bgap** at open circuit (**Bg1**).

3.1.5. Phasor Diagram

The classical *dq* phasor diagram is available for salient pole or non-salient pole machines, provided that machine is sinewound or approximately. As the machine couldn't be purely sinewound, all the phasors represented by **PC-BDC** refers to the fundamental space harmonic component. However, to take a good use of this facility a sinewound machine or much approximated is desirable and it has to be a concern in the design. Moreover, phasor diagram is drawn for one phase and it is tacitly assumed to be similar for the other phases. This means that balanced operation is considered, which is reasonable in this project.

3.1.6. Voltage, Current and Torque Loci

Regarding the operation envelope of machine and its drive, it's very useful to appeal at voltage phasor locus and compare it with the voltage limit circle of inverter. This makes possible to study the effects of field weakening and see how the phasor voltage varies with current locus, which means the circular arc whose radius is the phase current and displacement angle **γ**. This shows how much phase voltage is required from the inverter as **γ** varies. As a current regulated drive is assumed, it can place the current phasor anywhere inside the circle, provided it has sufficient voltage available to overcome the **EMF** and the impedance of the machine. In a variable speed drive, as the **EMF** and synchronous reactance increase in proportion with speed, the voltage locus circle or ellipse gets more close to the voltage limit circle. At the limit and with a certain value of **γ**, the drive may not have enough voltage to maintain the current, so the current becomes voltage limited. This is associated with saturation of the current regulator, which starts to lose control of the current waveform. Therefore this kind of analysis is useful to explore the variable speed drive and **γ** value to employ to get the field weakening and overcome the rising of **EMF** and inductance. In this theory it's possible to check some analytical formulations to compute the base speed for salient pole and non-salient pole machines, including the ideal **γ** that gives the maximum torque [8]. It's possible with this **γ** value to take all the advantages from the alignment and reluctance torque, however this value is not fixed because depends on current and varies with saturation.

A constant torque locus can be superimposed on the circle diagram, which is a rectangular hyperbola, offset from *q-axis* in the case of salient pole machine [8]. The ideal **γ** formulation can be used with constant torque locus to check when it's possible to achieve the same torque at a lower current, or the same torque at a higher speed as the voltage limit ellipse shrinks. However the theory behind this doesn't take into account the effect of iron losses. In practice, these parasitic effects distort the idealized circle and ellipse diagrams and the idealized torque loci. While the high speed behavior is important, the distortion is very significant. However this project doesn't deal with such conditions, so any concern about this.

3.1.7. I-Psi Diagram

During one electrical cycle, the electromechanical energy conversion per phase, **W**, is equal to the area of a closed loop traced by the point whose coordinates is *(i,ψ)*, which means phase current and phase flux linkage. The average torque can be computed as a function of phase number, **m**, and pole pairs, **p**.

$$Te = \frac{m * p}{2 * \pi} * W \qquad (\mathbf{3.1})$$

This calculation is extremely important to compute torque using **FEA**.

3.1.8. Iron Losses

The specific core loss calculation is computed by modified Steinmetz equation [34] to account for non-sinusoidal variation in **Bt** and **By**. The specific core loss includes a hysteresis term and an eddy

current term that are calculated inside de steel data base manager (**DBM**). The hysteresis term requires the peak flux density in each section and the frequency. The eddy current term requires the mean squared value of dB/dt in each section over one cycle. The method used to calculate the peak flux density and mean squared value of dB/dt is based on-load waveforms of **Bt** and **By**, as function of rotor angle calculated over 180º electric. The adjustment factor **XFe** gives final loss calibration.

In appendix D.8 the iron losses Vs **B** at a fixed frequency can be found. The computation is for rotor and stator iron used in the new project.

3.1.9. Slotting Ripple

Slot ripple refers to the modulation of **Bgap** caused by stator slot openings. Carter's coefficient is a well-known example but Freeman used a sophisticated procedure involving elliptical integrals to determine the harmonics in the flux density. Using **FEA** is also a powerful method for calculating the slot modulation and **PC-BDC** have calibration factors to use in **Match FE** to adjust the slotting effect.

Lawrenson's method is implemented by first determining the slot modulation in **Bgap** distribution using the method of Weber extended by Zhu and Howe [8]. Slot ripple is related to the concept of permeance harmonics. As the rotor rotates past the stator slots, the overall permeance is modulated at slotting passing frequency (**fsp**), causing the main flux to pulsate at this frequency. As permeance is a lumped-circuit concept rather than a distributed field concept, the calculation of flux variations is useful in this context.

3.1.10. Magnet Losses

In an ideal synchronous machine the field rotates in synchronism with the rotor and the flux density is time invariant throughout the rotor cross section. There is no tendency for eddy currents to flow anywhere in the rotor, so no losses in the magnets, rotor or shaft. Such ideal conditions would exist at constant speed in a machine with smooth cylindrical surfaces, no slotting, with sine distributed windings and with balanced polyphase sinusoidal currents.

However eddy currents are induced in practice by imperfections from the ideal synchronous machine. In such imperfections it's possible to detach: space harmonics in the stator ampere conductor distribution and time harmonics in the stator current waveform producing asynchronous field components that rotate forwards or backwards relative to the rotor; the modulation of the overall permeance of the magnetic circuit at **fsp**; the dips modulation at the air gap flux distribution due to stator slot-openings which rotate backwards at synchronous speed relative to the rotor.

To avail the magnet losses, it's assumed that they are caused by eddy currents which are due to variation of flux density in the magnets. The engineering analysis of eddy currents is mathematically delicate even in **2D** models and very few **3D** effects can be fully analyzed by classic methods. **3D** effects include the effects of finite-length and other shapes than simple rectangular blocks. The way used to avail the nature of eddy currents is calculating the ratio between a key dimension of the magnet, as the length, and skin-depth. Therefore if the skin-depth in the magnet is comparable with half length, it means at that frequency the eddy currents turn inductance limited [37]. In most cases the eddy currents are likely to be resistance limited as a result of the relatively high resistivity of magnets.

In this case, any further increase of resistivity will reduce the loss. Moreover, the loss will be reduced if the magnet is made thinner, which can be achieved doing segmentation.

When the magnets are buried inside the rotor of an interior rotor machine, they are less susceptible to eddy current loss. The asynchronous space harmonic components of the field are naturally attenuated away from the air gap, so the higher the space harmonic order is, the greater the rate of attenuation. However buried magnets cannot hide from time harmonics in the current waveform created by pulse width modulation (**PWM**). More discussion on this can be consulted [8].

3.2. SPEED PC-FEA

The simple magnetic circuit model can make crude allowances for saturation, even the nonlinear one. For thorough analysis of the magnetic field, **FEA** is far the most powerful. It is particularly effective computing details of local geometric features and the effects of arbitrary distributions of conductors and magnetization patterns. These details continually increase in importance because of the need to reduce torque ripple and acoustic noise.

In cases where magnetic saturation is present, it's not reliable to obtain the inductance by the storage field energy as it relies on the assumption that the inductance does not vary with current. Moreover, the storage energy in permanent magnets introduces another ambiguity. A more rigorous approach is using vector potential, **A**, directly with equation:

$$\Phi = \int A \cdot dl \qquad (\mathbf{3.2})$$

In this equation Φ is the flux linking the contour along **A** is integrated. In **2D** problems, the flux linking a coil is given by:

$$\Phi = A_{c1} - A_{c2} \qquad (\mathbf{3.3})$$

The values of A_{c1} and A_{c2} represent **A** values at the extreme coil side positions: go and return. So it's important that conductors positioning are known, for means of a conductor location vector (**CLV)**. If there is a complete winding with coil sides in different locations, the method can be extended by summing the fluxes with appropriate polarities according to the direction of conductors.

PC-FEA is a fully fledged **FEA** tool for **2D** magnetostatic analysis with a nonlinear solver and powerful post-processing. It will be used to substitute **FEMM** in this new project.

3.2.1. FEA Best Practice

The best practice using **FEA** passes to: supply good **BH** data from the materials; get a good mesh for torque calculations; check that boundary conditions are correct (Dirichlet and Neumann); check that element order is correct and choose an appropriate convergence tolerance to the iterative method

used, like Newton-Raphson in this case. Typically 10 iterations are enough to attain the solution. If more is required, probably the materials are not well prepared. This causes other concerns:

3.2.1.1. Materials

Most errors arising from material properties are a result of irregularities in the **BH** data: non-monotonic data; don't extend to a sufficiently high value of **B** or doesn't start from 0, or the interpolation used to obtain the **BH** points introduces spurious irregularities. Since particular care is needed with all **BH** curves, a very fastidious preparation process is needed to attain good results with virtual prototyping and with **FEA**. It will not be given reference to that in this work but further reading is advisable [34]. An example of this curves related to the iron used in the machine are presented in appendix D.6 and D.7. It can be found that **BH** data must be smooth, even at low flux densities, because points of inflection can cause slow or even convergence failure in nonlinear magnetic circuit or **FEA** solver. This smoothness can be checked with **μr** vs **B**. The **BH** curve is also included in appendix D.5.

3.2.1.2. Cogging Torque

The cogging torque is a very difficult calculation which requires a very good mesh density and various methods of torque computation to see if a reliable result is attained. Its analytical calculation is difficult and requires a series of simplifying approximations, so **FEA** is usually a good way to analyze it. These phenomena results from the interaction of permanent magnet **MMF** harmonics and the air gap permeance harmonics due to slotting. When it's present, there is a tendency of rotor align in a number of stable positions even when the machine is unexcited. The resultant pulsating torque doesn't contribute to the net effective torque and since it can causes speed ripples and induce vibrations, its reduction is usually a major design goal. In this work several methods to calculate the torque were used to give some contrast in **FEA** calculations. They can be distinguished between co-energy derivatives methods and Maxwell stress tensor methods, respectively: torque by co-energy and virtual work (**VW**); **MST** and Maxwell surface integral (**MSI**).

3.2.1.3. Elements Table

In this functionality local flux density values are computed in **PC-FEA** for one electrical cycle in each mesh element of iron regions. The element values for magnetic vector potential, flux density, field strength and relative permeability are stored in tables and the iron losses are calculated based on modified Steinmetz equation. This feature is very useful to compare the calculations with **PC-BDC** and to help giving a better judgment about **XFe** value to use, as it considers with more detail the flux densities waveforms.

3.2.2. GDF editor

The objective of this editor is creating the file that contains the necessary geometry and other necessary data to define the finite element problem. The problem is divided into regions and assigns nodes along the region boundaries, with appropriate boundary conditions already referred on external

boundaries. It is possible also to modify the node distribution and other properties, before the problem is passed to **PC-FEA** pre-processor for meshing. Then the lines geometry information and subdomain characteristics such as materials and current densities are passed to **PC-FEA**. This is a very useful feature because the process of achieving a good mesh starts here and is independent from **FEA** program itself. The boundary node distribution is an input for the mesh generator and the quality of mesh optimization is very dependent on the number of boundary points defined and the spacing between them. Most of the meshing errors arise from a poor initial distribution of nodes at the sub-domain boundaries.

This functionality is a clear advantage over **FEMM**, where there is no way to create subdomains inside a region and customize the mesh in each subdomain. It's necessary, for instance, when transient solver is used to calculate the magnets eddy currents. In the appendix C.3 it's possible to check an example of boundary node distribution in the machine studied. This configuration was used as default to all **FEA** calculations.

3.2.3. Mesh Generator

The division into finite elements is called meshing and it is done by any **FEA** program capable of reading **GDF** files. The triangular mesh generator (**TMG**) used has an auto adaptive algorithm which takes as its input the boundary node geometry and the maximum angle, producing first-order triangular elements. This represents the maximum angle allowed between 3 consecutive boundary nodes. Since there are further some optimization procedures applied, this angle was initial taken to the value of 100º. Mesh optimization is applied to bring it close to its ideal value of 60º. The optimization routines applied are: triangle area optimization, node centering, subdivision of the largest triangles, deletion of the smallest triangles and Delaunay test [33]. If more improvements to attain a good density mesh or solve errors are needed, it's possible to add new boundary nodes. These new nodes are placed on straight lines between existing nodes and if virtual arcs are used, the mesh generator can be instructed to place a given set of boundary nodes on an arc to improve the geometric modeling accuracy. This is done in this project because it attains good results. The appendix C.4 shows a mesh example for the motor studied based on the previous descriptions. That configuration was set as default to most of calculations using **FEA**.

For problems requiring a multi position solution and rotating mesh, **PC-FEA** starts with separate rotor and stator meshes. Then it has to identify the nodes at the opposing surfaces, defining for it a band that can be adjustable by the user to include more or less nodes. A good value to use in the project was achieved by several experiences, not too small value for not leaving some nodes behind but also not too large to not include extra nodes. A simple illustration of a rotating mesh is given in appendix C.5.

3.2.4. GoFER Routine

This functionality automatically sets up standard **FEA** calculations at **PC-FEA** script. The most important will be summarized.

3.2.4.1. Bgap Waveform

This routine produces an open circuit calculation with fixed rotor angle. Then flux density distribution measured at middle air gap for that rotor position is returned. The comparison with **PC-BDC** calculation is done by means of matching finite element (**Match FE**) tool.

3.2.4.2. Btooth Waveform

An open circuit **FEA** calculation is produced, in which the rotor position is stepped through a sufficient angle to determine the waveform of tooth flux density as the rotor rotates 180 electric degrees. As referred in tooth flux method, the entire phase **EMF** can be constructed from this waveform. The file returned can be compared and adjusted with X factors by means of **Match FE** in order to **PC-BDC** give good prediction, especially if the **EMF** is calculated under this method. The tooth flux is measured at the middle teeth length and the rotor steps were defined so the points obtained are normally spaced at intervals of 1 electrical degree.

3.2.4.3. Cogging Torque

This feature obtains the variation of cogging torque caused by the interaction of the magnetized rotor with slotted stator on open circuit. The data is returned to **PC-BDC** by **Match FE** where it's possible to determine the effect of skew in cogging torque waveform. As this calculation requires precision, especially in machines where the cogging is small, a good mesh optimization is needed like described above, as well as a high number of rotor steps.

3.2.4.4. I-Psi Unskewed

The main goal of this on-load unskewed calculation is to get the average **EM** torque from the energy conversion loop, in a *sinewave* drive. It's of great value for calculation with highly saturated **PM** machines, especially with interior magnets where *d-axis* synchronous reactance (**Xd**) and *q-axis* synchronous reactance (**Xq**) may vary strong with current. The result is valid even when the winding is not sine distributed and also takes into account any variation in the level of saturation as the rotor rotates, so permeance harmonics are included. In such cases it's the only rigorous method for calculating the torque as it includes all **EM** torque produced by phase currents. Cogging torque is not but since **i-psi** loop is only to calculate the average **EM** torque and the average cogging torque over one cycle is zero, it has no effect on the result. This is another clear advantage over **FEMM** software that always uses instantaneous torque methods like **MST**, which is very dependent of mesh quality.

The elements table already referred can be obtained in this routine and, as in the last, the number of rotor steps are important for smoothness and solution accuracy.

3.2.4.5. I-PSI Skewed

This is a special variant of **i-psi GoFER** that performs multiple **FEA** computations corresponding to a series of slices which are phase shifted to reproduce the effect of skew. This phase shift can be effected either by phase shifting the current waveform or by physically rotating one slice relative to the next [32]. The calculations were performed with 10 slices since good results were obtained. The **i-psi**

loop data can be imported into **PC-BDC** and compared with internal calculation, like with *i-psi* loop unskewed.

3.2.5. Transient Solver

Most **FEA** for electrical machines are magnetostatic, requiring the solution of Laplace equation in air and steel regions and Poisson equation in magnet regions. So it doesn't admit time varying phenomena such as eddy currents. To calculate them it's necessary to solve the diffusion equation. The transient solver used in **PC-FEA** has this purpose, limited to a **2D** calculation in a transverse plane and restricted to a single conducting region. Eddy current carrying regions can be modeled using the transient diffusion equation [39]:

$$curl\ (v\ curl\ A) = -\sigma * \frac{\partial A}{\partial t} + \sigma * (v \times curl\ A) + curl\ (v\ B_r) \qquad (\mathbf{3.4})$$

The solution of this equation requires a time stepping algorithm such as Crank-Nicolson. The term $\partial A/\partial t$ can be approximated using an incremental strategy at time interval Δt [39]. Storing the information about **A** in each mesh element for the eddy current carrying regions, it's possible to estimate the mean loss density in that element, as it rotates through an electrical cycle.

Finite element solutions in **2D** must satisfy the zero net current condition across each conducting region separately:

$$div\ (J) = 0 \qquad (\mathbf{3.5})$$

Using **PC-FEA** transient solver, this condition is only satisfied over the whole solution domain and not over individual conducting regions. An approximate result can be obtained by suppressing the conductivity of all magnets, less the one that is being calculated. Considering that losses must be equal in all magnet blocks, the final result is obtained by multiplying the result for one block by the number of poles. This relies on the assumption that eddy currents in any magnet do not affect the eddy currents in any other magnet. This is characteristic of resistance limited eddy currents and to attain good predictions using this software, the design must guarantee it. It is also desirable in the **EM** point of view.

3.3. Motor CAD

This software is based on a thermal analytical lumped circuit model. The thermal network is composed by resistors and power sources. Resistances are used to model the main heat transfer paths within the machine and their value is dependent upon the dimension and the materials thermal conductivity. The machine losses contribution are modeled as the thermal equivalent to electrical current sources, therefore power sources. Many applications, as in this project, do not have a steady state operation so in order to obtain a reasonable transient calculation time, lumped circuit techniques

are required, rather than computer fluid dynamics (**CFD**) or even **FEA**. The **CFD** accuracy is not as good as with **EM FEA** due to the complexities of geometry and turbulent fluid flow. Moreover, can be very time consuming, weeks or even months, to construct a model and then calculate it. Therefore its use is best to calibrate analytical formulations.

As most of models studied in next points are nonlinear and fluid properties, air or water, vary with temperature, it's necessary to perform a calculation for each temperature determined at all nodes in lumped thermal circuit. This means that an iterative procedure is needed for both steady state and transient analysis.

3.3.1. Winding Layer Model

Most of electrical machines have random wound mush winding in which is impossible to model the position of each conductor. Even with precision and form wound windings it is often not necessary to model each individual conductor. For this reasons a layered model is used to represent the winding in thermal circuit, as it gives indication of layers temperatures and has physical relationship to the geometry and slot fill used. As the slot is composed by a mix of copper, insulation, impregnation and liner, if their lengths and the slot dimensions are known, it's possible to calculate the thermal resistance for each one, according to the material thermal conductivity. Substituting the conductors by layers of copper and insulation within the slot liner and define a set of thermal resistances, it's possible to identify the winding hot-spot at slot center. Some calibration of this model using thermal **FEA** is advisable. More topics about this model can be found [19].

3.3.2. Losses Calculation

For **BPM** it's useful to have models that take into account the temperature and load to calculate the losses. If the copper loss is inputted at a specified temperature, then it changes according to the winding temperature, based on the resistivity variation [19]. Particularly, if **NdFeB** magnets are employed, it's very useful to consider the flux drop in the magnets with the temperature increase. Defining the steady state operation for machine developing a constant torque, it's possible to account with temperature increase in the winding due to current to compensate the flux lost in the magnet. Some formulations can be found to calculate the copper and iron losses at the winding and magnet temperature, starting with defined loss values at known winding and magnet temperatures [19].

3.3.3. Interface Gaps

The accuracy of a motor thermal performance is critically dependent upon the estimation of the many thermal contact resistances within the machine as stator lamination to housing, and slot liner to lamination. The correct estimation of contact resistances can be crucial, especially in heavily loaded machines where a large loss through even a small thermal resistance leads to a large temperature difference. The contact resistance is due to imperfections in touching surfaces, and the easiest way to quantify it is base the thermal resistance on an average interference air gap. Some typical values for different kind of materials can be found in [19] based on Holman and Mills books [40], [41].

3.3.4. Bearing Model

The bearings are a very complex component in terms of heat transfer. It's a composite component with an inner and outer race, balls, grease and air. All these elements and the lubricants give a big level of uncertainty for thermal resistance determination. Some work has been done [42] to give more data of typical values for an equivalent gap that can model it.

3.3.5. Convection Heat Transfer

The convection heat transfer calculations for all external surfaces of the motor use convection heat transfer correlations for each particular surface. A process of dimensionless analysis is followed to obtain a functional relationship between the physical properties and the fluid parameters. This makes the resulting correlations applicable to all shapes and with any fluid material, in a laminar or turbulent flow. A set of dimensionless numbers are used in the process: Reynolds number (**Re**), Grashof number (**Gr**), Prandtl number (**Pr**), Nusselt number (**Nu**). Once heat transfer coefficient (**h**) is determined using **Nu**, the thermal resistance is calculated for a given surface area.

3.3.5.1. Natural Convection:

This is the heat transfer process that is considered between the housing and the ambient, defining a totally enclosed non ventilated (**TENV**) cooling. The convection correlations for horizontal cylinder and vertical flat plate can be consulted [19], based on Simonson book [43].

3.3.5.2. Forced Convection:

Considering enclosed channels the formulation for **Re** is given in [19]. This is particularly important as it defines the transition from laminar to turbulent flow. If laminar flow is present, the correlation that defines **Nu** is given in [19] based on Mills books [41]. If turbulent flow is present, **Nu** is given in [19] based on Gnielinski formula [44].

3.3.6. End Space

This area of machine cooling is one of the most difficult to predict accurately as fluid flow, air in this case, in the end space region of an electric motor is usually much more complex than flow over its outer surfaces. This is because the fluid flow depends on many factors including the shape and length of the end winding, added the surface finish of the rotor, end sections and turbulence. Several authors have studied the cooling of internal surfaces in the vicinity of the end windings. In the majority of cases, they propose the use of formulations given in [19] which represent a curve fit of **h** with local fluid velocity for surfaces in contact with end space fluid. The main goal to obtain an accurate estimate of the end space cooling is to select an appropriate correlation and then estimate the local velocity seen by all surfaces in the end space region. The default used is Schubert correlation and can be consulted in [19] as well as ways of estimating the local fluid velocity.

If there are end cap vents open, it allows an amount of flow in and out of the end space regions. However it will not be considered in this project as the team feedback from Agni 95R considering this

feature is not good. There were some problems with gravel and other particles that enter inside the motor and damage the rotor and brushes.

3.3.7. Duct Wall Friction

The duct wall roughness is used for calculating the pressure drop in a water jacket or through ventilation cooling system. It is important for ensuring that system pressure is calculated properly and the parallel path flow rates are estimated correctly. The duct wall resistance is predicted using formulations from Miller book [45] based on Colebrook-White equation which forms a good estimate of turbulent flow area of Moody chart [19].

3.3.8. Air Gap Model

The air gap heat transfer model can be made to be solely based on conduction or to include convection as well. The convection model is considered in this project due to work developed by Taylor [46]. It determines the increase in heat transfer coefficient over that for pure conduction due to convection induced between two concentric cylinders rotating relative to each other. He found that heat transfer is made by pure conduction when the flow is laminar but there is an increase in heat transfer when **Re** passes a critical value. Above it, the flow takes on a regular vortex pattern. Above a higher critical **Re** value, the flow becomes turbulent and the heat transfer increases further. The formulations can be consulted in [19].

The slotting and saliency effects are not included in the models. However a safe margin is given to obtain an over prediction on rotor temperatures if the flow is turbulent, which is a good hypothesis base. More information can be consulted in [19] based on the Gazley book [47] and Hayase [48].

3.3.9. Insulation Lifetime

The insulation lifetime is very important in machine design and is dependent on the winding hot spot temperature. The estimation method is based on Montsinger model [52] to calculate the rate of lifetime loss as the temperature of the winding increase.

3.3.10. Thermal FEA

When winding layer model is applied, calibration with **2D** finite element may be necessary. The **2D FEA** is set up with housing temperature calculated in Motor CAD used as boundary condition. The active copper and stator losses are used in the finite element calculations. The results can be compared with the layer model and the calibration must be done if the temperatures difference is superior to 5%. To do that procedure, the impregnation goodness can be used to adjust the values and therefore it loses physical meaning. However it is not too important because it's only a means of calibration. What really matters is the material used in impregnation and its thermal conductivity.

3.3.11. GoTAR Routine

This is the standard method for linking **SPEED** programs to Motor CAD software, in a very similar way of **GoFER** but now using Windows® Active X because the software packages are different.

The geometry is passed between the tools, as well as winding definitions and losses. A steady state or transient performance can be executed in an iterative way: Motor CAD return adjusted parameters back to **SPEED** so that parameters are calculated at the correct temperature. This provides a mean of automatic calibration for **SPEED** thermal model.

3.4. Electromagnetic & Thermal Project

Once the tools that will be used are presented and the main models described, it's now important to have an idea of how they will connect to obtain the final virtual prototyping. Since all this software packages are full Active X compatible, their interconnection using a Windows® system is automatic. This issue is very important as it allows co-simulation between **EM** and thermal design, to adjust the temperatures in steady state or transient operation, and so update resistance and losses taking into account the cooling system. As **PC-FEA** module is common to all **SPEED** packages, the data interchange is done by **Match FE** tool. This feature makes possible the comparison between **GoFER** numerical results computed by **PC-FEA** and the analytical **PC-BDC** calculations. This allows calibrating **PC-BDC** analytical models with **FEA** results. The next flowchart illustrates the procedure and the different tools' capabilities summarized.

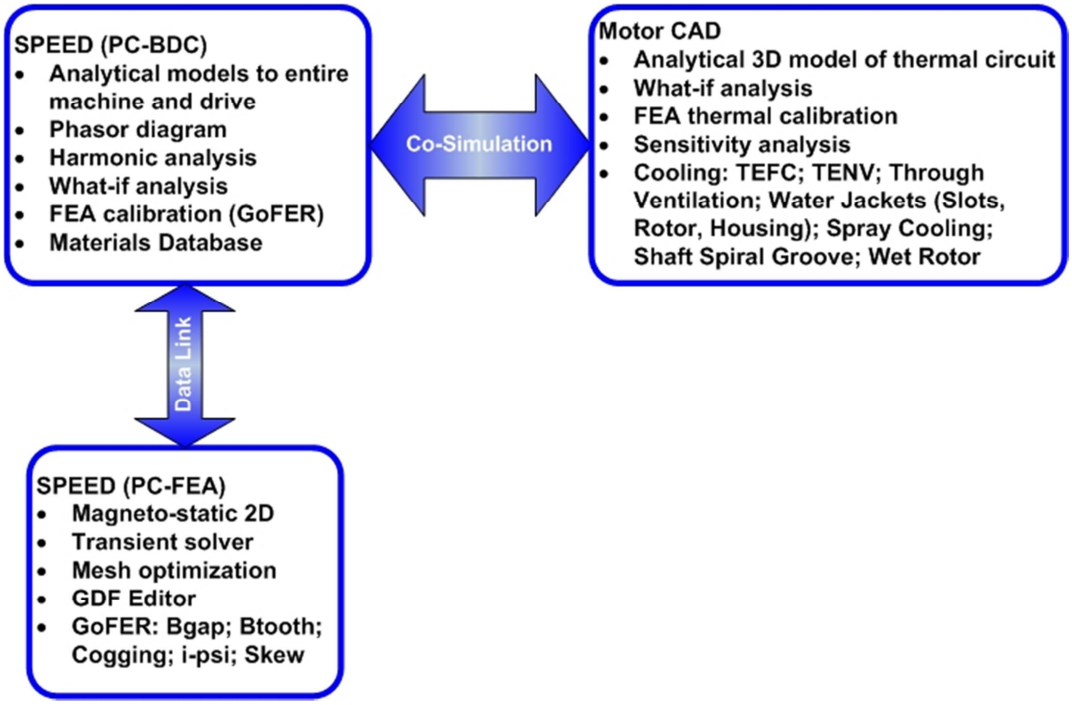

Figure 3.4 – Software packages connection.

Similar project approach has been done using **SPEED** and **CFD** software to make the **EM** and thermal project in same logic of data interchange. More information is addressed in [61].

4. Prototype MM03_V3: Electromagnetic Project

This chapter presents the new prototype design, focused on **EM** project using **PC-BDC**. It starts with a spoke rotor **IPM** machine that already exists and it's calibrated. Changes were made on that machine in order to introduce the first design options and study its results. This has the advantage of check with more confidence the effects of small changes and understands what is important, performing a "what-if" analysis. The visual feedback from **CAD** outline editor is useful to minimize errors and give a first idea of design viability.

4.1. Electromagnetic Basics

The first design considerations will be based in the analysis of some key equations, taking into account the project scope. The following formulations reproduce the **EM** basics [30]:

$$\begin{cases} E_{q1} = \dfrac{\omega}{\sqrt{2}} * \psi_{1d} \\ \psi_{1d} = k_{s1} * k_{w1} * T_{ph} * \Phi_1 \\ \Phi_1 = \dfrac{B_{g1} * D * L_{stk}}{p} \\ T_{ph} = \dfrac{C_{pp} * 2 * p * T_c}{P_{pth}} \\ MLT = 2 * L_{stk} + 2 * L_{et} \end{cases} \qquad (\mathbf{4.1})$$

It can be verified that **Eq1** is related to fundamental component of **PM** flux linkage (**ψ1d**) by Faraday law. The expression represents the module of this vector in the phasor diagram. It states that is necessary a high flux linkage at open circuit to get the highest **EMF** possible. This has interest because the alignment torque is proportional to this component, more specifically the first harmonic, **Eq1**:

$$T_{ei} = \frac{m * p}{\omega} * E_{q1} * I_{q1} \qquad (\mathbf{4.2})$$

The first term is constant for a given machine, so to maximize the alignment torque and achieve a high **TRV** is necessary to get a high **EMF**. This has the effect of decrease the necessary armature current to get the same torque value, which is good for the cooling system because there are few losses to dissipate. The equation states also that *q-axis* component of phase current is responsible for torque production. This principle can be used in space vector modulation using **FOC**, like is being developed inside the project.

It's important to achieve the highest value possible of **Eq1**, which means the highest value possible for **ψ1d**. The flux linkage equation states that the ideal way to maximize it is not have skew in

the machine and use a winding with a full pitch coil in order to get **Kw1** equal to 1. Moreover, **Φ1** has to be as high as possible and the same with turns in series per phase. Regarding the last ones, **TC** is the main variable to play and its main effect is increasing the machine reactance, however it can saturate the current regulator. Therefore a reasonable value is given for starting and then the current and voltage loci will avail the best number of turns to use, in order to guarantee the variable speed drive at speed range given. The number of parallel paths in phase winding (**Ppth**) can be used to adjust the resistance and inductance, because the parallel connections in the winding have the effect of current decreasing. The other degree of freedom is **Φ1**, mainly with fundamental air gap flux density, **Bg1**. The spoke rotor type allows flux concentration in the rotor, which permits a high flux density in the air gap, therefore this is the main variable to maximize as it only depends on magnets and air gap used. The best is choosing the grade with highest **Br** taking into account the temperature that is expected to find in the magnet. The stack length and stator bore diameter have big influence in the overall weight, so as first approach is better define them in the maximum limit to maximize **Φ1** and then check the weight to see if the limit is exceeded or not. Using this procedure for a first iteration is important to note that if stack length increases, the mean length of turns (**MLT**) increases too and winding resistance gets higher. To compensate this effect could be good to have slots with big area. As the machine will have a short diameter, it implies that few slots must be used to maximize the slot area and the tooth width. This point is very important because as seen before, is expected to have a machine very saturated in the tooth and stator yoke. Therefore to avoid extreme values of current to achieve peak torque is important to guarantee the maximum area possible for tooth flux. This has the effect of decreasing flux density in the tooth, **Bt**, and machine will deal better with saturation.

Once the basics are defined, is useful to take some conclusion about the total torque that can be developed with a salient pole machine:

$$T_{tot} = m * p * \left[\psi_{1d} * I_{q1} + I_{d1} * I_{q1} * \left(L_d - L_q\right)\right] \qquad (\mathbf{4.3})$$

$$\begin{cases} \psi_{d1} = \psi_{1d} + L_d * I_{d1} \\ \psi_{q1} = L_q * I_{q1} \\ I_{d1} = -I_{sp} * \sin\gamma \\ I_{q1} = I_{sp} * \cos\gamma \end{cases} \qquad (\mathbf{4.4})$$

In the equation is possible to check two torque components: alignment and reluctance. Alignment torque, as already seen, results in interaction between **EMF** and current. Reluctance torque results in interaction between stator current and inductance variation as the rotor rotates. This component requires phase advance to be used. As it decreases the necessary current to achieve the same torque level, it is not the worst case scenario for **EM** and thermal point of view. This means that is best to direct the project without considering phase advance and then study it in a last phase.

4.2. Design Options

The basic design options will follow, based on last assumptions. As this project is very complex and has many variables, only the most relevant will be described.

4.2.1. Materials

This topic reflects all the materials necessary to make the **EM** project. For the winding the choice passes to use copper, as it's a classical solution. However, researches using laminated winding with aluminum are being developed with good results [49], as many others [55]. As it's not a simple solution it was left behind even with weight advantages. About the magnets, iron and shaft more considerations are necessary.

4.2.1.1. Magnets

Several types can be considered. The following table helps to systematize ideas and make the best choice, regarding the experience in the last design.

Property		Units	Alnico 5-7	Ceramic	Sm_2Co_{17}	NdFeB
Remanence	B_r	T	1.35	0.41	1.06	1.2
Coercivity	H_c	kA/m	60	325	850	1000
Energy product $(BH)_{max}$		kJ/m^3	60	30	210	250
Relative recoil permeability	μ_{rec}		1.9	1.1	1.03	1.1
Specific gravity			7.3	4.8	8.2	7.4
Resistivity		μΩ-cm	47	$>10^4$	86	150
Thermal expansion coefficient		10^{-6}/°C	11.3	13	9	3.4
Temperature coefficient of B_r		%/°C	-0.02	-0.2	-0.025	-0.1
Saturation H		kA/m	280	1120	> 3200	> 2400

Figure 4.1 – Magnet types and properties [8].

It can be seen that **AlNiCo** has low coercivity field strength, **Hc**, therefore it's more directed to applications where the machine is not heavily loaded, which is not this case. **Sm-Co** is much better on that and is widely used in specialist application with high temperature requirements. However it has the highest specific gravity, which is bad when the weight is an important variable. Ceramic or Ferrite magnets have the lowest remanence field (**Br**) and this variable is crucial in this design process. The last solution is **NdFeB**. In fact it has all the good properties needed for the design: high **Br** and high energy product, high **Hc** and good specific gravity for the energy product developed. The main drawback is the high temperature coefficient of **Br**, which means that magnet loose **Br** with temperature increase. However as it was identified the need for an extreme cooling strategy, is possible to develop some special features in **EM** and thermal design to mitigate this disadvantage. In the appendix D.9 can be find a comparison between different magnets: **NdFeB** (N38EH; N35AH; N33AH) [14] and **Sm-Co** (RE(SM)Co5 159/159; RE(SM)Co5 175/119; RE2Co17 222/199) [14] using magnet **DBM** of **SPEED**. Independently of grade, is possible to check that **NdFeB** magnets have the highest energy product.

If choice passes to **NdFeB** is important to take some considerations about manufacturing process and choose the right kind and grade in the several categories available. The principal categories of **NdFeB** regarding the manufacturing process are sintered and bonded. Since raw material of sintered is metal, it's necessary to make them into particles for the machining. Bonded there is no such need as the raw material is powder. So in the pressing process, sintered is compacted in the presence of an externally magnetic field, which guarantees the direction of magnetization in place and higher **Br**. To bonded magnets there is no need of external magnetic field and it's possible to magnetize the magnet in any direction, however the energy product will be much lower comparing with an anisotropic magnet. The advantage of these magnets is that no machinery is needed as the powder is pressed into the shapes already chosen. Taking this into account, the option will be sintered **NdFeB** because is the strongest. The only constrain is that standard shapes must be used, like parallelepipeds or cubes. This is due to the manufacturing process explained. Regarding the coating and since this prototype will not work in hard environment, a simple coating with **Zn** or **Ag** is enough.

To decide the magnet grade, the first approach was choosing those with highest temperature allowed because there was no idea about the thermal behavior of the machine in the first design iteration. The disadvantage is the price, however machine design is an iterative process and this was only the first iteration. Further corrections and adjustments in design are natural. In the manufacturer point of view, magnets typically have a large tolerance on **Br**, more or less 5%. When a magnet grade is new, most magnets may be towards to the lower end of the tolerance band. The magnet manufacturer usually improved the magnet manufacturing process with time and most magnets now are towards the upper band. Therefore an average value was used to **Br**, as can be consulted in the appendix D.2. It's possible to check the main properties of grade N35AH, used in this design.

4.2.1.2. Iron

The iron is the key material for any magnetic circuit. Its properties, regarding saturation polarization and specific losses, are crucial in the **EM** and even in the thermal project. As already stated this machine has a high **TRV**, therefore saturation is an important **EM** characteristic to deal. Moreover, to attain a high **Bg1** may be interesting explore small air gaps with the strong magnets already chosen. This cause some concerns about forces developed in the iron and shear stress in the air gap, beyond saturation already referred. The ideal is to have an iron with high tensile strength, high permeability and high saturation polarization. In general iron cobalt alloys can achieve the two last referred, however the first is more difficult. Moreover, a thin lamination to minimize the eddy currents loss and good interlamination materials are important in order to achieve the best thermal behavior and the lowest losses possible.

All these requirements were achieve with iron cobalt alloy VACODUR® 49 [13]. This product is specifically directed to high performance motors with maximum power density and low losses. Moreover, the same alloy can be optimized for best magnetic or mechanical properties. It means that manufacturing process can be changed to achieve the highest tensile and yield strength or the lower specific losses and highest permeability, without changing the main composition. So this permit to apply in the stator the alloy to optimize the magnetic properties, losing in the mechanical variables

referred but maintaining the good qualities of iron cobalt. Then in the rotor can be applied the alloy optimized to mechanical properties which guarantee high tensile strength. There is no problem to deal with high rotating stacks, submitted to a higher shear stress, vibrations and high forces due to the high air gap field. The specific loss of rotor iron is higher but as it's not expected to have great losses on the rotor, no problem on this.

Regarding the saturation polarization, it guarantees linear behavior until 2.35 T which is typical in this kind of alloy. This property is very important in the design because as saturation is not a problem, the typical rule of thumb which states **Bt** and **By** in open circuit with values of 1.5 T is no more an issue to concern. So high values can be reached, like 1.7 T, and the natural consequence is increasing **Φ1** and **Eq1**. Results about the advantage of using iron cobalt alloys in high power density machines and VACODUR® 49 applications can be found [59].

The **BH** data for **DC** curve of VACODUR® 49 can be consulted in [50], both for rotor and stator. This was the data used to prepare all the necessary iron characteristics, as stated in section 3.2.1, using steel **DBM** from **SPEED**. The main properties can be found in appendix D.4, including loss values used to calculate the coefficients of Steinmetz equation.

4.2.1.3. Shaft

As discussed in section 2.1, the only concern on this material regarding the **EM** project is guaranteeing a non-magnetic shaft. Moreover, has to be cheaper and with high tensile strength because it has to support high forces at low speeds. The most common material with standard utilization in these applications is stainless steel.

To choose the best alloy, the criterion was searching for the highest tensile strength and at same time with good machining properties. Stainless steel 455 is relatively soft and formable in the annealed condition. A single step aging treatment develops exceptionally high yield strength with good ductility and toughness. Is very easy to fabricate and joins high strength with corrosion resistance. All this properties and good price push this solution towards the final choice. Basic properties can be consulted in appendix D.3 [21]. As the shaft is not considered in FEA calculations, it was not necessary to define **BH** curve in **SPEED DBM**.

4.2.1.4. Construction Details

This topic has interest regarding the iron stack and the magnets setting in the spoke rotor.

To fill the interface gap between magnets and rotor stack is good practice using glue line to guarantee durable bonds with outstanding impact and peel resistance. This is achieved with Loctite® 392 as can be seen in the datasheet [51]. It´s recommended for bondline gaps until 0.1 mm, so it's ok for the typical metal-metal interface gaps seen between magnets and rotor iron. In the appendix A.7 can be seen a figure that illustrate this procedure for an **IPM** machine. There are several ways to assembly the magnetized permanent magnets, linking manual and automated production. More information is addressed in [56].

For iron lamination is important to know that cobalt iron besides being expensive requires carful processing, mainly if thin gauges are used. This justifies the choice of Vacuumschmelze products,

because all the stacking process is done by the manufacturer. Moreover, VACODUR® 49 is assembled with proper interlamination material, the VACSTACK®, which consists in a complex composite of glue, insulation and oxidation layer offering the best electric resistivity. Regarding these considerations, no special worry has to be taken in the machining and assembly of thin gauges. All the technological processes needed are entirely fulfilled by the manufacturer in order to maintain the properties described. The thinnest lamination available was chosen to guarantee the lowest eddy currents loss: 0.1 mm. Precise stacking and low geometrical tolerances avoiding magnetic deterioration and expensive mechanical finishing are guaranteed, using either skewed assembly or not. High filling factors are possible, approximately 98%, which is the value used in this design.

4.2.2. Design Type

According to classical theory **AC** machines should have sine distributed polyphase windings, supplied with *sinewave* current. Once the drive operates with *sinewave* current, it's possible to use phasor diagram to analyze the machine. Sine distributed windings are required for space vector theory used in **FOC**, because if there is any saliency the inductances should ideally vary sinusoidally with rotor position and *dq* equations using Park transformation can be used. In consequence **EMF** waveform is perfectly sinusoidal. Therefore to make a good use of space vector modulation and Park transformation, avoiding approximate calculations, is necessary to guarantee that machine is sinewound.

To get a sinusoidal **EMF** there are several ways to perform it. At open circuit, rotating magnets create a rotating magnetic field which generates induced voltages in the windings. So, one way is profiling the magnet surface to get a sinusoidal flux distribution in the air gap, using bonded Halbach magnets. As in this geometry the magnet has parallel magnetization, the profiling has to be done in the iron polar piece which increase even more the already expensive manufacturing process described in section 4.2.1.4. Another solution is using a *slotless* machine, however the torque density is very low due to the large air gap and it's not a good solution for this application. Other way is choose a winding that filters out the harmonics in the air gap flux distribution, manipulating the winding factors to maximize the first harmonic and eliminating the others. However to guarantee this is generally necessary a combination of slots/pole superior to 3, which is very high for this application. As the machine will be very saturated, is important to have few slots for the same diameter in order to have wider teeth and more area to the conductors. Taking this procedure not only the winding resistance is decreased due to higher slot fill gross, but also the tooth flux is higher because the tooth area is bigger. The only care needed is with machine weight because copper has the higher specific gravity, so put more copper turn machine heavier. A compromise is needed between the tooth width and slot area. The other thing to pay attention is the cogging torque because it has to be minimized. A very low cogging is obtained if the slot and pole numbers are chosen so that least common multiple (**L.C.M**) between them is large [2]. When the number of slots is close to the number of poles, lower **L.C.M** is obtained. This goes in the opposite direction of the previous discussion, where the desirable is use few slots. One solution can be exploring fractional slot winding mixed with skew and both

problems are solved: no cogging and sinusoidal **EMF** is granted. This will decrease **Eq1** and torque as discussed in section 4.1, but it's the consequence that has to be accepted in the design process.

As stated, is important to choose the adequate slots/pole combination, which has to fulfill the last requirements referred. Starting with the pole number is important to avail if the 8 poles used in first design can be maintained or not. Generally, higher the pole number, higher the magnets weight and cost increase, beyond the increase in the frequency and losses. But lower the pole number, higher the required stator yoke thickness to avoid saturation. Since this iron alloy is appropriate to deal with high saturation fields, the yoke thickness can be maintained at the expense of high **By**. The important is minimizing the number of poles to achieve a low **fsp** and have reduced losses. The 8 poles for the rated speed of 6000 **RPM** give a frequency of 400 Hz, which is exactly specified in VACODUR® 49 datasheet in terms of specific losses. As first attempt, the 8 poles can be assumed and the following step is checking the best slot number.

The main concern choosing the slots number is to maintain the greatest common divisor (**G.C.D**) of slot and pole number superior to one, otherwise problems with unbalanced magnetic pull will emerge [2], [15]. Analyzing some typical fractional slot combinations used, the choice passed to the famous Papst design which became very popular in the automotive industry. This combination has 12 slots and 8 poles, guaranteeing good symmetry properties because typically no unbalanced magnetic pull is verified. At same time a low **fsp** is obtained, which is good to reduce the iron losses in the rotor due to the slotting effects. However it has some problems with cogging torque, mainly when small air gaps are used. Since skew is already in mind to achieve sinusoidal **EMF**, is possible here manipulate the skew factor to turn the machine sinewound and at same time reducing the cogging.

Typically is stated that larger slots could be not so good in the cooling because is harder to extract the heat. However an intensive cooling strategy will be adopted so this isn't a big disadvantage.

4.2.3. Geometry

This point makes reference to the main options taken regarding the radial and axial cross section variables.

4.2.3.1. Radial Cross Section

The important variables are grouped by topics to indicate the main concerns in its definition. In appendix A.6 the presented variables for this geometry can be consulted.

- **RadSH**: The inner shaft radius was defined with the same dimensions of Agni 95R [16], as depicted in section 1.3.

- **Rad1:** Rotor radius is important regarding the moment of inertia. The goal is reducing it much more when compared to the values of Agni 95R. As discussed is section 2.3, the maximum rotor radius to consider is 3 cm.

- **Gap:** To attain the highest **Φ1** and maximize **Eq1** and the alignment torque, small air gap is needed independently of the other problems with cogging already discussed. Therefore as first

iteration in the design 0.5 mm was used. This air gap length is standard enough to guarantee a manufacturing process and rotor assembly without great problems and high costs.

- **BetaM:** To avoid significant pole-to-pole leakage, including zigzag flux, a special care was taken with the width of tooth tips or overhangs. It has been found that zigzag leakage flux has significant influence on the cogging torque with **PM** machines. As it varies with the rotor position, the procedure was minimizing it to a fixed one. The starting point take into account some formulations developed [38] and then **FEA** was taken to empirically verify the best measure of iron pole arc.

- **Inset:** Regarding the discussion taken in section 3.1.10, the goal was inset the magnets as deep as possible, only constrained by hub diameter. To hide the magnets from flux pulsation in the air gap, the necessary inset value was taken to obtain a hub with 3 cm as required.

- **MagWid:** Magnet width was defined in order to achieve a peak air gap flux density of 1.4 T at open circuit. This thumb rule was reached after many **FEA** performed in order to check the best value in the air gap to obtain **Bt** and **By** in the range discussed in section 4.2.1.2.

- **Rad3:** Stator outer radius was defined to start with a stator yoke of 5mm, as it was considered good for a first iteration. **FEA** gives more indications to support this decision. It was defined having in mind the length of frame thickness in order to achieve the total ideal diameter of 12cm.

- **Slot Type:** The choice passed for a type with straight shape, without round corners to increase the area available. The preferred was the square or flared type. In appendix A.2 can be seen an example with the design variables. All fillet radiuses in the picture were defined as zero in order to increase the slot area.

- **TWS:** Tooth width is very important due to saturation. The first attempt was giving it a high value and then checks with **FEA** the **Bt** obtained, as well as winding resistance and machine weight. This is the critical area to optimize the weight because hub, magnets and rotor iron were already defined in order to achieve the require peak air gap flux density and pole-to-pole leakage minimization. This variable and stator yoke must be modified until attain the required weight and performance.

- **SO:** Cogging torque is very dependent of slot opening. Typically higher **SO**, higher the cogging but it has to be confirmed using **FEA**. As a first approach, the lowest value possible was used, based on constructive limitations. It was found to be 1.5 mm. Moreover, the flux pulsation deep in the magnet is very dependent on this value, therefore is important to minimize it.

- **TGD:** The saturation in tooth tips is very important because when the machine is heavily loaded the tips have permeability close to the air value. This has the same effect of an open slot, which is bad for torque ripple. Only with **FEA** is possible to get the best value. As first approach

was used 1.5 mm for radial depth of tooth tip which is higher than usual. This was defined on the ground that is expected high saturation in tooth tips.

- **SOang:** Same considerations are taken here. Slot opening angle has to be linked to **TGD** in order to deal with saturation, mainly at **Ppeak**. Some judgment is needed using **FEA**.

- **SD:** Slot depth was mainly used to adjust the yoke thickness, if **Rad3** is in this maximum, or to adjust the slot area. It is not convenient to use big values as it increases the tooth reluctance, so was considered for starting the value of 1.6 cm.

4.2.3.2. Axial Cross Section

The procedure is equal to the last point. In appendix A.4 the variables presented for this geometry can be consulted.

- **Lstk:** As discussed in section 4.1, stack length was maximized taken into account the necessary space to the end windings and machine end space for cooling. The picture in appendix A.5 illustrates the relation between stack and end winding length.

- **FrLgth:** Frame axial length defines the end space of the machine and the total length without shaft. As first approach, it was considered that 1 cm for the end space is good enough. If an intensive cooling strategy is used there is no need to have a big area in the end space region to extract the heat. This turns easier to achieve the ideal length required.

- **FrThk:** Frame thickness only can be optimized when the cooling is being studied. For a first estimation of machine total weight, 7.5 mm was used.

- **CapThk:** End cap thickness has the standard value of 5 mm, however it has to be submitted to mechanical optimization.

4.2.4. Winding

This term is related to the totality of coils in the machine. As 3 phases are used, the phase windings are displaced by $2\pi/m$ (electrical rad) from each other around stator periphery. This defines a balanced winding, which is very important in this project. This guarantees that resistances and inductances in all 3 phases are equal. The **EMF** waveforms are balanced in the sense that they have the same waveshape and are displaced in time phase by 120º at the fundamental frequency. This winding will be supplied by balanced currents.

The arrangement of conductors in the winding is critical in determining the waveform of the **EMF**. The quantity of cooper is also important to minimize the losses. Regarding the choice made to the slot/pole combination, the best winding will be presented concerning also all manufacturing issues.

4.2.4.1. Winding Type

Once the goal is obtain a sinewound motor, it seems logical to design the winding to maximize the fundamental winding factor and minimize the winding factors for all the harmonics. A satisfactory practical arrangement is often to design for relatively small 5^{th} and 7^{th} harmonic winding factors, leaving the 3^{rd} harmonic to be suppressed by star connection. This connection was assumed in the project and higher order harmonics were ignored on the supposition that their magnitudes decrease when harmonic order increase.

On the other hand, **MMF** harmonics contribute to the differential leakage inductance. The combination of a winding with high **MMF** harmonics with a sinusoidally magnetized rotor will produce a sinusoidal **EMF** with high inductance. To calibrate this inductance and guarantee the required drive to the team, the number of turns **TC** and **Ppth** connections in the winding are used. If all coils in one phase are in series, each conductor carries the phase set point current (**Isp**). However, if they are connected in any series/parallel combination, with **Ppth**, the conductor current will be Isp/P_{pth}.

The first step was chose between concentrated or distributed winding. Concentrated winding is very attractive by cost reasons but has also some drawbacks. To obtain a high winding factor and lower torque ripple is sometimes necessary an irregular distribution of teeth [2]. For a first design iteration is easier to start with a simpler configuration and avoid irregular teeth as some of them become thinner and saturate easier. Moreover, after contact with a winding company in Portugal, *Fernando A. Lemos*, that hypothesis was cut off as they don't manufacture this kind of winding. The choice passed to use a fractional slot overlapping winding, if possible with double layer. It means that every slot contains two coilsides, typically one coilside in the bottom layer and the other in the top. In practice is important by manufacturing reasons to have equal number of coilsides in every slot. Double layer windings are a priority to use since they have better properties such as shorter end windings and more sinusoidal **EMF**, comparing to single layer. Using fractional slot is difficult to get sinusoidal **EMF** due to the few slots used, however double layer guarantees the double number of turns in each slot which increase the **EMF**. In terms of manufacturing process a phase divider using Nomex® can be performed and is important to implement due to mechanical reasons. In appendix A.8 is possible to see a slot sketch with a phase divider.

There were already defined 12 slots and 8 poles. Therefore the number of slots/pole/phase is equal to 0.5, which means that is necessary to define 4 poles in the winding facing the 8 poles in the rotor. As first attempt, it's considered coils per pole (**CPP**) equal to 1, as usual in fractional slot type. Having 4 poles in the winding, it means that 8 coilsides per phase are present, to distribute along 12 slots. So for 3 phases it gives 24 coilsides, which is exactly the double of slots number. It means that a double layered winding was guaranteed. As it's not possible to have a non-overlapping one, the coils **Sp** chosen is equal to 2 forming an overlapping winding. However is important to point that **Sp** is higher than pole pitch, which means that coils are not short-pitched or chorded. As consequence, no filtering effect will happen in the harmonic content of air gap flux density distribution. This is not necessary a problem because it was already discussed that skewing the stator is an acceptable solution regarding the design options taken.

4.2.4.2. Slot Fill Gross

Slot fill gross is a measure of the amount of copper in the slots of an electrical machine. Generally speaking, the higher slot fill gross, the higher the efficiency. As it's not easy to achieve a high slot fill in manufacturing, this is an important parameter that somehow links the level of manufacturing difficulty with the machine performance. Formulations about the typical slot fills can be consulted [54].

The values of slot fill gross with hand wound are between 45% to 50%. Larger values are possible only for segmented stator which was not considered in this design. Assuming a wound made with a machine, it's reasonable to assume a slot fill gross of 54%, leaving 6% for impregnation.

The conductors positioning in the slot make difference in terms of slot leakage inductance. If the conductors are crowded towards the bottom of the slot, the slot-leakage inductance is increased but if they are near the slot opening the slot leakage inductance is decreased. This is an important manufacturing issue to take into account.

Once the slot dimensions and slot fill were fixed, **TC** and number of strands (**Nsh**) were the manipulated variables to change the phase resistance and one strand diameter respectively.

4.2.4.3. All Phases Connection

The following picture illustrates the winding connection for all 3 phases. It gives a visual help for the considerations taken above. Using this layout is possible to define the **CLV** which states the positions of all coils and number of conductors in all phases. This is very important when the winding is defined using **FEA**.

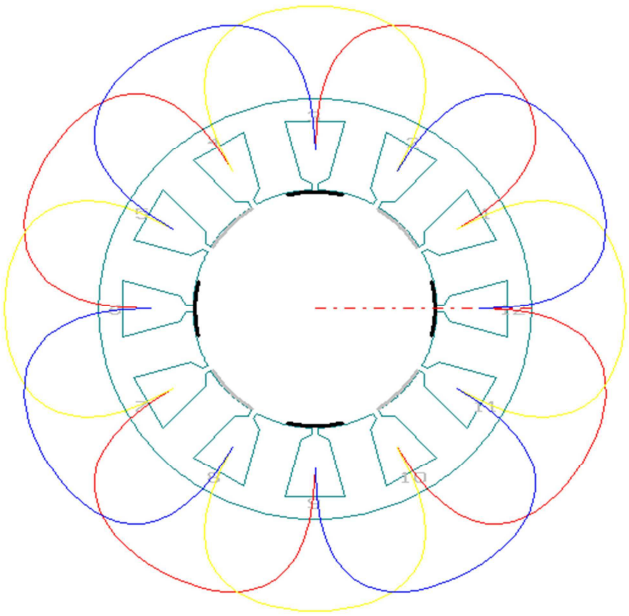

Figure 4.2 – PC-BDC winding: All phase's layout (RYB).

4.2.4.4. Winding MMF

The following image displays the distribution of air gap **MMF** around the rotor for all the 3 phases together. It's constructed under the assumptions that steel is infinitely permeable and the stator windings are represented by current filaments on a smooth bore cylinder at angles corresponding to the centre lines of their respective slots. It's also showed the 1st electrical harmonic of **MMF** distribution, both related to an electrical angle of 25º.

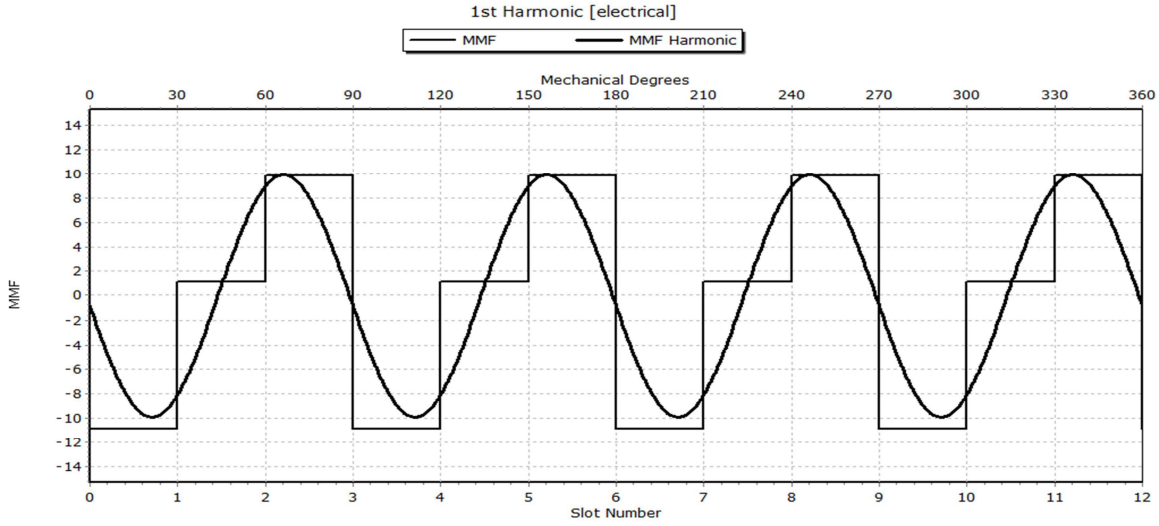

Figure 4.3 – PC-BDC winding: Total MMF.

The armature reaction flux density in the air gap is proportional to this **MMF**. As can be seen it's far from sinusoidal. Even with a sinusoidal flux density distribution due to the magnets in the air gap, the sum will not be sinusoidal which give arise to a differential leakage inductance. The *squarewave* **MMF** has 4 cycles spanning 360º, which means 8 poles distribution like defined.

4.2.4.5. MMF Harmonics

The next picture shows the Fourier analysis of previous **MMF** distribution.

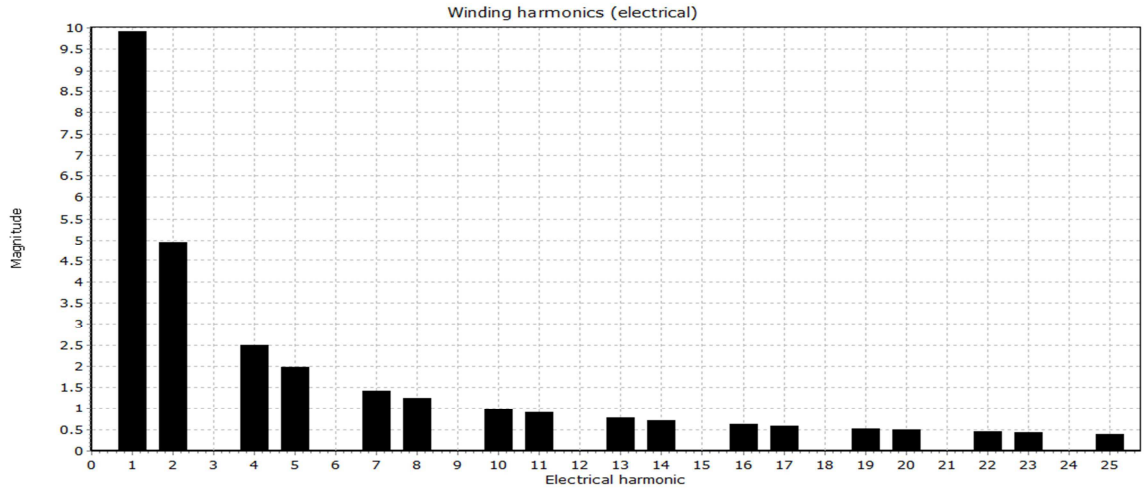

Figure 4.4 – PC-BDC winding: MMF Fourier analysis.

The individual harmonic components are multiplied by a function to account for the modulating effect of the slot openings [8]. This spectrum can be thought of as a filter which modulates the harmonics in the air gap flux distribution. In fact the winding factors chart can help more on this and take more conclusions about the waveshape of **EMF**. All harmonics are present except the triplen which is very characteristic of fractional slot windings and states the analysis made on last section. Moreover, in this 12/8 machine, the lowest harmonic is also the working harmonic, which means the 1st electrical harmonic or the 4th mechanical harmonic. This can be seen in the spectrum of mechanical harmonics where the first to appear is the 4th one. It has advantages in electrical point of view because when sub-harmonics tend to appear they increase the differential leakage inductance further. This is a good property of Papst design.

4.2.4.6. Winding Factors

The next picture shows the winding factors as a bar chart. They are calculated directly from the Fourier analysis of the winding distribution, normalized to the Fourier components of a full pitch unskewed winding.

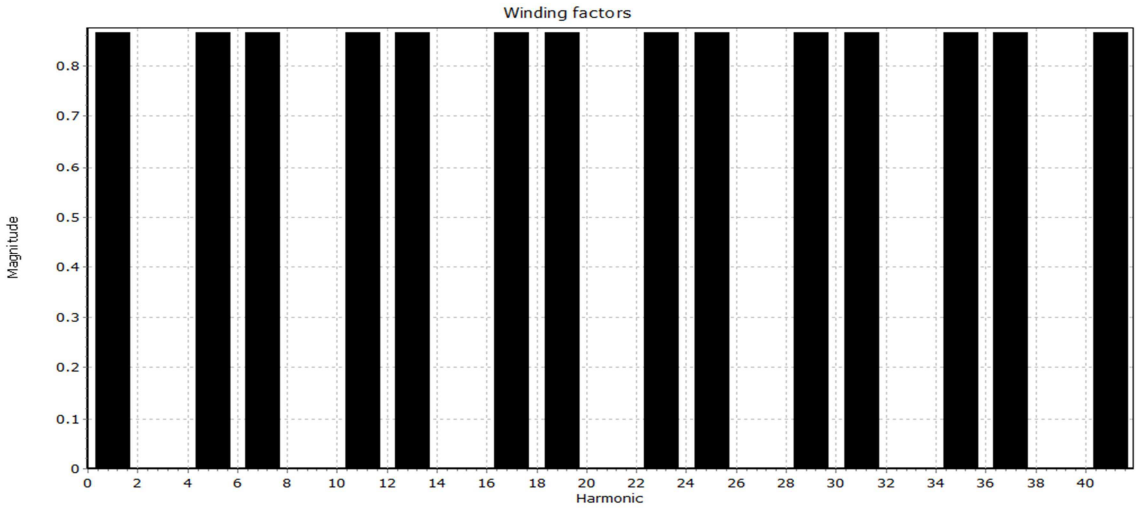

Figure 4.5 – PC-BDC winding: Unskewed winding factors.

All the winding factors have the same value, which is 0.866. This is not too high and shows one of the disadvantages of using Papst design. It's never possible to obtain a higher value than this independently of coil **Sp** used. Moreover, the filtering effect is too few as all the harmonics have the same winding factor, except the triplen. This design has only the capability to filter the 3rd harmonic however it was not necessary because the winding is connected in star. When it's the case, the 3rd harmonic components of two phases are in phase and in line-line connection they are subtracted from one another, resulting in the complete elimination of 3rd line-line **EMF** harmonic. The full pitch winding used practically don't filter the most troublesome 5th and 7th harmonics of air gap flux density. These results proof that changes are needed to obtain a sinusoidal **EMF**, passing for stator skew to modify the winding factors.

4.2.4.7. Görges Diagram

The next image shows the Görges diagram for 1st **EMF** harmonic.

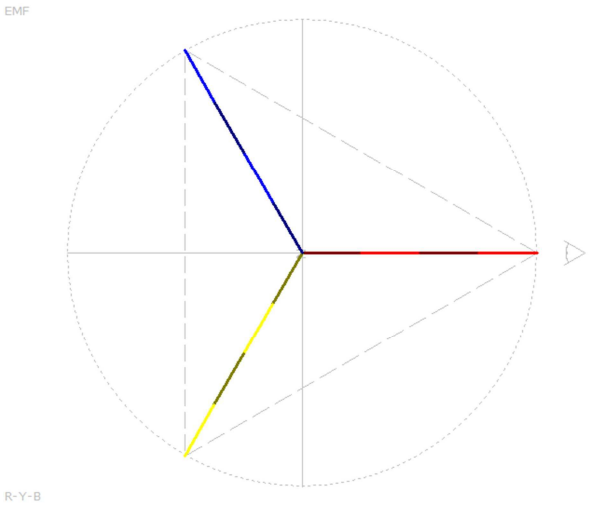

Figure 4.6 – PC-BDC winding: Görges diagram for 1st EMF harmonic.

This diagram shows the **EMF** vectors of the individual coils and how they add up to produce the total **EMF** per phase. It permits to check the phase sequence and adjust the necessary offset, which means the number of slot pitches between start of phase 1 and 2. The phase sequence is correct when these phasors are viewed as rotating anti clockwise in the order **RYB**. This is only conventional, and guarantees that rotor rotate anti clockwise due to the Lorentz forces developed. It can't be seen as something that is right or wrong.

Analyzing the diagram is clear that phase sequence is correct, as it was defined. Also when the phase sequence is correct, the negative sequence and zero sequence voltages should be zero. This is verified with the following results:

$$\begin{cases} V_1 = 41.57\, e^{j\,0}\ V \\ V_2 = 0\, e^{j\,137.73}\ V \\ V_0 = 0\, e^{j\,36.03}\ V \end{cases} \qquad (\mathbf{4.5})$$

This state that the sum of the 3 phase **EMF**'s is zero, in other words there is no zero sequence around the wye. This is important because with a delta connection a large current could be attained. The suppression of 3rd harmonic by the winding factor already exposed in last section contributes to this result. Moreover, is possible to check that all **EMF** phasors are spaced by 120 electric degrees and the centroid lines describe an equilateral triangle which means that perfectly balanced 3 phases **EMF**'s are obtained.

4.2.4.8. Radial Forces

Radial forces are undesirable attractive forces between the stator and the rotor while tangential forces act on the rotor to produce torque. As the rotor rotates the force varies as a result of the interaction between the magnets and the teeth. It was necessary for mechanical reasons to verify if

the winding give arise to unbalanced magnetic pull. Once this rotor has no eccentricity, is expected that such problem don't appear. Moreover, the **G.C.D** of slot and pole number is superior to one which is also a good indication. The following picture depicts the forces development for one arbitrary rotor position:

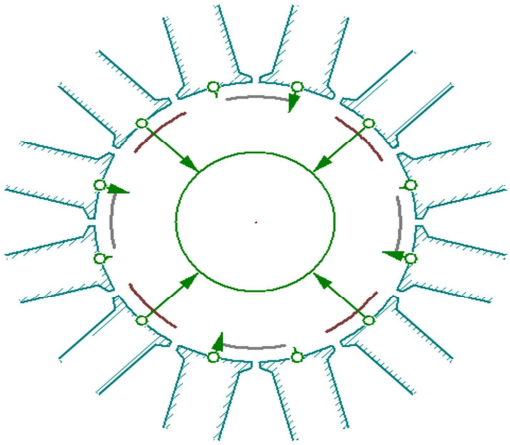

Figure 4.7 – PC-BDC results: Radial forces.

For this slot/pole combination the net force on the rotor is zero, so there is no unbalanced magnetic pull. The radial magnetic force density is proportional to the square of the normal component of **Bgap**. The tangential is typically neglected, since the permeability of the iron is much higher than air. As can be seen later using **FEA**, the flux lines leave rotor surface almost perpendicularly. More can be seen to avoid the winding asymmetry that originates unbalanced pull [2].

4.2.4.9. Acoustic Noise

Magnetic noise results from magnetic forces that make the stator vibrate. The forces that cause this noise are mostly the radial ones [2], already seen in the last section. To better avail this effect has also interest the magnitude squared of **MMF** harmonics. The following figure shows it.

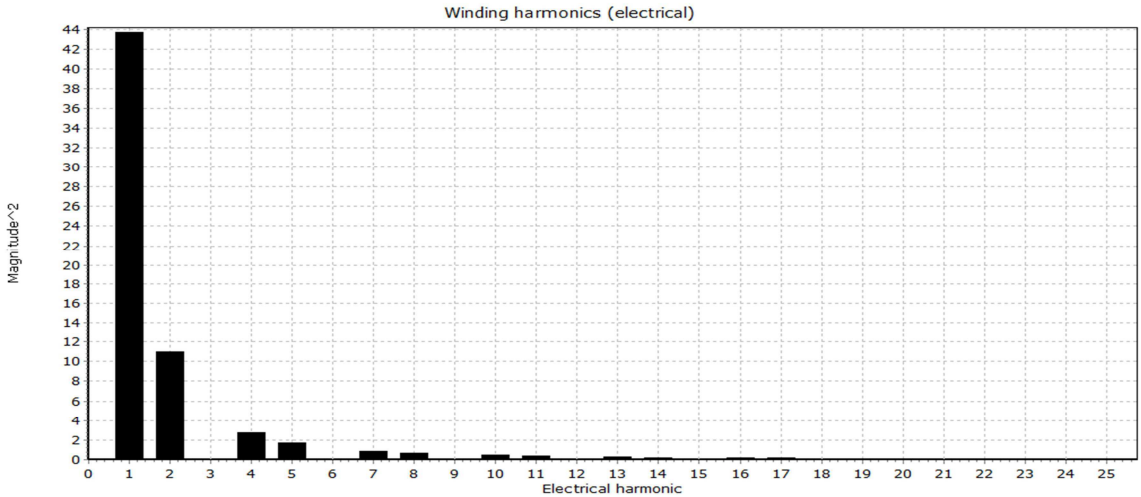

Figure 4.8 – PC-BDC winding: MMF harmonic squared.

It can be seen that there is some contribution to acoustic noise from 2nd, 4th, 5th harmonics. It could be significant in other applications but since this machine is to a race car, no special worry should be taken on this.

4.2.5. Losses

This point will present the relevant results and considerations about losses calculations, in all types to consider. Copper losses calculation are based on Joule law and iron losses on Steinmetz equations as already stated in section 3.1.8. There are in continuously development new models, like ArcelorMittal® iron loss model, which can be consulted [57].

4.2.5.1. Iron Losses

Regarding the considerations taken in section 4.2.1.2 about the iron manufacturing, it was decided to use in this project **XFe** equal to 1. In fact, high values are common to compensate uncertainties that exist in steels data, especially when the values of flux density or frequency are different from those at which the steel data was measured. However it's not the case, since the data for specific loss at rated frequency is available and the manufacturing process of Vacuumschmelze don't make significant changes in the cobalt iron properties. As explained, this fact was important in the final decision for the iron to be used. Moreover, **Bt** and **By** were scaled using the ratio of the "air gap voltage" to the open circuit **EMF**, which permits to give an overestimation on the losses computed by **PC-BDC**. Further checking is necessary to compare these results with elements table results using **PC-FEA**.

4.2.5.2. Windage & Friction Losses

This two loss components were join together. To calculate the friction losses low friction bearings were considered, namely SKF E2. The power loss curve can be consulted [63]. These bearings with synthetic base oil and lithium thickener are well adapted to applications where the weight is important. Typical examples include electric motors up to 37 kW, which is near from the maximum power required.

To calculate windage losses a script in Microsoft® Excel using visual basic (**VBA**) was made to compute it for several speeds, based on Saari formulations [6]. The following table resumes both losses calculated.

Rotation (RPM)	Friction Loss (W)	Windage Loss (W)	Total
500	2	0.0023	4.0023
1000	3	0.011	6.011
2000	4	0.0582	8.0582
3000	5	0.154	10.154
4000	6	0.31	12.31
5000	7	0.53	14.53
6000	8	0.8	16.8
7000	9	1.16	19.16
8000	10	1.62	21.62
9000	11	2.18	24.18

Table 4.1 – Windage and friction losses.

To make the calculations for other speeds, the following quadratic interpolation was used. In the equation the exponent **NWFT** is always equal to 1.

$$W_{wf} = W_{f0} * \left(\frac{RPM1}{RPM0}\right)^{(NWFT+1)} \qquad (\mathbf{4.6})$$

4.2.5.3. Magnet Losses

For interior magnet machines all the eddy current calculations were based on a circuit model which uses the sub-transient time constant obtained from an analytical field solution [8]. This model was used for loss component due to interaction between current time harmonics and winding space harmonics, as well as flux pulsation component caused by permeance harmonics. The flux modulation was calculated by *i-psi* **GoFER** and the relevant harmonics were used to compute the magnet losses with **PC-BDC.** All the analytical calculations made consider that **NdFeB** has 1.2% of conductivity relative to copper.

The transient solver results using **PC-FEA** were used to conclude about the number of magnet segments to apply. It was only necessary to check if eddy currents are resistance limited because the transient solver calculations only make sense in this case. It was developed a script in Microsoft® Excel using **VBA** to compute for each rotation speed the **fsp** and skin depth (**λ**). The following table shows the results.

Rotation (RPM)	FSP (Hz)	λ (mm)
500	100	60.17
1000	200	42.55
2000	400	30.08
3000	600	24.56
4000	800	21.27
5000	1000	19.02
6000	1200	17.37
7000	1400	16.08
8000	1600	15.04
9000	1800	14.18

Table 4.2 – Skin depth and slotting passing frequency.

Once the magnet dimensions are known is easy to compare the highest value of skin depth with half of the biggest magnet dimension. It was seen that skin depth is much higher than that magnet dimension, therefore confidence can be obtained with transient solver results. This means that any eddy currents in the magnets will be resistance limited.

Magnets are often divided into blocks which are isolated from one another electrically. They can be segmented in circumferential direction or in axial direction in order to keep the individual blocks small due to manufacturing reasons. However in the project can be explored this to attain other objective, namely to break up the eddy current paths into smaller loops which increases the effective resistance presented to the eddy currents. As already stated, if the eddy currents are resistance limited, this will decrease the associated power loss. The segmentation effects fall outside the scope of **2D** analysis, so for rapid calculation using **PC-BDC** approximate methods were used [8].

4.2.5.4. Proximity Losses

Proximity losses were not considered in this project. The main concept is that current in one conductor is influenced by the current flowing in neighboring conductors. This result in an effective increase of AC resistance and copper losses, besides that gives local areas with higher current density. As this machine will not work at high speeds and the wound can be made in order to minimize these losses, this component was neglected.

4.3. Open Circuit Calculations

Once the main design options and variables were decided, a simple calculation can be used to conclude about the following steps that have to be done in the design. The open circuit calculation is a way to give the first models calibration, adjusting **PC-BDC** results with **PC-FEA** by means of **Match FE**.

4.3.1. Open Circuit GoFER's

The basis of **GoFER** routines used to calibrate the analytical calculations was depicted in section 3.2.4. Some considerations will be done regarding the configurations used because it's important for final **FEA** result.

The entire solution was oriented so that *x-axis* coincides with a stator slot centre line. The starting point of solution domain is always referred to this position. The area covered by **FEA** solution, or solution domain, was defined as the highest common factor between the number of slots and the number of poles. This has the aim of minimizing the solution time, however it's important to check if the winding shares the same symmetry due to slot/pole combination. Since Papst design has perfectly symmetry, there is no problem on this and **FEA** solution is represented by 3 slots and 2 poles.

Regarding the rotor configurations, the shaft was not included in calculations because a non-magnetic shaft is used. The number of layers used in the air gap to compute torque was 4. This is the regular value for small air gap machines like this.

A smaller solver tolerance was used to make the solution more precise, independently of computation time. The maximum number of iterations for Newton-Raphson method was defined as 30 on the grounds that in this range indicates insufficient smoothness in steel data, as discussed in section 3.2.1.

The method of interpolation used to iron **BH** curve is B interpolation [34]. **PC-FEA** then made linear interpolation between these points.

4.3.1.1. Bgap GoFER

This **GoFER** calculates **Bgap** for a fixed rotor position, defined in this case to be aligned with *x-axis*. The following picture shows the post-processor result.

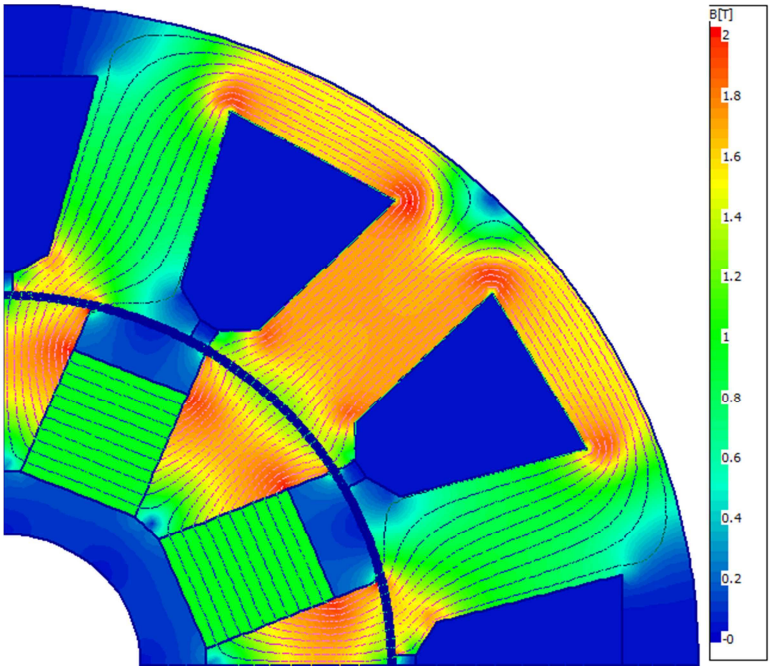

Figure 4.9 – PC-FEA post processor: Bgap GoFER.

It's possible to verify that flux density leaves the rotor polar piece almost perpendicularly, which states that the main field component is radial and the tangential can be neglected. Moreover, the rotor iron, tooth and stator yoke have values according to the range discussed in section 4.2.1.2, close to 1.7 T. This indicates that magnet, tooth and stator yoke dimensions are good to attain the design objectives. The next picture compares the **Bgap** over 180 electrical degrees obtained using **PC-FEA** and **PC-BDC** by means of **Match FE**.

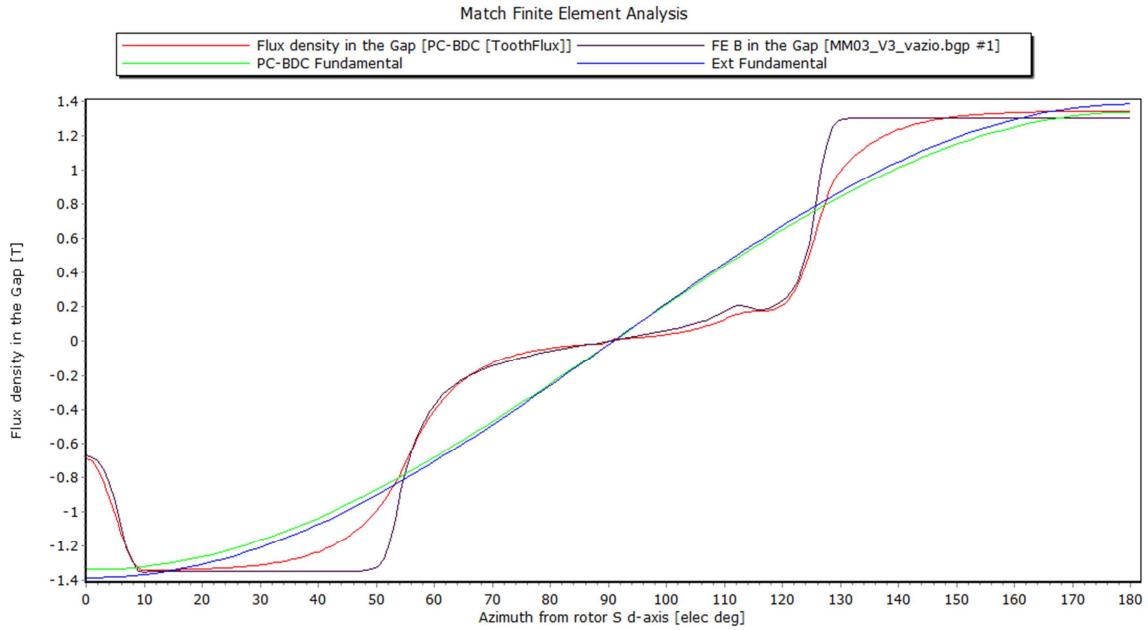

Figure 4.10 – Bgap Match FE: Red - Bgap (PC-BDC); Black - Bgap (PC-FEA); Green - PC-BDC fundamental; Blue - PC-FEA fundamental.

Typically the static flux distribution **Bgap** returned by the appropriate **GoFER** is modulated by slot openings. This give arise for some problems when it's compared with **Bgap** calculated under BLV method because the slot openings are smoothed out by the theory of Carter coefficient. However in this project there is no such problem as the **EMF** is calculated under the tooth flux method.

The **FEA** result indicates a peak value of air gap flux density in the order of 1.35T, which is close to the value discussed in section 4.2.3.1, giving good indications about **MagWid** used. The calculations performed with **PC-BDC** are adjusted to **PC-FEA** results by means of the following X factors depicted in section 3.1.2: **XBrT**, **XBetaM**, **XFringe**. **XTTarc** is adjusted by means of analyzing figure 4.9. As the flux is the first thing to be calculated, is possible to see that all the flux from rotor polar piece finds its way into the stator tooth so it means that **XTTarc** is 1. Figure 4.10 shows good agreement between both distributions as well as the fundamental components, indicating that calibration process was well succeed.

The slot opening used is vanishing small but nevertheless a significant modulation in **Bgap** is introduced, as can be seen in the black curve. The **PC-BDC** results were adjusted to reflect that modulation by means of other X factors.

4.3.1.2. Btooth GoFER

As referred in section 3.2.4, this **GoFER** is very important to determine the **Bt** waveform and the phase **EMF** because **PC-BDC** calculations are based on tooth flux method. The **PC-FEA** post processor result is the same that exposed in figure 4.9. The variation of **Bt** and **By** over 180 electrical degrees is exposed in the following graph.

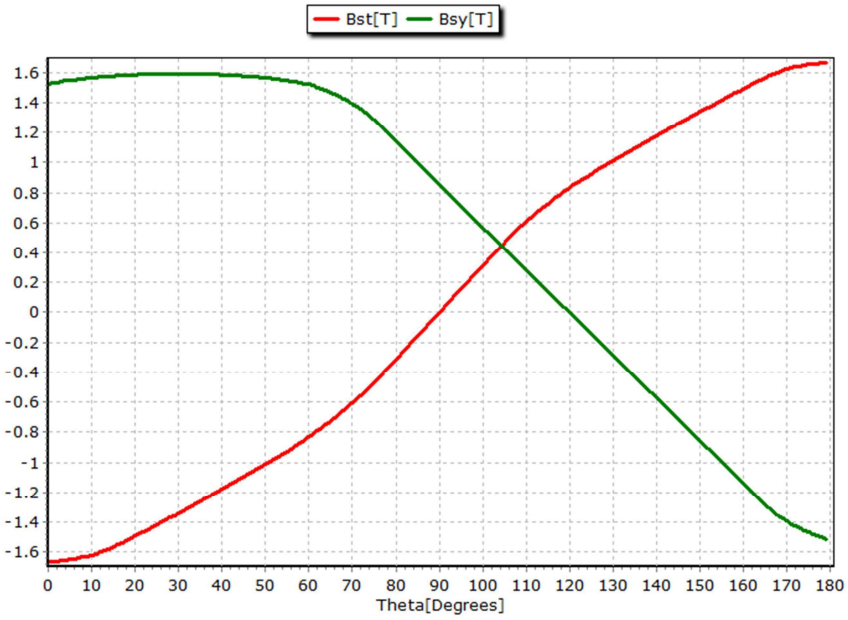

Figure 4.11 – PC-FEA post processor: Bt and By over 180 electrical degrees.

Is possible to see that **Bt** waveform is more or less sinusoidal, while **By** has a flat top shape. The maximum value of **Bt** is 1.72 T and **By** is 1.65 T, confirming the analysis of last section.

Regarding the discussion about slot opening effects the **Btooth GoFER** has no such problem. As the rotor rotates, the overall flux level does vary at **fsp** because the total permeance of the magnetic circuit is modulated at this frequency. Usually it's only when the tooth flux waveform is differentiated that slot ripple appears and is often too small to be clearly discernible in the tooth flux itself. This explains why the slotting effect is apparent in the **Bgap** flux distribution and in tooth-flux **EMF**, even though it may not be immediately obvious in the **Btooth** waveform. The following images regarding the **Match FE** comparison between **PC-BDC** and **PC-FEA** calculations illustrates this principle.

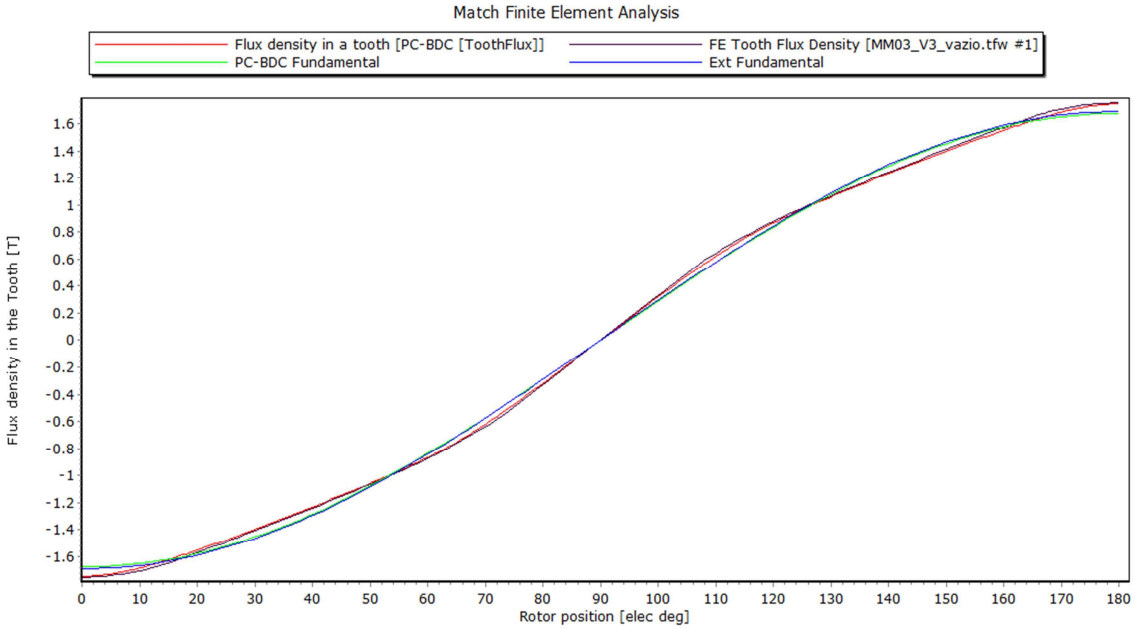

Figure 4.12 - Btooth Match FE: Red - Bt (PC-BDC); Black - Bt (PC-FEA); Green - PC-BDC fundamental; Blue - PC-FEA fundamental.

As stated, in this waveform the slotting effect is not seen. The waveshape is uniform and it's possible to check the good agreement between both results, after adjusted the following X factors: **XBtpk**, **XTw**. Others were also used to adjust the flux density values computed by **PC-BDC**, namely in the stator and rotor yoke. The factor **XBtpk** was adjusted based on the analysis of figure 4.9. The objective of this parameter is adjust the effective tooth arc used for "flux collection" at stator surface, in such way that will define the correct integration limits to apply the Simpsons rule. As observed on the figure, more or less 98% of the tooth head collect the flux lines from rotor polar piece. This defines the parameter and states that practically all the tooth arc is used to collect flux and produce **EMF**. These adjustments give also very good agreement in fundamental components, less than 1% of difference.

The next picture shows the single turn/tooth **EMF**, which represents the generated **EMF** waveform by differentiating **Bt** waveform. Is possible to check that fundamental components are identical and so are the areas under the curves and the rectified mean values. The **FEA** waveform contains higher order harmonics. These will appear in the phase **EMF** waveform of the machine. In other fractional slot motors some of these harmonics are reduced or eliminated when the tooth **EMF** waveforms are combined into the phase **EMF** waveform.

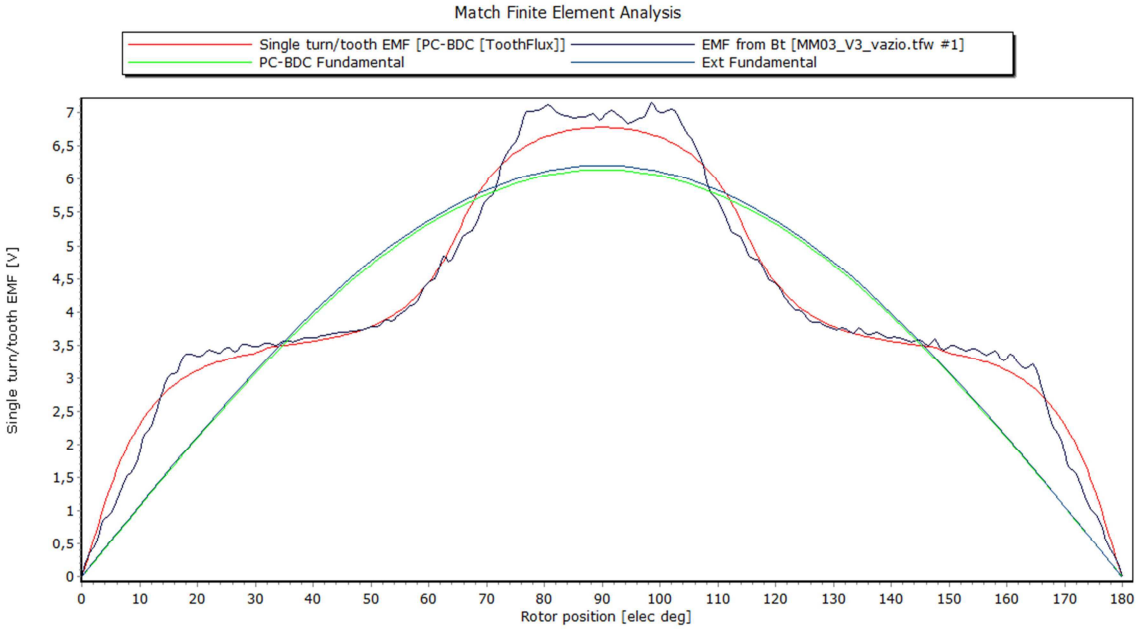

Figure 4.13 – Single turn/tooth EMF Match FE: Red - EMF (PC-BDC); Black - EMF (PC-FEA); Green - PC-BDC fundamental; Blue - PC-FEA fundamental.

The X factors determined before give also good adjustment here, which was a good indication in the design process. The operation of **Btooth GoFER** is similar to the action of this search coil wound around a single tooth. The addition of tooth fluxes or tooth **EMFs** is a straightforward summation of waveforms in the correct phase relationships and no winding factors are involved. This logic permits to obtain the phase **EMF**, exposed in the next picture.

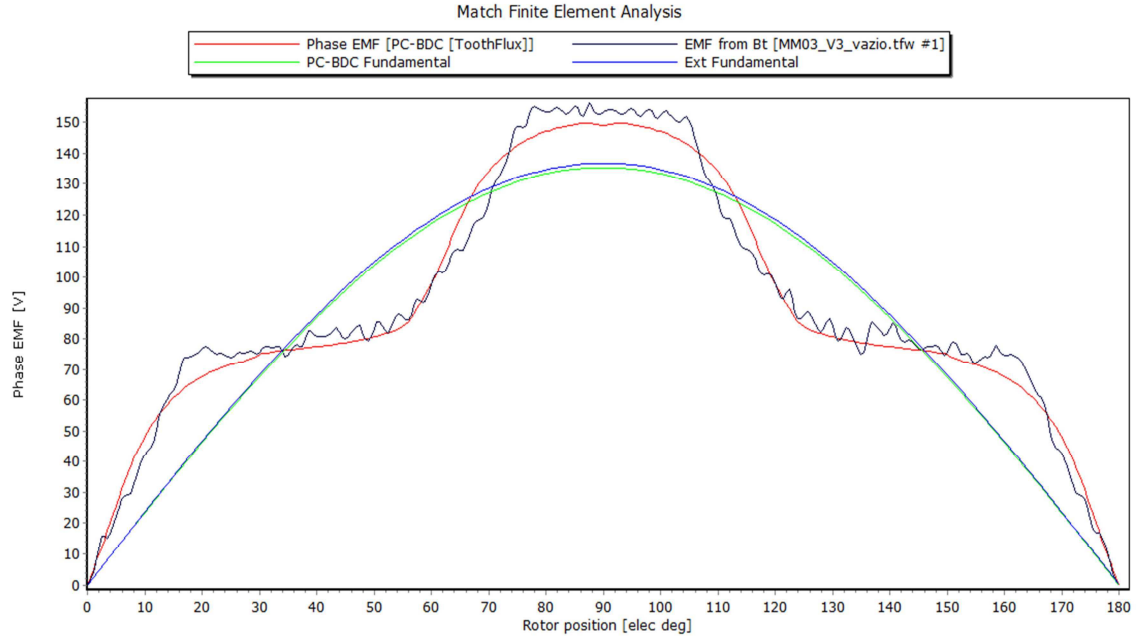

Figure 4.14 – Phase EMF Match FE: Red - EMF (PC-BDC); Black - EMF (PC-FEA); Green - PC-BDC fundamental; Blue - PC-FEA fundamental.

The higher order harmonics appear also in phase **EMF** computed by **PC-FEA** as analyzed before. Same X factors were used here and the good agreement between **PC-FEA** and **PC-BDC** results are clear, even in the fundamental components, with a difference in the range of 1%.

This result shows that phase **EMF** is far from be sinusoidal, which confirm the analyses stated in section 4.2.4.1. Moreover, the two possible methods to check the phase **EMF** agree: this conclusion is taken with the operation of **Btooth GoFER** and the discussion in section 4.2.4.1 was based on winding factors. This means that a full pitch search coil gives an **EMF** waveform that is almost a replica of **Bgap** distribution, apart from the effect of permeance harmonics. The **EMF** of the entire winding can be derived from this coil **EMF**, but by means of the classical winding factors as stated also in section 4.2.4.6.

The results obtained for line-line **EMF** can give more indications.

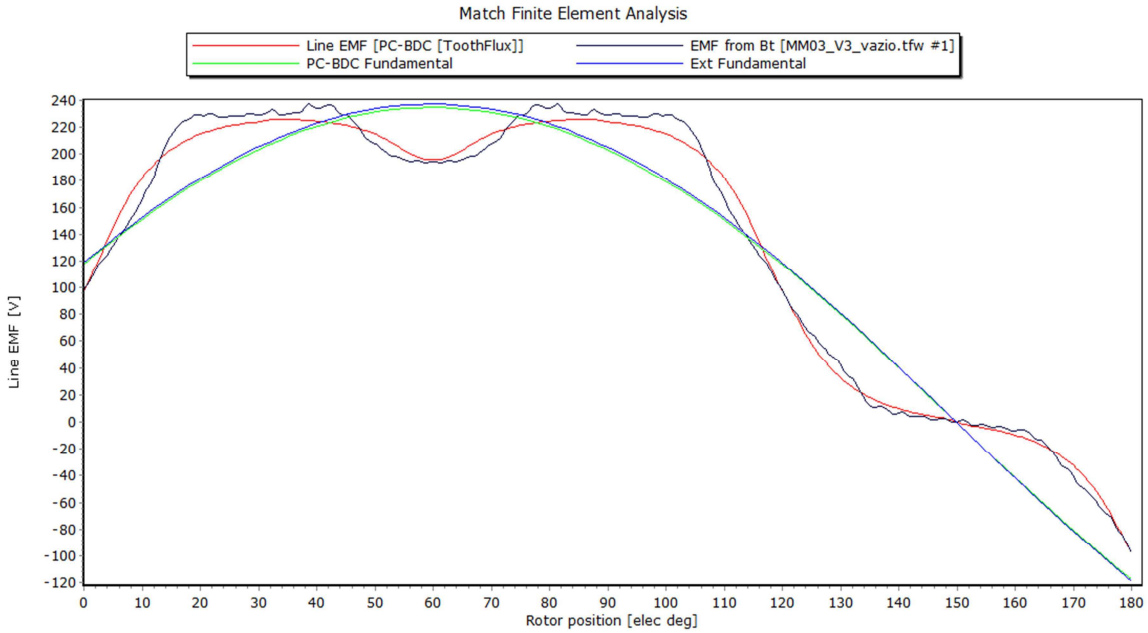

Figure 4.15 – Line-Line EMF Match FE: Red - EMF (PC-BDC); Black - EMF (PC-FEA); Green - PC-BDC fundamental; Blue - PC-FEA fundamental.

About the agreement between waveforms and its fundamental components the conclusions are the same. This line-line **EMF** is near from a flat top waveform which may be bad for torque ripple. The phenomenon is principally due to variation of permeance in the air gap and the interaction between the air gap flux and the space harmonics in the **MMF**. Its reduction is important to improve the machine life time and give better behavior against noise and vibrations. It is considered an acceptable value for this application if less than 5% of peak torque is achieved. This departs on the basis that car inertia will filter much of this effects and this application doesn't require a precise positioning control like in servomotors for instance.

Analyzing *i-psi* loop is possible to have a better idea about the flux linkage in open circuit.

4.3.1.3. I-PSI Loop Unskewed GoFER

The *i-psi* **GoFER** is designed for on load conditions, but it can be run with zero current. In that case it returns the flux linkage of an entire phase winding. The flux linkage is calculated from **A** values averaged over each slot, as depicted in section 3.2. This method helps to make the resulting waveforms smoother by removing numerical "noise".

Following picture reproduces *i-psi* loop obtained with **PC-FEA**. As the models are already calibrated and **PC-BDC** results are almost the same when comparing to **PC-FEA**, only the **FEA** computation will be exposed.

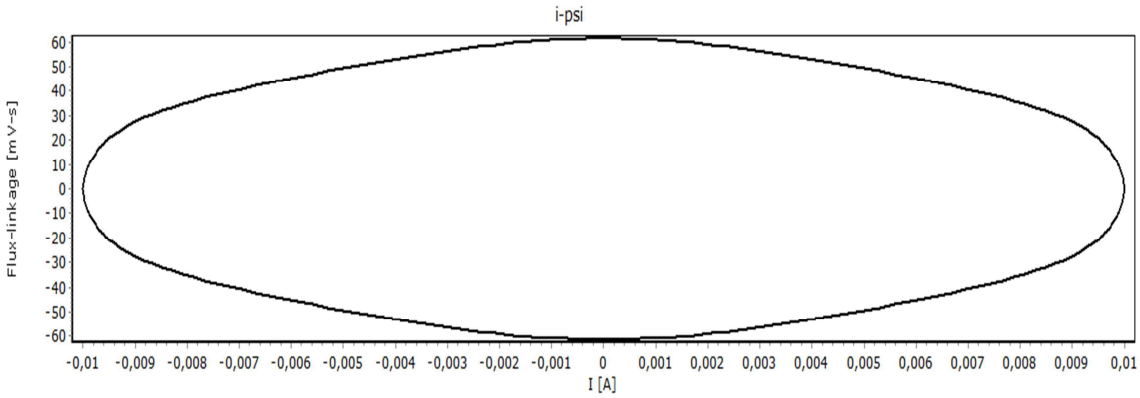

Figure 4.16 – I-PSI Loop Match FE: Black - I-PSI Loop (PC-FEA).

As can be seen, the values used for the current are very small. It's not possible to run it with zero current but this is a good approach for an open circuit calculation. The diagram is not perfectly elliptical which means that flux linkage has some harmonic content while the current is perfectly sinusoidal. The analysis of flux linkage will give more details.

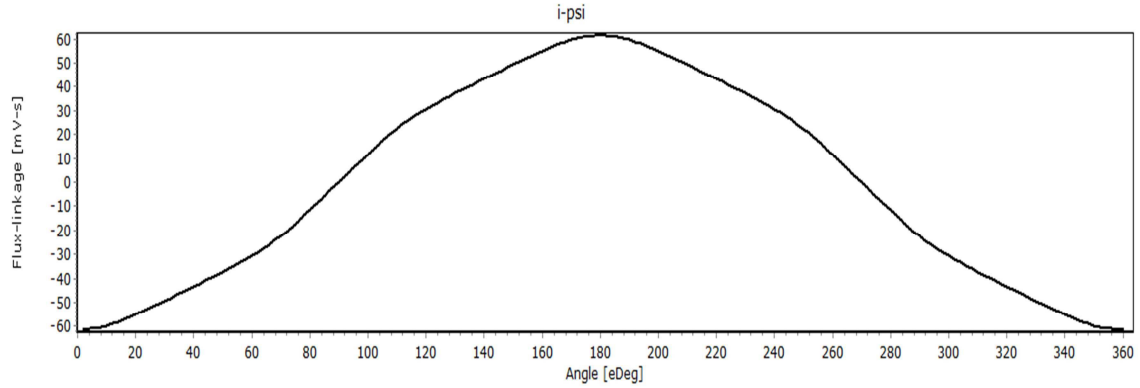

Figure 4.17 – Flux linkage Match FE: Black - Flux linkage (PC-FEA).

In fact flux linkage is not as sinusoidal as the current which justifies *i-psi* loop waveshape. Moreover, for the first 180 electrical degrees the evolution is very close to the **Btooth** waveform depicted in section 4.3.1.2. This give very good indication for the calculations establish until this phase. The cogging torque **GoFER** could give more idea about the skewing effects.

4.3.1.4. Cogging Torque GoFER

This calculation is susceptible to errors if particular care isn't taken with the mesh, rotor steps and convergence tolerance, as described in section 3.2.4. To improve the results, four different methods of torque calculation were applied: co-energy, **MST**, **VW**, **MSI**. System co-energy is evaluated at each rotor step and the differences are divided by Δθ to give instantaneous torque; **MST** is evaluated at two different radiuses in the air gap and averaged; **VW** is evaluated in the air gap region; **MSI** is applied in the air gap [32]. The **DC** components from the cogging torque waveform were removed.

Using **Match FE** was possible to skew the cogging torque in order to find the skew angle that eliminates it. The following pictures illustrate the procedure while the harmonic content of the cogging, unskewed and skewed is left, respectively, in the appendix C.1 and C.2.

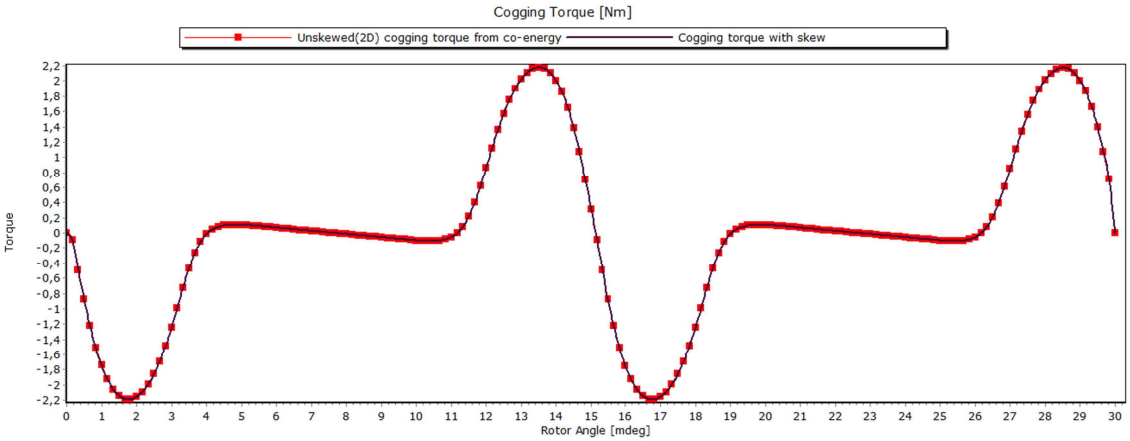

Figure 4.18 – Cogging Match FE: Black - Cogging (skew=0); Red - Unskewed (PC-FEA).

All the different torque methods gave the same result for the cogging in terms of waveshape. The only difference is in the peak value and the biggest difference is in the order of 2%. This means that result is reliable and mesh refinement is good. This torque method is based on co-energy and the value is 4.37 N.m peak-to-peak, even with a so small **SO**. It's a high value, typical when Papst design is used. This indicates that skewing is needed to bring the value to zero. The next picture illustrates it.

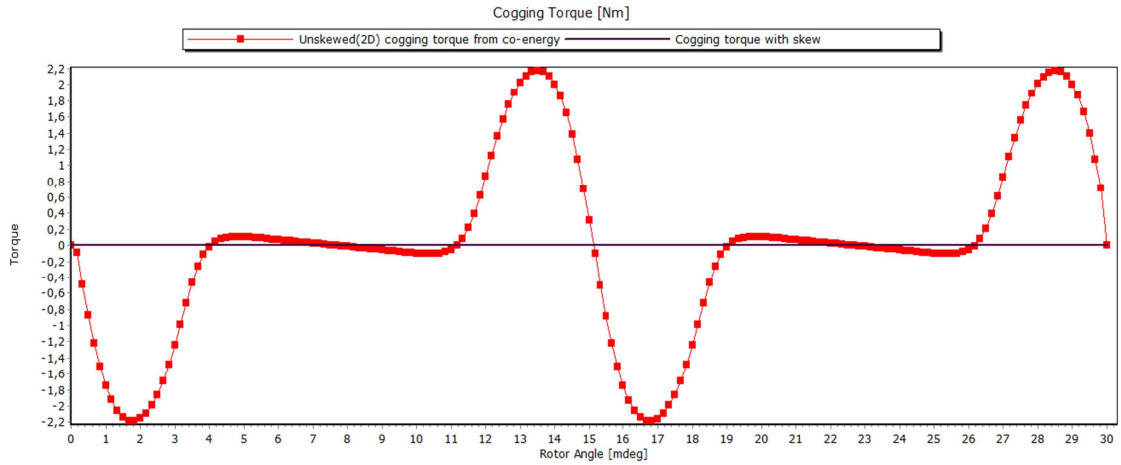

Figure 4.19 – Cogging Match FE: Black - Cogging (skew=0.5); Red - Unskewed (PC-FEA).

When the skew is equal to 0.5, which means 50% of slot pitch, the cogging torque is reduced to zero and the same happens naturally with the harmonic content. When skew is equal to 1 the cogging torque is also zero. However the lowest skew angle must be chosen in order to give the highest value possible for **Ks1** and obtain the highest torque with less current, as analyzed in section 4.1. This value was used in all calculations to guarantee a sinewound machine. The mean to calculate the true skew angle can be consulted [30].

4.4. On Load Calculations

In this project this kind of performance was based in **PC-BDC** static design. This means that calculations are for a single operating point at a fixed temperature. As the most critical operating point of the machine is in **Ppeak**, this single point is assumed to be at 42.5 kW @ 6000 **RPM**. The value assumed for battery voltage (**Vs**) is 520 V, a little bit below the value exposed in section 1.3 to give some margin to internal voltage drops. For a first estimation in the calculations, it was considered that all components were at ambient temperature of 40ºC. According to flowchart depicted in section 3.4, is then necessary a co-simulation to adjust the correct temperatures in transient operation. This issue will be approached later.

In the static design the current is forced with an ideal waveform. As requirement is to attain a *sinewave* drive, a 3-phase balanced *sinewave* current system is forced in the armature. **PC-BDC** uses the phasor diagram to calculate the required voltage at machine terminals, when the current is specified by **Isp** and **γ**. The maximum voltage available from the inverter is represented as a circle in the phasor diagram, when voltage and current locus is selected. The mode of operation selected to determine this maximum voltage was a six step in 180º electrical. This means that every transistor is switched on for 180º electrical and there is no chopping. Therefore the current waveform is the natural result of the applied voltage waveform together with the impedance and **EMF** of the machine. Therefore to check if the current regulator is saturated, which means if supply voltage **Vs** not exceeds the sum of **EMF** and the resistance voltage drop of the motor together with any additional voltage drop in the power transistors, the voltage and current loci was used. Some margin to allow for inductance voltage drop Ldi/dt was given.

Other possible study is using a dynamic design which simulates the complete drive system for this *sinewave* current control. As there are another works focused on this topic inside *Projecto FST Novabase* and to turn the analysis simpler, this was not considered in this project. In fact **PWM** is more complex in *sinewave* drives because all three phase-legs are active all the time and the 3 transistors are normally conducting at any instant.

In the appendix A.1 is represented the complete circuit with machine and drive. It includes **DC** source, power electronics, connection leads, equivalent machine circuit and wye connection. The filter represented is not considered and it's only ornamentally.

4.4.1. I-PSI Skewed GoFER

This on load calculation considers the current **Isp** that is necessary to the machine develop the **Tpeak** with **γ** equal to zero, due to the reasons depicted in section 4.1. Once the machine in the referred operating point is heavily saturated, several **FEA** were performed to find the necessary **Isp** to reach **Ppeak** at corner speed (**Nc**). The value obtained for **Isp** was 267 Apk.

To illustrate the effect of using skew, the following pictures show the open circuit results with skew equal to 0.5 in order to give some comparison with results for machine on load.

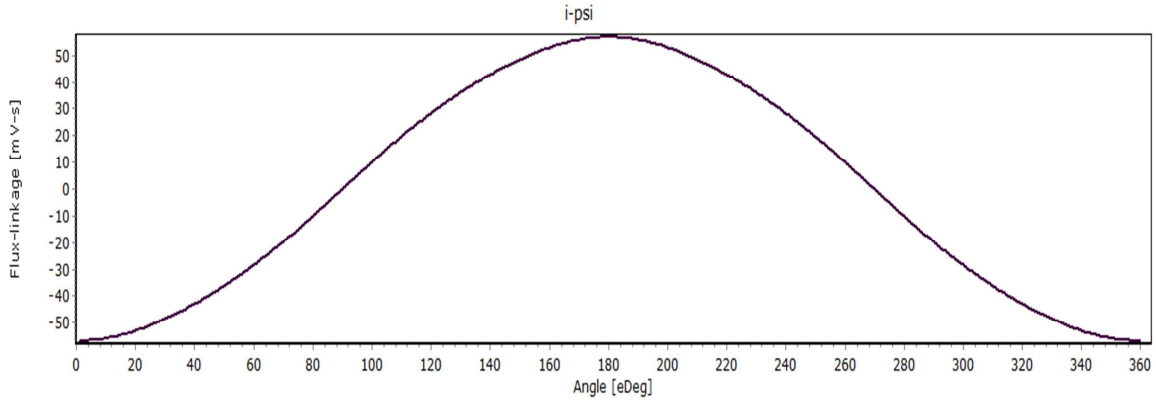

Figure 4.20 – Match FE skewed: Black - Flux linkage (PC-FEA).

This result states a phase flux linkage perfectly sinusoidal and coincident with fundamental component. The skew that eliminates cogging is also enough to guarantee a sinewound machine. The following figure illustrates the phase **EMF** in open circuit.

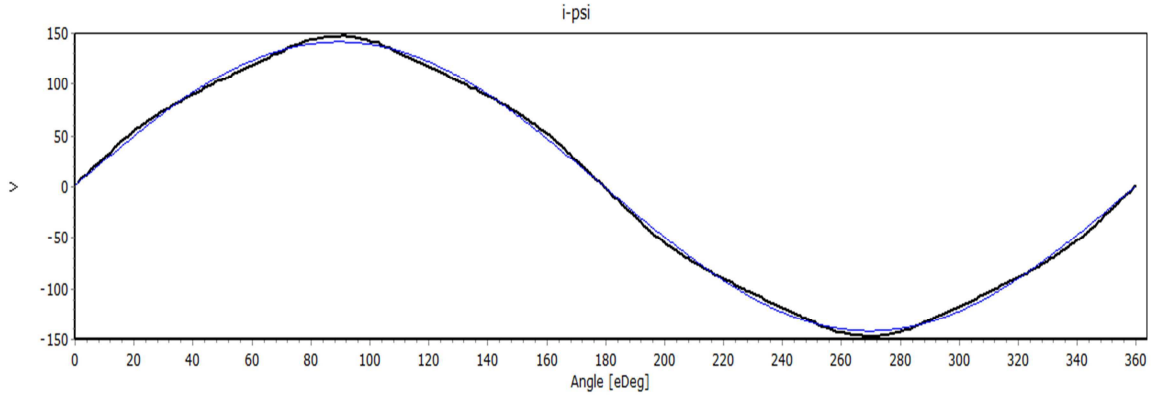

Figure 4.21 – Match FE skewed: Black - Phase EMF (PC-FEA); Blue - PC-FEA fundamental.

The phase **EMF** is much more close to sinusoidal waveshape than the first unskewed result depicted in figure 4.13. This gives very good indication for the next steps of design process. The fundamental component is therefore close to **EMF** waveform as can be seen on blue line. This result states that phasor diagram can be used with confidence as the **EMF** and current are sinusoidal, so fundamental components represent with accuracy the real ones.

Running the *i-psi* skewed **GoFER** with machine under load for the current **Isp** determined to attain **Ppeak**, the **PC-FEA** post-processor result is illustrated below.

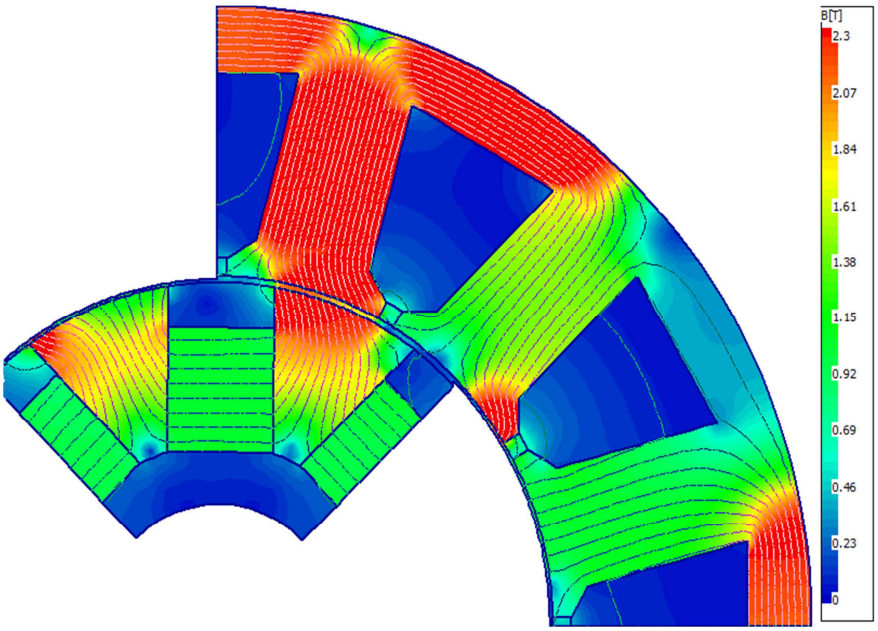

Figure 4.22 – PC-FEA post processor: I-PSI skewed GoFER.

It's possible to check that machine is heavily saturated in this working point, as expected. The peak values of **Bt** and **By** are respectively 2.37 T and 2.4 T. This is a little above of saturation polarization value of VACODUR® 49, which indicates that the tooth width and stator yoke are well dimensioned for this working point. The peak value in the tooth tip is a little bit higher, 2.46 T, which can be considerate acceptable for this iron and therefore there is no need to make changes in **TGD** or **SOang**. The maximum flux density attained by rotor polar piece is 2.43 T, which indicates some saturation. Therefore it will have influence in **Eq1** that needs to be studied.

Saturation causes great variation in **Xq**, which can decrease a lot between no load and full load. In a lesser extent **Xd** is also affected by saturation. So it's important to avail the produced torque in these conditions and adjust **Xd** and **Xq** by means of **Match FE**. Next picture exposes the *i-psi* loop on load.

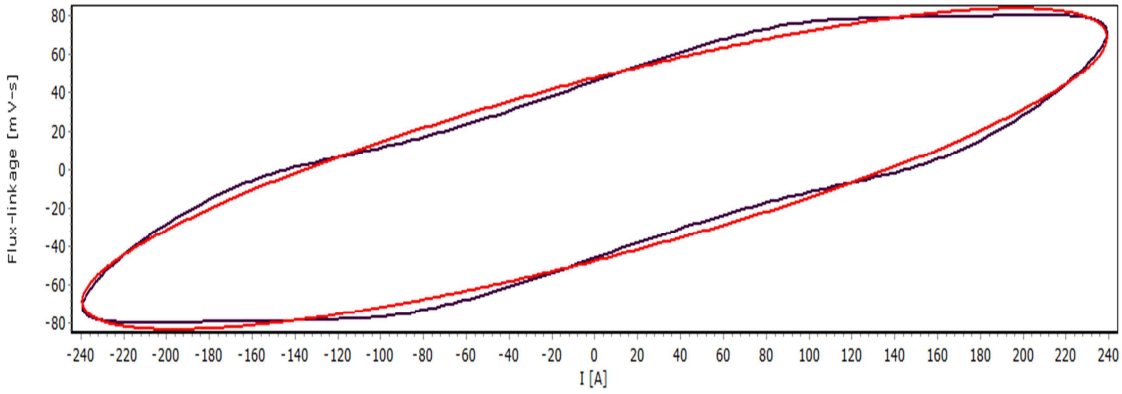

Figure 4.23 – Match FE skewed: Black - I-PSI Loop (PC-FEA); Blue - I-PSI Loop (PC-BDC).

The first thing to note is that black *i-psi* loop is not perfectly elliptical. Saliency, permeance harmonics but mostly saturation distorts it. In a highly saturated machine the inductances saturate and there is even uncertainty as to what happens to **EMF** under these conditions. Superposition does not apply and therefore *d-axis* flux cannot be uniquely partitioned into separate components attributed to the magnet and *d-axis* armature current.

Initially, both loops didn't match and was necessary use X factors **XCd**, **XCq** and **XLdiff** to establish the result stated and account for saturation effects. Then was possible to analyze and compare the average electromagnetic torque from **PC-FEA** with **PC-BDC** as depicted in section 3.1.7.

To initiate the adjustment process, the best was start with flux linkage waveform because the currents always match. The next picture shows the result and is clear the saturation effect, which appears by means of a flux linkage with a flat top waveform when compared with fundamental component.

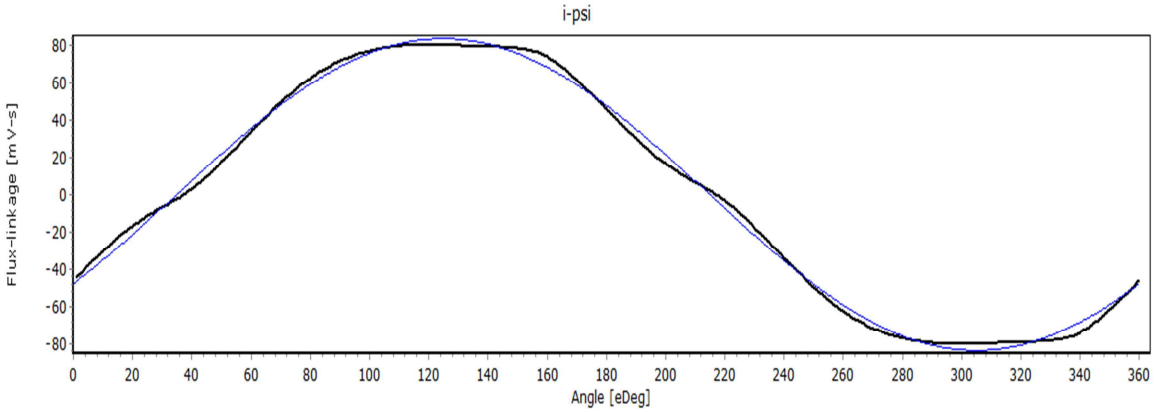

Figure 4.24 – Match FE skewed: Black - Flux linkage (PC-FEA); Blue - PC-FEA fundamental.

Before calibrating the models, it was seen that saturated flux linkage waveform was too large and too far to the left compared with **PC-FEA** waveform. Phasor diagram will provide the logic for the adjustments and decide the correct values for X factors.

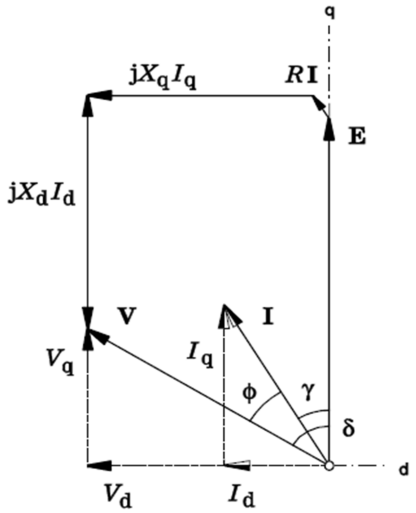

Figure 4.25 – General phasor diagram.

Flux linkage is what generates the fundamental component of phase voltage (**Vph1**), so the focus on the phasor diagram was in this quantity and having in mind that **γ** is 0. To perform the matching it was necessary to reduce **Vph1** and retard its phase. Reducing **Xq** will achieve this effect by shrinking the voltage **Xqlq**. Due to the saturation of the iron polar piece, adjustment was needed to be done in **Eq1** too, by means of other X factors. This saturation of pole face causes a reduction in **Eq1** leading to a reduction in the alignment torque. The **Xq** adjustment is done by means of **XCq** while **XLdiff** had the same value on the grounds that differential leakage inductance will saturate in the same way as **Xq**. However is important to note that differential leakage isn't a significant part of total reactance.

The final result for the average torque matches, resulting in 68.45 Nm. This value corresponds to **Te**, therefor to obtain the torque in the shaft (**Tsh**) is necessary to subtract the mechanical losses resulting in 67.63 Nm. The **Ppeak** is attained at 6000 **RPM** and the analytical model is perfectly calibrated with the numerical.

In order to avail the saturation effect, is interesting to compare **Xq** and **Eq1** values for saturated and unsaturated condition. The following table illustrates it.

Condition	Xq (Ω/ph)	Eq1 (V)
Saturated	**0.724**	**84.73**
Unsaturated	**0.95**	**100.4**
Difference (%)	**23.8**	**15.6**

Table 4.3 – Saturated and unsaturated Xq and Eq1.

Is possible to check that **Xq** is much more affected by saturation that **Eq1**. Both effects will reduce the torque developed, so to attain the same power is required more current to compensate it and naturally the cooling system has to dissipate more heat due to the higher copper losses. Before passing to **PC-BDC** calculations is necessary to check the losses using **FEA**, namely in the iron and magnets.

4.4.2. I-PSI Elements Table

The calculation has to be made using *i-psi* **GoFER** unskewed on load. The result is not the same but the unskewed calculation tends to give higher peak values on the tooth and yoke field as depicted in section 4.3.1.2. In this computation losses tend to be higher than with skew so the analysis is on the safe side. Moreover, the idea is only to compare the losses in qualitatively terms and check if the base idea to define **XFe** has reliability.

The same working point was used and the basis to compute the iron losses was depicted in section 3.2.1. In appendix C.6 can be found the post-processor result of losses calculation using **FEA**.

The following table exposes the comparison between losses calculated in **PC-BDC** and **PC-FEA** using elements table.

Iron losses (W)	PC-BDC	PC-FEA
Hysteresis	**83.4**	**85**
Eddy Currents	**401.6**	**353.2**
Total	**485**	**438.3**

Table 4.4 – Losses: PC-BDC and PC-FEA.

This state that even with **XFe** equal to 1, the losses in **PC-BDC** calculated with **Bt** and **By** on load are higher than those calculated with **FEA**. The difference can be seen as high enough to take account from manufacturing changes in the iron properties that increase the iron losses. As explained in section 4.2.1.4, there is no need to guarantee a big security margin as it's not expected to obtain great changes in iron data due to the manufacturing processes of Vacuumschmelze. This analysis confirms that **XFe** equal to 1 is a good approach for iron calculations.

4.4.3. Magnet Flux Pulsation

Even when the windings are perfectly sine-distributed and carrying perfectly sinusoidal current waveforms, the flux in the magnet pulsates at **fsp** because of permeance harmonics. A real winding has space harmonics in its **MMF** distribution even when the currents are balanced and sinusoidal, which produces additional flux pulsations in the magnet. The resultant flux pulsation cannot be calculated analytically, but must be determined by **FEA**. To do it, *i-psi* **GoFER** unskewed on load for the same working point was performed. The considerations taken in last section about the adequacy of results are equal here. This is a purely magnetostatic calculation, assuming *a priori* that any eddy currents in the magnet will be resistance limited. This fact was already proved in section 4.2.5.3.

The following picture shows flux pulsation and the harmonic reconstruction of the waveform.

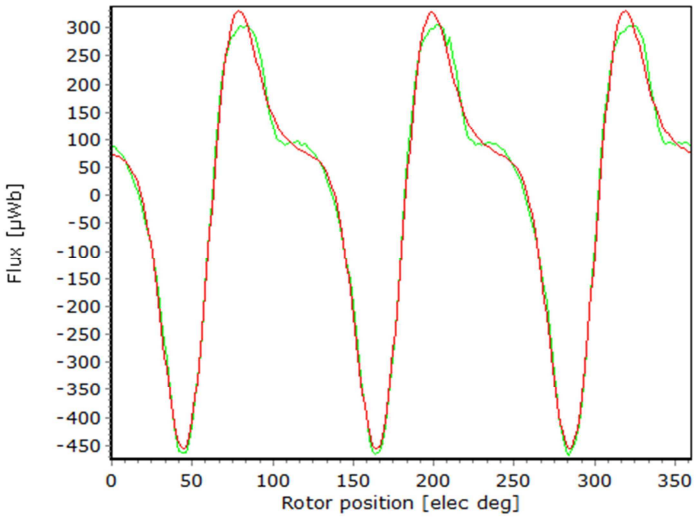

Figure 4.26 – Match FE I-PSI: Green - Flux pulsation (PC-FEA); Red: Harmonic reconstruction.

The magnet flux pulsation was successful reconstructed until the 9^{th} harmonic, so for future calculations of magnet losses the flux pulsation considered is exposed in red line. This simplify the computation time without losing the important information of flux variation.

To get a more reliable idea if magnet segmentation is necessary, the transient solver is executed to analyze the magnet losses due to eddy currents.

4.4.4. Transient Solver

Using *i-psi* **GoFER** on load for the working point discussed, the transient solver was executed. The configurations had into account the topics discussed in section 3.2.5. The next picture shows the **PC-FEA** post-processor results for one magnet and rotor aligned with *x-axis.*

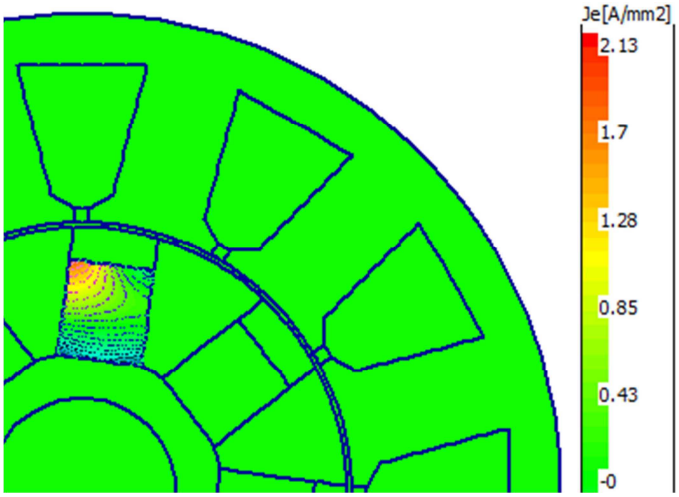

Figure 4.27 – PC-FEA post processor: transient solver.

The peak eddy current density observed in the magnet has the value of 2.13 A/mm^2 which is a high value. This magnitude depends on the load conditions, so for the most exigent working point this is the worst result. It can be seen that eddy currents are not uniform along the magnet cross section and their distribution depends on the rotor position. There is some correlation of current density with the slot openings. This is due to the slot harmonics in the **MMF** distribution as well as the slot openings themselves.

Using elements table was possible to get the value of eddy current losses. For one magnet the value obtained was 10.6 W. Since the eddy currents are resistance limited and the machine has 8 poles, the total magnet losses expected is 84.8 W. This is a relatively high value which means that segmentation may be considered. This has the advantage of losses reduction and guarantees a better behavior on the cooling system. It also minimizes the flux drop in the magnets due to the temperature increase, which is important to attain in a high **TRV** machine.

For a first approximation in the design and taking into account manufacturing issues, the number of magnet segments used in the circumferential direction was 16. In the axial direction no segments were defined, which means that magnet extends normally the whole length of the machine.

These values were introduced in **PC-BDC** to calculate the magnet losses, based on the flux pulsation determined in section 4.4.3 and in considerations taken in section 4.2.5.3.

4.4.5. Demagnetization

The demagnetization withstand capability is a critical property of a **BPM** machine. Even partial demagnetization is unacceptable, so the design must provide safeguards to prevent it. The aim was to make sure that magnet operating point stays above the knee of magnet curve. It´s necessary to check

the values in all points on the magnet cross section because they might not be all the same. This reason justifies the use of **FEA** and the analyses must be done to the worst case scenario.

The temperature is critical because **NdFeB** has negative temperature coefficients for **Br** and **Hc**, which means that both decrease when the temperature increases. Moreover the knee moves to a lower value of **Hm** and less current is required to demagnetize the magnet. The value used for reference in the knee point was 0.2 T, taken for a typical grade of **NdFeB** working at 200 ºC [68].

To the maximum current applied is considered the current that drives the machine to **Ppeak** at rated speed, 267 Apk, as depicted in section 4.4.1. The worst case scenario is defined as the value referred applied in order to demagnetize the magnet filed, which means that armature reaction is studied in the negative *d-axis*. The following picture illustrates the post-processor result using **PC-FEA**.

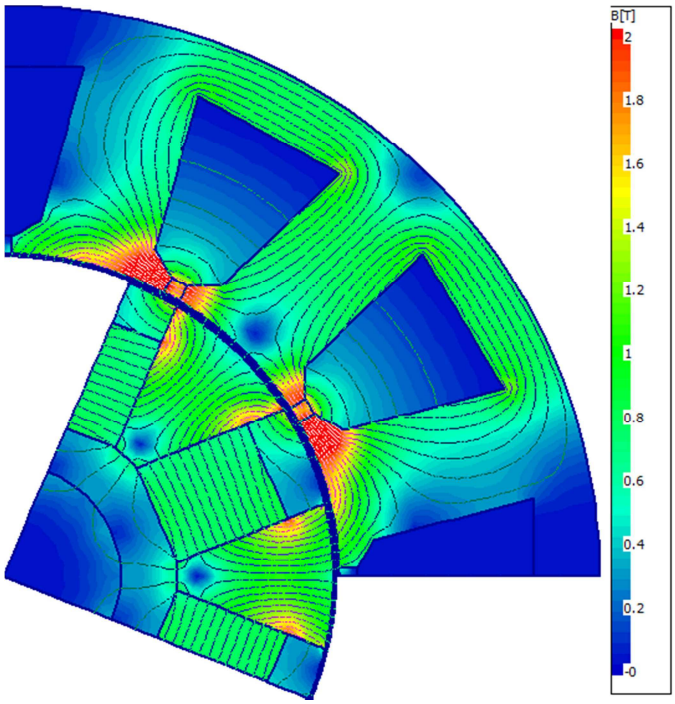

Figure 4.28 – PC-FEA post processor: single load point.

The lowest flux density value in the magnet is 0.55 T, which is above the 0.2 T referred for **NdFeB** working at 200 ºC. This is the worst case scenario because if the temperature decreases the value corresponding to the knee decreases too. Moreover, this is an exaggerated analysis because the peak current will never be used in the negative *d-axis*. This means that design process guarantee the necessary measures to explore the machine over the entire envelope defined by the team, without any **EM** problems.

4.5. PC-BDC Results

Since all the necessary calculations and model calibrations in open circuit and load condition were done, it is reliable to check the analytical results given by **PC-BDC**. This allows having an idea of this

design success as well as improving some details to get it better. A good starting point is check the current and voltage locus to analyze the saturation of current regulator as defined in section 4.4.

4.5.1. Phasor Diagram

The following picture illustrates the current and voltage locus in phasor diagram, taking as reference the picture 4.25.

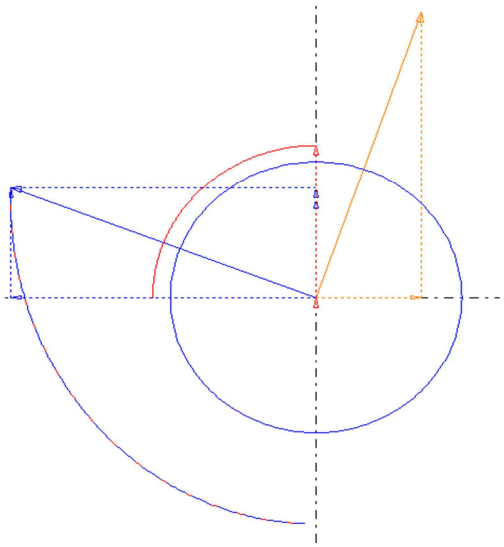

Figure 4.29 – PC-BDC phasor diagram: Blue - Voltage; Orange - Flux linkage; Red – Current.

The picture shows that there isn't enough voltage to drive the necessary current to the machine for the peak operating point. The machine reactance is too high, so changing **Ppth** in the winding connection to reduce the reactance may be a solution. Since 4 poles are considered, the connection can consider 2 poles in series with the parallel of the next 2 series poles. The new result is given in the following picture.

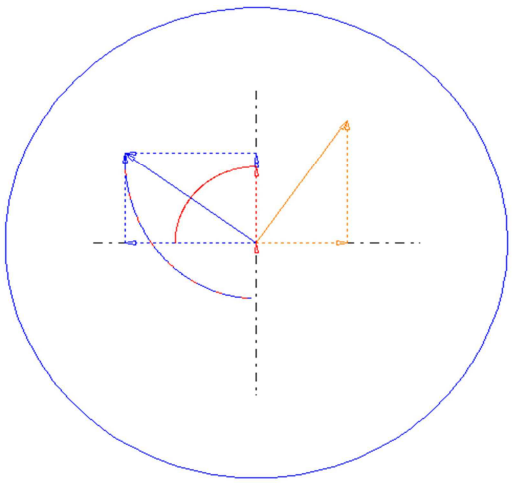

Figure 4.30 – PC-BDC phasor diagram: Blue - Voltage; Orange - Flux linkage; Red – Current.

The entire phasor diagram is defined inside the voltage circle limited for a six step 180º operation. This means that maximum voltage available from the inverter is enough to drive the machine until the base speed of 6000 **RPM** at **Ppeak**. There is some difference between **Vph1** and the circle limit, however this is done to drive the machine until the 9000 **RPM** and compensate the **EMF** and reactance increase with speed. This will be useful to study the machine in entire operation envelope.

An illustration of the suggested winding connection is given in appendix A.9.

4.5.2. Simulation Graphs

The following figures give illustration for the most important **EM** variables defined in this design.

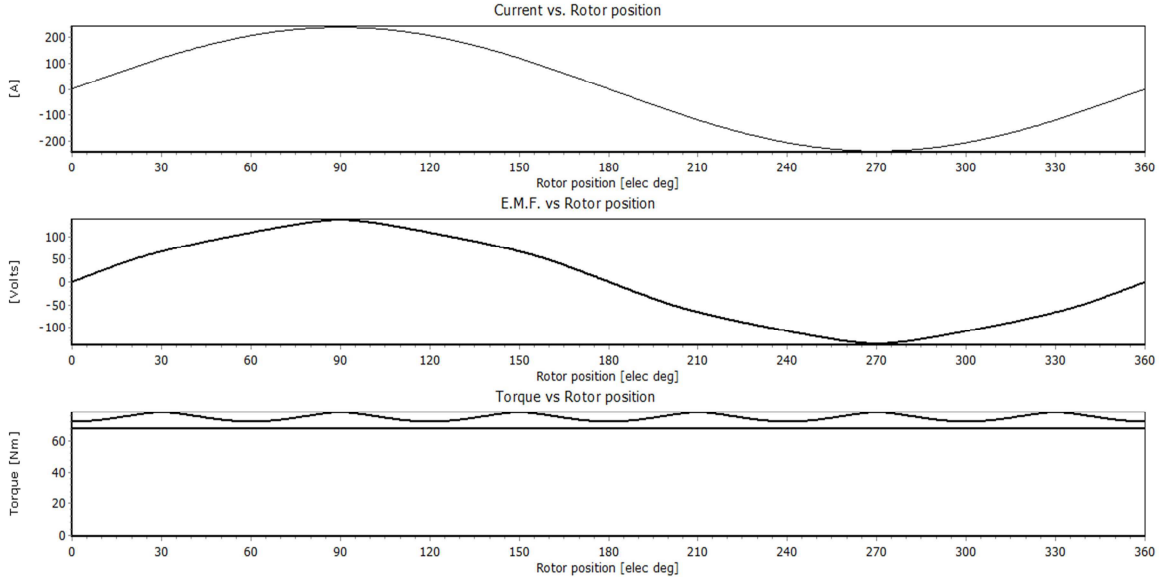

Figure 4.31 – PC-BDC graphs: Current, EMF and Torque Vs Rotor position.

As depicted in section 4.4.1 the phase **EMF** is close to sinusoidal waveshape, however some torque ripple is observed. This is mainly due to the harmonic content of line-line **EMF**.

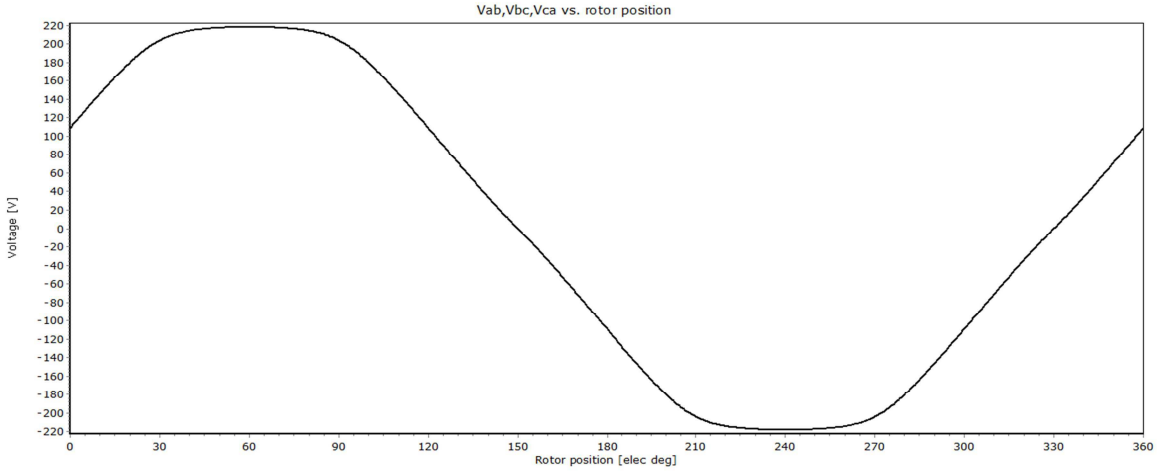

Figure 4.32 – PC-BDC graphs: Line-Line EMF Vs Rotor position.

The line-line **EMF** has a flat top waveshape which is the main cause for the torque ripple observed. It's important also to see the effect of skew in the air gap flux density.

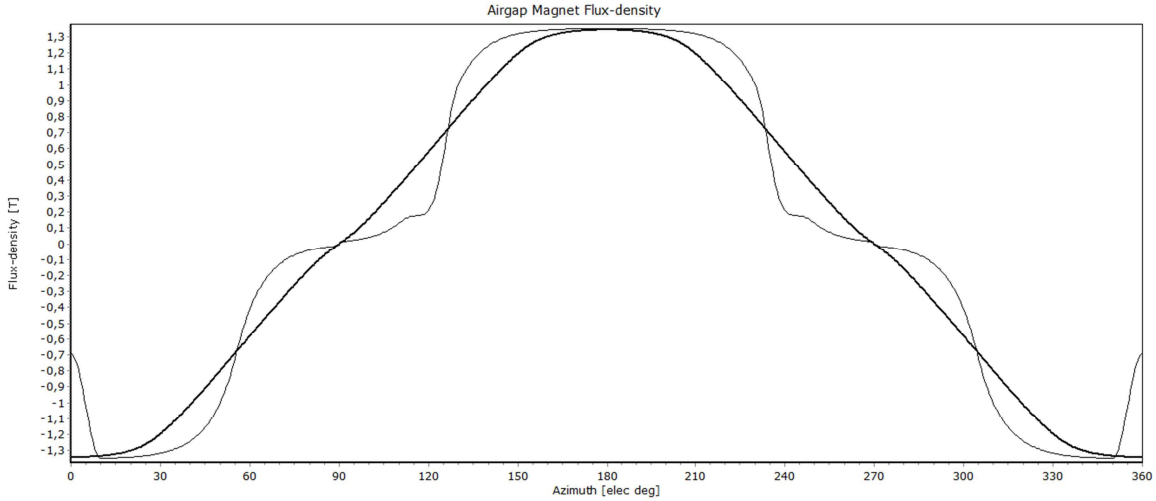

Figure 4.33 – PC-BDC graphs: Air gap flux density Vs Rotor position.

This graph gives good illustration about the skew effect. The dark line represents **Bgap** obtained after skewing the stator while the clear line represents **Bgap** without skew. The effect of harmonic filtering obtained with skew is evident and in conjugation with the skewed winding factors, mainly those related to 5^{th} and 7^{th} harmonic, is possible to have filtering effect in this waveshape, resulting the **EMF** already showed.

Harmonic analysis allows quantifying some of these aspects.

4.5.3. Harmonic Analysis

The harmonic analysis was performed for 21 harmonics, which was found to be a good value to focus the important aspects in the design. The most important harmonics were considered until 11^{th} order. The following pictures show harmonic analysis for the most relevant **EM** variables.

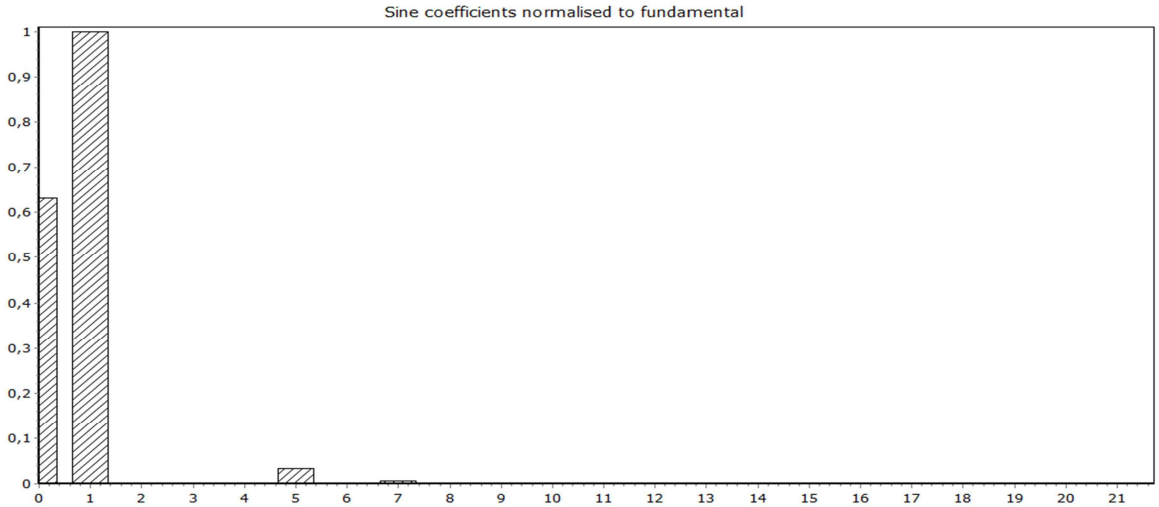

Figure 4.34 – PC-BDC harmonics: Line-Line EMF.

The **DC** component displayed represents the half cycle mean value for all the symmetrical waveforms. The harmonic coefficients are normalized to the fundamental, which shows as 1. The 3rd harmonic in line-line **EMF** was suppressed by wye connection as it can be seen on the figure. The flat top waveshape is mostly due to the presence of 5th harmonic. It was not filtered enough by the correspondent skewed winding factor, causing most of the torque ripple observed. The harmonic analysis in the torque will give more information.

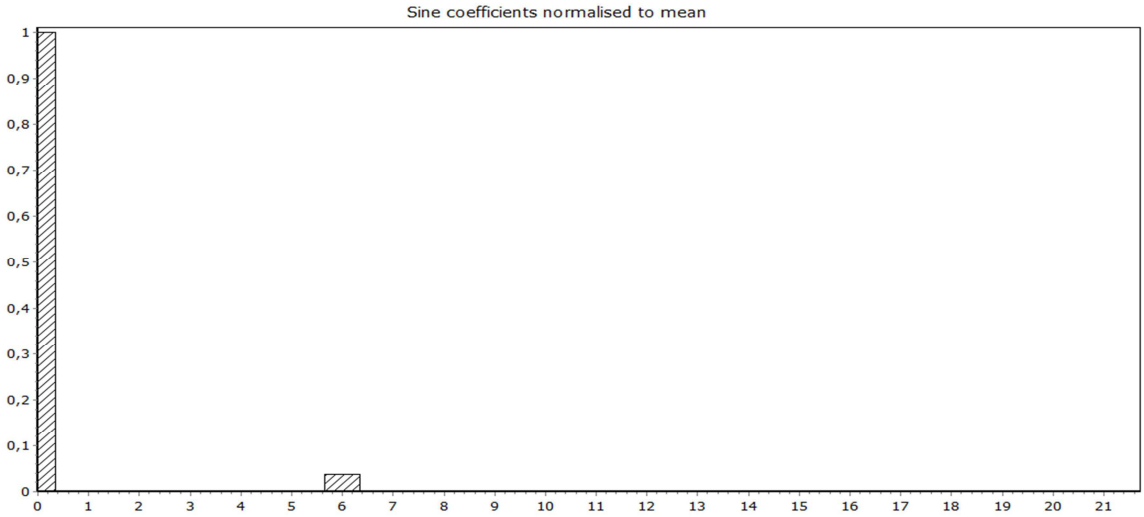

Figure 4.35 – PC-BDC harmonics: Alignment Torque.

In this case the coefficients are normalized to the mean value, which shows as 1. Is notable that non-zero torque harmonics are those of order 6*k*, where *k* is an integer. In this case only the 6th harmonic is relevant and justifies the variation observed in figure 4.31. After checking the maximum and minimum value attained and relates the difference to **Tpeak**, the torque ripple attained is 4.4 % of **Tpeak**. This is in the limits established for the project as depicted in section 4.3.1.2.

The following table shows the total harmonic distortion (**THD**) for most important variables in **EM** design in order to establish a balance and check the success to attain a sinewound machine.

EM Variables	THD (%)
Line-Line EMF	**3.34**
Bgap Skewed	**6.1**
Bgap Unskewed	**18.32**
Bt	**0.67**
By	**1.11**

Table 4.5 – PC-BDC THD results.

The results exposed give very good indication. The low **THD** attained indicates that this motor can be treated as a sinewound machine. The filtering effect of employing skew reduces the **Bgap THD** in almost 12%, reflecting the analysis done in figure 4.33. The flux densities in tooth and yoke are almost sinusoidal, which justify the result for phase **EMF** computed with tooth flux method, as depicted in figure 4.31.

4.5.4. Design Sheet Results

Next table summarizes other important results regarding the machine performance.

Variables	Results
LgthOEnd	181.2 mm
WireDia	2.025 mm
Rph20	25.9 mΩ
LDiff	0.027 mH
Ld	0.3288 mH
Lq	0.288 mH
Psh	42.5 kW
Nc	6000 RPM
J	28.9 A/mm^2
WCu	2.4 kW
WFe	485 W
WMag	9.2 W
δ	53.85 º
PF	0.59
Dtot	116 mm
Mlgth	212 mm
Wt_Tot	7.72 kg
Wt_FeR	1 kg
Wt_RSS	3.14 kg
RotJ	8.56 E-4 kg.m^2

Table 4.6 – PC-BDC overall results.

The result obtained for wire diameter indicates that this value is high, even for a machine wound. To get a better performance in the wound process may be useful to consider not a single wire but divide it into **Nsh** strands. In this case the wire diameter is smaller by the factor of $1/\sqrt{N_{sh}}$ so it's enough to consider **Nsh** equal to 2. In appendix A.3 can be consulted a graphical example of this implementation.

The axial length of the end windings indicates a good result to give 1 cm for the machine end space region. The final length is near for the recommended 20 cm.

Regarding the inductances, differential leakage inductance is small despite of high harmonic content of **MMF**, which indicates that there is no special concern in the differential leakage. The inductances over *d-axis* and *q-axis* indicate that machine has little saliency.

The circumferential segmentation used in the magnets allows great reduction in the losses when compared with **FEA** transient solver results. This value will be maintained in the design process.

The total weight achieved give very good indications to maintain the current geometric variables in the design process. Giving a margin of 3 kg for frame, end caps and bearings, the final result will be close to 10 kg. Moreover, using a spoke rotor the weight is reduced in a relation of 1:3 relatively to a massive iron rotor. This result is proving the advantage of applying this geometry in the project.

The total moment of inertia is greatly reduced when compared with Agni 95R results depicted in section 2. The reduction is in the order of 1:28.

5. Prototype MM03_V3: Thermal Project

This chapter presents the complete machine's thermal project using Motor CAD software. Since a good **EM** design was achieved, is important to get the correct temperatures in all components to have a better idea about the real machine performance. Those temperatures are dependent of the cooling used, materials chosen as well as many other options that are important to clarify.

The process starts with **GoTAR** routine, then the main cooling options are defined and the final results are obtained using the lumped thermal circuit at steady state. Duty cycle operation is a specialized feature, directed to analyze specific exploration regimes. To perform the necessary sensitivity analyses and check the important cooling paths is more easy and quick to look at steady state operation. Then, since the cooling is defined, the duty cycle analysis can be performed.

As this machine doesn't have steady state operation in this application, some simulations were done with **PC-BDC** and **PC-FEA** to check when machine starts to saturate at rated speed **Nc**. It was verified that when shaft power (**Psh**) is equal to 25 kW, the machine had some saturation in the rotor polar piece. Therefore this was the working point defined to analyze the machine at steady state, which means that losses obtained with **PC-BDC** are passed to Motor CAD to give input to power sources used in the lumped thermal circuit. Machine geometry and winding definitions are also exported to perform the complete cooling system. The most general design options, which are transverse to entire project, will be presented as a starting point.

- No encoder was modeled because there was no indication by the team about the use of position sensing. However this can be an important issue to deal in thermal point of view if will be considered in near future.
- Shaft used is the standard solid type, with dimensions depicted in chapter 4.
- No potting on end windings cavity is considered on the basis that liquid cooling is good enough to extract the heat. Moreover potting is more difficult to implement and is expensive.
- No mounting is considered, which is good because represents the worst case scenario. Mounting can have a significant impact on thermal behavior. In fact, 35% - 50% of total loss can be dissipated through the flange, for instance, in servo motor designs.
- No sleeve is used in the rotor. This is based on the assumption that magnets in the spoke rotor are mechanically well attached to the iron and no special concern is needed to fluid seal.
- End cap and bearing dimensions are not optimized. The Motor CAD intelligent geometry scaling is used to obtain average values to these components, related to machine's overall dimensions. More mechanical study is needed on this.
- The ambient temperature considered is 40 ºC. In normal working conditions is expected to find a lower temperature, however 40 ºC is a standard value used in industry and can be seen as a worst case scenario.
- The motor is considered to be oriented in horizontal position, like Agni 95R on FST04e. This feature has strong influence in natural convection cooling, between housing and ambient, because it modifies the convection correlation to be used.

- The altitude is not considered in this project due to the typical conditions of formula student competition. However is important to note that altitude has a significant effect on convection cooling, especially at high altitudes where air pressure is significantly lower leading to lower hear transfer coefficient (**h**) and thus a hotter machine.
- Is considered that machine don't have a large temperature drop across the active section, which means that is expected to find a low temperature gradient in the axial direction. This assumption is due to the short axial dimension required.

5.1. Materials

This topic makes reference to the materials applied in thermal project, beyond those already referred in section 4.2.1. As this is very important to overall machine performance, a reference is given in appendix E.1, in table format, where materials' thermal properties are exposed.

5.1.1. Housing & End Caps

Overall machine weight is an important requirement, therefore using lightweight materials in this components may compensate other choices that are necessary to introduce more weight in the machine. This happens with iron and shaft, because VACODUR® 49 is heavier than regular silicon iron and stainless steel is typically a material with high specific gravity. On the other hand, softer and smoother materials have advantages in contact resistances, having lower values comparing with hard materials. As the housing and end caps have an interface gap resistance between them, the choice passes to use a smoother material on booth. The most common and cheap material found is aluminum, which guarantees small contact resistances between the housing and end caps besides improving the contact resistance with housing and stator laminations. This gap is a function of how well the rough laminated outer surface of the stator is prepared before the housing is fitted. This feature is crucial in the overall thermal performance.

Since the material is chosen, is necessary to select the alloy to use. The best compromise is having an alloy with good machining properties, resistant to corrosion and good emissivity. This was found with Aluminum alloy 6061 [20], which has good acceptance for applied coatings allowing an anodized chemical treatment. This improves the material emissivity as can be consulted in table on appendix E.5. Moreover this material has good workability, relatively high strength and high resistance to corrosion. This last property is very important if a cooling using water jacket is implemented directly in the housing. More properties of this alloy can be consulted in appendix D.1.

5.1.2. Insulation & Impregnation

Before defining the insulation and impregnation materials, is important to establish the machine thermal class because the choice depends on it. Maximum winding temperature allowed will define the thermal limit exploration of the motor, which will be important to determine the maximum time to explore **Ppeak**. However how much better is class insulation the more expensive is the material and manufacturing processes involved. It was found some materials with thermal class H at good price

and very well established in the market. Insulation and impregnation materials that allow maximum winding temperatures superior to 180º C become more difficult to find and are much more expensive. It's the case of insulation materials with class N or R. Therefore, for first iteration in the design start with thermal class H materials is a good point. Even if the maximum temperature allowed is not attained it means that insulation lifetime will be longer when compared to thermal class F or B. This is important because there are expensive manufacturing processes that cannot be avoided, as referred in section 4.2.1, which means that obtaining a prototype as durable as possible must be a priority.

Conductor insulation separates the wires and turns of a coil. The standards are not as high as they are for groundwall insulation, resulting in the thinnest insulation component. Conductor insulation is often a thermoplastic material where both crystalline and amorphous regions improve thermal resistance, mechanical properties and insulator flexibility. The most common used in electrical machines are ester-imides or amide-imides. Polyimide films have very low nominal thicknesses, typically from 6 μm to 0.4 mm, which is very good to decrease the thermal resistance and increase slot fill gross. A tough polyester film widely used in small size machines is based on **PETP** membrane. An example is Mylar® film but it doesn't support so high temperatures as required in class H insulation. An analogous synthesis to conventional polyester **PETP** was found. It's called **PEN** and is high performance thermoplastic polyester, improved with two benzene chains as can be depicted in appendix E.2. This simple feature allows increasing the thermal resistance, turning possible its utilization even as thermal class N material.

The product selected to be employed as insulator, based on **PEN** polymer, is Teonex® [69]. It has typically the double of aramid paper thermal conductivity, high mechanical strength, good dielectric properties and resistance to hydrolysis. It´s supplied in a range of thickness from 25 to 125 μm, so the lowest was chosen.

Other important issue to take into account is winding impregnation. Its main functionality is improving winding thermal conductivity and reducing the hot spot value. It also gives mechanically reinforcement, protecting it from moisture, dirt and chemicals. The most common materials are impregnation varnishes and resins. In the impregnation varnishes approximately half of the volume is an evaporable solvent, which is replaced by air when the varnish hardens. Therefore, polyester based varnishes including solvents have mostly been replaced by impregnation resins that are polyester or epoxy based. They don't contain solvents and are chemically hardening impregnants. In common machines, polyester resins are used because they have a low price and are easy to handle. Epoxy resins are very reliable but have higher price when compared with polyester resins, so the first approach is using this impregnant type. However the insulation impregnation process is important to select the final product to use. Slot insulation is composed of several different components, one of them is often an air gap. It can appear in undesired places when the impregnation has not been complete or when are bubbles in the varnish. To avoid these gaps and attain a machine that guarantees high performance standards in the thermal behavior is advisable to use **VPI** process. This eliminates air pockets in the impregnation and avoids partial discharges in the insulation, increasing their lifetime and reliability. The only constrain is choosing a polyester resin that is adequate to this technology.

It was found an unsaturated polyester resin in special acrylic monomer, with very good thermal properties, typical 3 times the thermal conductivity of common resins. The Dobeckan® LE 6500 is directed to **VPI** and is used for low and medium voltage [70].

5.1.3. Slot Liner

The main function of groundwall insulation is to galvanically separate the coil from the iron core of machine. Slot insulator has to guarantee good mechanical strength since sharp edges may occur in the slot. Aramid paper is a good material for this purpose, because it has good thermal resistance and impregnation properties. This means that aramid papers efficiently absorb the resin, fixing it well to the surface when compared to polyester films used with the same purpose. Since an impregnation material and **VPI** is planned, this permits to reduce the interface gap between the liner and stator lamination. This interface resistance has great influence in the winding average and hot spot temperature.

Aramid fibers are also very tolerant to mechanical stresses, even heat and moisture simultaneously guaranteeing better heat resistance than polyester films. The typical aromatic polyamide used for this purpose is Nomex®. There are several thicknesses available, and naturally the selection passes to the lower possible. It's common to find applications in small motors with 0.18 mm of thickness, so as a standard it will be adopted in this project too [71]. A graphical illustration of a liner inside the slot can be consulted in appendix A.3.

5.1.4. Top Stick

This component is also known as slot wedge and is very important mechanically because it holds the stator windings in the slots formed between the stator teeth. Slot wedges are made either magnetic or nonmagnetic material. The magnetic ones are good to reduce slot ripple in the air gap flux density caused by permeance harmonics, reducing also the eddy current losses in the rotor. The weak point is the mechanical resistance, which justifies its substitution to the nonmagnetic wedges. The ideal is somehow having both properties: mechanical resistance and magnetic behavior.

This was found in SPInduwedge product [72], based on thermoset epoxy which is a thermal class H material. Parts modeled from epoxy are hard, rigid, combining high mechanical strength with good electrical properties. A figure with a top stick inserted in the slot is referred in appendix A.8.

5.1.5. Bearings

Since this component is not optimized in design process, could be used a standard solution in order to explore a worst case scenario. It can be defined using a material for the inner and outer race that leads to the higher interface gap between bearing, shaft and end cap. The most common material used to hold and guide the balls is chrome steel 52100 [73], very similar to stainless steel in terms of contact resistance. This means that using this material the interfaces obtained are: stainless-stainless related to inner race and shaft; stainless-aluminum related to outer race and end cap. This is certainly worse than the typical polymer cage found in SKF E2, therefore thermal analysis will be on safest side.

5.2. Cooling Options

This topic focuses the main definitions for heat transfer modulation to be applied in the machine's virtual prototyping. Since the models are already referred in chapter 3, this will give some complement, quantifying the important variables.

5.2.1. Natural Convection

This process defines heat transfer between housing and ambient. Convection correlations based on Simonson´s formula are applied to different machine parts, depending of their geometry. For housing and radial area of end caps is applied the correlation to a horizontal cylinder and for end cap axial area is applied the correlation to a vertical flat plate.

In rigor, could be considered a forced convection cooling between the housing and ambient based on air displacement due to the car moving, which defines a blown over system. However, since the main cooling path is the liquid cooling, that modulation is not expected to affect too much the final result. Besides that, it introduces more complexity in the modulation process. This justifies the option for a **TENV** cooling system between housing and ambient instead of **TEFC**.

5.2.2. External Radiation

This process takes place in form of electromagnetic waves mainly in the infrared region. Radiation emitted by a body is a consequence of thermal agitation of its composing molecules. In a **TENV** machine this dissipation to the ambient can be equal or even exceed natural convection. As this machine will be liquid cooled, this is the main cooling path. However to give a complete modulation of all heat transfer processes, is important to quantify the materials emissivity and view factor. This is used in calculation of external radiation heat transfer coefficient at housing and end caps.

The emissivity values for anodized aluminum can be consulted in appendix E.5, both applied to housing and end cap. Regarding the view factor the simplification used is that surfaces with a clear view of the ambient have their view factor set to 1. In fact this happens both for housing and end caps, because when water jackets are used there is no need of exterior housing fins. They are the critical components to define this variable.

5.2.3. Interface Gaps

The different interface gaps considered in project are dimensioned for an average manufacturing process as they are function of materials hardness, surfaces smoothness and air pressure. In appendix E.6 can be consulted the vales used for all contacting surfaces. Special attention is needed to the bearing effective gap, defined as depicted in section 3.3.4, and to interface between stator lamination and housing. This is the most critical one because it defines the effectiveness of cooling system to extract the heat from winding and iron. A sensitive study in this variable is necessary to understand the impact that an average manufacturing process cause in machine performance.

5.2.4. End Space

The heat transfer coefficient is defined with two terms: one to account for natural convection when reference velocity is zero and another that increase forced convection due to rotor rotation. The coefficients are defined according to published data comproved by measurements done in prototypes. The Schubert relation corresponds to such set of data, typically used by default in these studies. To complete the correlation is necessary to estimate the local velocity seen by all surfaces in end space region. Regarding the rotating surfaces is easy to calculate as it's just the components peripheral velocity. For non-rotating components it's more difficult and the process is calculating the reference velocity using analytical formulations [19] where a multiplier defines the rotor smoothness. A lower value is applied when no wafters or fan is used and the end space air is still. This is a good starting hypothesis, which defines the initial end space cooling configuration.

5.2.5. Losses

This topic is very important to define the complete lumped thermal circuit model. Losses are the power sources in the circuit and its values depend on temperature. On the other side, temperature depend also on losses which means that is important to define how this relation is established. Moreover, there are some kinds of losses that are important to define how they are calculated and applied in the circuit. For instance is the case of bearing losses. As explained, the bearings are not an optimized component in the design and the values based on power loss curve exposed in section 4.2.5.2 are an approximation for a worst case scenario. This guarantee that results will be on the safest side, however is important to define how this component is represented in the lumped thermal circuit. It is defined by two nodes, each one representing the inner and outer race and losses are splitted equally between them. On the other hand, windage losses values are inserted as defined in section 4.2.5.2 and equally divided between stator bore node and rotor surface node.

Iron losses are divided between the losses developed in the teeth and yoke. To give more physical meaning of temperature gradient along the teeth, it is represented by 3 nodes. This means that total teeth losses are divided by 3 and applied in each node, while the yoke losses are inputted directly in the stator yoke node. Rotor iron losses are applied in the rotor node and the same with the magnet losses.

Copper losses are splitted between active and end windings according with formulations based on winding layered model [19]. There are two nodes for each end winding, front and rear and losses are divided between them according to their volumes. The first calculation to define the cooling system is done at steady state operation in the working point of 25 kW at **Nc**. The best approach is consider that machine has to develop constant torque at steady state and the loss variation takes into account the temperature and load, according with explanations and formulations referred in section 3.3.2.

In appendix E.8 can be consulted the equivalent lumped thermal circuit of the machine to working point referred. It's possible to check the losses distribution as explained.

5.2.6. Liquid Cooling

In section 2.3.6 was identified the need of using a liquid cooling strategy to perform the peak **TRV** required. However there are several types of liquid cooling to consider and the best selection has to be made. For instance, rotor water jacket has known some applications in specialist **BPM** at aerospace industries. The ducting system is placed between the magnets and attains good performance for heavily loaded machines. However, its mechanical implementation is expensive and hard to setup. Besides that, magnet segmentation is used to reduce the losses so it's not really necessary to extract the heat from magnets in this way. Another possibility is using slot water jackets. It's also common for very highly loaded machines like this, even small machines. The main setback is again the mechanical setup, needing a very specialized wound to manipulate at same time ducts and conductors, turning the process very expensive. Moreover, the ducting system reduces slot fill gross which increase the phase resistance for same slot area. Other possibilities in liquid cooling are wet rotor and spray cooling. The first is widely used in pumps and the second in large machines with high volume end windings. Both have more fluid concentration in the rotor parts and end windings. Since that major losses expected in this project occur in the active cooper, probably the best and simpler approach is using water jackets in the housing. This allows extracting the heat from the active winding part and also from end windings in the end space region. If will be necessary to improve the cooling in end space region a spray cooling strategy could be used by means of housing and not the shaft as it's typical. With this solution no more ducts are needed, said in rotor or stator iron because the main cooling path is defining in the housing. Moreover, it turns the cooling process more standard and cheaper to implement. The important thing to guarantee mechanically is a small interface gap between housing and stator laminations to get the better dissipation possible of the heat.

5.3. Winding

Some winding results were exposed in section 4.5.4, as well as other options discussed along chapter 4 and in this one, namely in insulation and impregnation used. Those data is transferred from **PC-BDC** to Motor CAD to perform the first cooling approach. Then the iteration between **EM** and thermal model is necessary to converge to the final steady state solution, as depicted in section 3.4.

Before starting to configure the housing water jacket cooling, is necessary to define the winding layered model approached in section 3.3.1 and calibrate it using thermal **FEA**. The design sheet results show that copper losses are the most relevant in the design, which means that is imperative to take a good modulation of winding.

5.3.1. Layered Model

This model establishes the necessary set of thermal resistances to represent the temperature rise within the winding and define how the winding is coupled to stator lamination nodes. Setting the thermal resistance of slot liner at the boundary of stator slot, is possible to place layers of copper and insulation within slot liner, as shown in the next figure on the left.

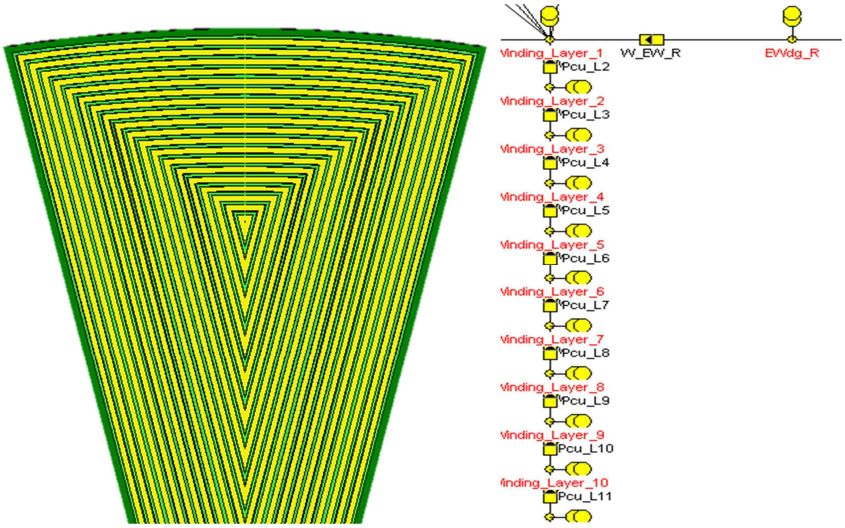

Figure 5.1 – Winding layered model (left); Set of 10 thermal resistances (right).

Since the copper and insulation lengths are defined and areas known from machine geometry, is possible to calculate a set of thermal resistances that represent the layered model by choosing the number of target layers to represent the winding. Highest the number of layers, more accurate will be the analytical model to predict the temperature in the winding. It was found that 20 layers give good representation, after some simulations and check the minimum number that guarantee no variation in the winding hot spot and average temperature. In figure 5.1 it's possible to see the thermal resistances set for first 10 layers. The layered winding model permits good visualization of components proportion in the slot: liner, copper, enamel and impregnation. That amount of material in layers is the same as in the actual machine. An alternative view can be seen in appendix E.7, where the conductors in the slot are exposed. It represents the equivalent conductor's distribution in the slot for this layered model.

5.3.2. Thermal FEA

To give sequence to previous choice, it's necessary to calibrate the model using thermal **FEA** and improve accuracy with it. The base for this procedure was depicted in section 3.3.10. A steady state analysis was performed for the working point defined as nominal, without any special configuration in the cooling. The objective is only to have notion about the qualitative results and take some conclusions based on comparison between layered model and **FEA** output, as next table shows.

Winding	Layer Model (ºC)	FEA (ºC)
Hot Spot	**86.2**	**88**
Average	**80.11**	**82.18**
Minimum	**72.78**	**69.35**

Table 5.1 – Uncalibrated results: Layer model Vs FEA.

The results are near, however is possible to get a better approximation in the winding hot spot. This value is critical in the machine performance so even a difference inferior to 5% is advisable. The next figure shows **FEA** post-processor output, after calibration using the impregnation goodness.

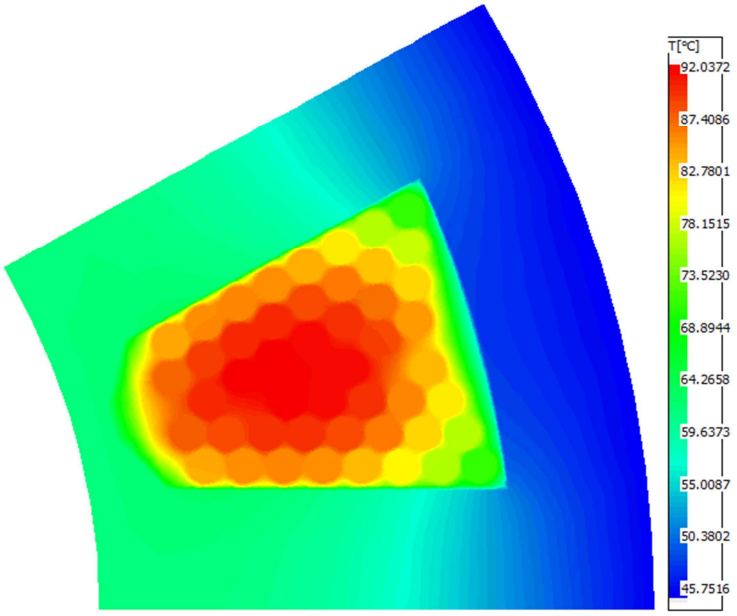

Figure 5.2 – Thermal FEA post-processor.

The result obtained with **FEA** for hot spot is at 92 ºC, as can be seen on post-processor label. The winding layer model result for the same hot spot is at 91.5 ºC, so the model is now well calibrated to proceed with next calculations and select the best configuration for housing water jackets.

5.4. Housing Water Jacket

To start the modeling of housing water jackets, it's necessary to analyze the mechanical constrains to the implementation. Safe margin was given when frame thickness was defined, namely to fin base and cover thickness. Starting with the value of 7.5 mm defined in section 4.2.3.2, is possible to define 2 mm for base and cover thickness in the aluminum alloy. This is good for a standard machining process and weight optimization. Therefore maximum channel height possible is 3.5 mm, which is a reasonable value for starting. If more is needed the frame thickness has to be increased, at the expense of more weight. An illustration of these dimensions can be depicted in appendix B.1 where a radial cross section shows the height of rectangular channels, the thickness between aluminum and stator lamination and top or cover thickness.

When pure water is used as liquid coolant, is necessary to give some attention to corrosion effects. The first approach is avoiding the use of another duct wall material, as rubber for instance, because it defines another thermal resistance and another interface gap, in this case between aluminum and duct wall material. The ideal is somehow put the water in contact directly with the housing material. In fact, this idea was in mind when the aluminum alloy was chosen for this purpose. Aluminum has good corrosion resistance and the anodized treatment improves it even more. This allows defining the ducting system without any additional material, which increase the efficiency of cooling. It's only needed to define the average duct wall roughness for aluminum to calculate the

pressure drops in the channels as depicted in section 3.3.7. This value was defined according to published data on Miller book [45] and the table consulted is exposed in appendix E.4.

5.4.1. Water Jacket Options

Since the team requirements defined in section 1.3 are clear when related to flow rate to use in the pump, the same doesn't happen to the type of flow definition. There is freedom to select the best option, or a constant flow rate or a flow rate proportional to speed. The first option was chosen on the basis that a constant flow rate will improve the cooling at low velocities when compared with second one. This can be important when a duty cycle analysis is performed for the different competitions, guaranteeing that winding hot spot don't attain a so high temperature, allowing a better exploration in thermal limits. The expense is on the higher pressure drops, always constant for the flow rate defined as 50 cm^3/s. This can be stated analyzing the following equation which relates **P** with **Q** by means of flow resistance, **R**, due to fluid friction at duct wall surface:

$$P = R * Q^2 \qquad (\mathbf{5.1})$$

The squared term in flow rate reflects the typical turbulent nature of flow. So if pressure drop turns too high, a sensitivity study can be performed to achieve the best channel dimension and optimize the velocity and duct resistance.

The flow rate is also affected by parallel paths number (**Ppch**) in a similar way that **Ppth** affects phase current and decrease machine's reactance. Lumped circuit modulation connects with same logic very different areas of expertize like electromagnetism, fluid mechanics and thermodynamic. So the higher the **Ppch**, less the flow rate obtained. This could be useful when there is a higher pressure drop, however the cooling becomes less efficient because the flow and velocity in the channel decrease, leading to a laminar flow. The turbulent flow eddies at higher velocities and the consequence is enhancing heat transfer when compared to laminar flow. Therefore, as first approach in the design, is considered that all the channels are in series performing a zigzag housing jacket. This allows more flow rate in all channels and turbulent flow is achieved. The concern is in the fluid velocity, because highest velocities may wear out material surface due to particles in the coolant.

In a water jacket application the coolant temperature could be different from outside ambient. For a transient analysis, fluid may be run through the machine for a certain period to reach a steady state temperature before starting the transient. However, there is no indication by the team on this variable, which is very dependent of the outside cooling system and the radiators efficiency. As first approach the ambient temperature of 40 ºC was used for inlet temperature of coolant (**Tinl**). This is not a bad approach for competitions with short performing time, like autocross or acceleration. However for endurance more care is needed here.

5.4.2. Axial Vs Spiral Water Jacket

To make the decision about the ducting system to implement in the housing, the main options to analyze are axial and spiral ducts. Both are standard enough to guarantee a feasible solution at good

price, using well known industrial procedures. The axial water jacket has more advantages in this geometry taking into account the channel area available for same channel number. This can be understood in the mechanical point of view. The spiral structure is done connecting the duct defined on housing top with duct defined on bottom, performing one channel. Then this structure is repeated along the axial length, forming a group of channels with a certain shape in the azimuth cylindrical direction. This means that channel width is dependent on the axial length. On the other hand, with axial channels the duct geometry is defined in radial cross section and the channel is extended along the axial direction. The connections between the channels are performed with "end-knees" in the end cap structure. This means that channel width is dependent on the machine perimeter. Therefore, if perimeter is higher than axial length, the axial structure guarantees best behavior regarding the water flow across the ducts. In fact it's what happen in this project, as can be seen in the results depicted in section 4.5.4, where is easy to check that machine perimeter is higher than total motor length (**Mlgth**). Next picture give geometry illustration in this two different approaches.

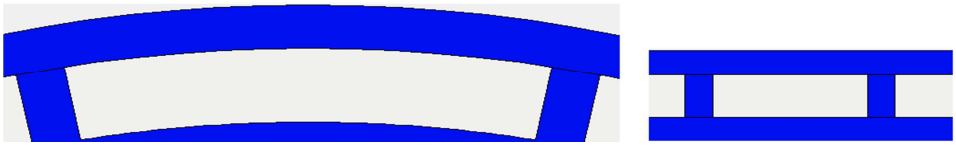

Figure 5.3 – Ducting system: Axial duct (left); Spiral duct (right).

The results obtained at steady state operation for the working point defined are exposed in next table. It confirms the previous considerations and helps to select the best ducting system. The simulation was performed for the same ducting geometry, flow rate definition, **Q**, **Tinl**, **Ppch**. Geometry variables regarding fin, cover and base aluminum thickness were the same as defined in section 5.4, as well as the channel height. The channel width has changed to attain the same channel number in both configurations and perform the comparison for same conditions.

Duct System	TWhs (ºC)	TWav (ºC)	TMag (ºC)	ReC (%)	Flow Type	Vf (m/s)	Ph (kPa)
Axial ducts	**110.4**	**104.5**	**91.1**	**289.1**	**Turbulent**	**0.74**	**5.22**
Spiral ducts	**109.3**	**103.5**	**90.2**	**455**	**Turbulent**	**1.3**	**26.2**

Table 5.2 – Comparison results: Axial ducts Vs Spiral ducts.

The first thing to note is that temperatures are very similar in both strategies so the selection criteria will not be for this side. The advantage will be on fluid flow characteristic, like expected regarding the previous discussion. In fact, the less area available in spiral ducts allows achieving the same turbulent flow at the expense of a much higher pressure drop due to the increase of duct wall resistance. Both flow types are turbulent which has to be a demand in the project, however the same temperature profile is achieved with axial ducts guaranteeing a small critical **Re** (**ReC**). This means that for axial ducts it's not necessary such a turbulent flow as it is in the spiral system to attain the same temperatures. The natural consequence is lower velocity and pressure drops in channels, performing a balanced flow across the housing, as can be consulted in appendix E.3. These reasons justify the choice for axial water jacket system.

5.4.3. Channel Geometry

The last performance considers the channels with rectangular shape. However there are several geometries that can be performed. The most common are circular and rectangular therefore a comparison between both is interesting to define which one will be used. In simple terms, rectangular ducts are expected to be better because there is more area available for flow. This also means that less material is present which bring advantages in the weight. It's expected that to perform an equivalent thermal performance with circular ducts more channels are needed to increase the useful area to dissipate heat. The weight could be higher due to more material present between channels.

Once housing water jacket cooling type was selected, several simulations were made with different dimensions for circular ducts in order to compare with the same rectangular channel analyzed in last section. The simulation conditions and initial variables are the same for those explained in last section. The next picture illustrates 4 different geometries analyzed.

Figure 5.4 – Circular channels: Circular 1, Circular 2, Circular 3, Circular 4 (left to right).

On the left, the ducts diameter was performed to the maximum in order to fulfill the same frame thickness used in rectangular channels of last section. The next pictures in the right shows a progressive increase in the frame thickness, namely 9.5 mm; 10.5 mm and 12 mm respectively. The objective was check the effect of diameter increase and consequently on area. The following table compact the results and allows taking conclusions.

Geometry	TWhs (ºC)	TMag (ºC)	ReC (%)	Flow Type	Vf (m/s)	Ph (kPa)	Mw (kg)
Rectangular	**110.4**	**91.1**	**289.1**	**Turbulent**	**0.74**	**5.22**	**10.33**
Circular 1	**108.4**	**89.5**	**646.2**	**Turbulent**	**1.51**	**50.2**	**10**
Circular 2	**110.6**	**91.3**	**525**	**Turbulent**	**1**	**7.5**	**10.8**
Circular 3	**109.7**	**90.5**	**466.7**	**Turbulent**	**0.78**	**6.4**	**10.52**
Circular 4	**110.7**	**91.3**	**381.8**	**Turbulent**	**0.52**	**2.1**	**10.6**

Table 5.3 – Comparison results: Circular ducts Vs Rectangular ducts.

All solutions give a turbulent flow which is a good starting point. The high **ReC** gives good indications about the nature of turbulent flow and for all solution states that laminar flow limit is widely passed.

The lightweight solution corresponds to the system *circular 1*, seen on the left in figure 5.4. It permits achieving a little bit less temperature in winding and magnets at expense of a higher pressure drop in the housing. In fact is the ducting system that leads to a higher pressure drop mainly due to the high duct wall resistance associated with the small area available. In this system there is almost no space between the circular ducts to achieve a similar thermal performance when comparing with rectangular channels. This means that are necessary 50 channels connected in series to attain a little better thermal performance and a small reduce in the weight, comparing with 16 channels for the rectangular system. In practical terms, such system is more difficult to implement and therefore more

expensive, mainly due to the small spacing between the circular ducts to implement the “end-knee” connection. For this reason such system is not worthwhile.

The next ones have better behavior regarding the pressure drops due to duct area increase created by the housing thickness enlargement. However the consequence of place more material is increase the weight, which is already in the limit required by the team. The system *circular 3* is the best from that series exposed. The thermal performance is very similar to the rectangular channel, a little bit better due to the improvement in fluid velocity (**Vf**). However is a little bit heavier and have the same drawback with the channels number because is required to connect 30 in series. This means that the small improvement in the thermal performance doesn’t compensate all the next drawbacks, even more when the weight is in the limit. This justifies the option for the rectangular channel system.

5.4.4. Channel Dimensions

For this machine is already stated that the best cooling is a zigzag water jacket with rectangular channels in axial direction. To optimize this structure it’s only needed to define the best channel dimension to perform the best thermal and fluid flow behavior. In section 5.4 some basic definitions were stated regarding the mechanical manufacturing. However the fin thickness was not referred because the channel type was not defined. This dimension can be depicted by means of figure 5.3 and in order to maximize the channel area and use the less material possible, is desirable to employ the thinnest fin. Regarding manufacturing constrains, 2 mm is a standard value to start. Fixing the channel height in the maximum, the thermal performance of the machine at steady state could be analyzed by means of a sensitivity analysis. This allows assessing the impact of parameter change in the thermal model by variation of a single or multiple parameters. Selecting one parameter turns the analysis more simple to optimize the design. The best way is check the ratio fin pitch/thickness (**Fpt**), because once fixed the fin thickness is possible to increase the channel width by increasing **Fpt**. The next graph shows the variation of pressure drop in the housing with **Fpt** increase.

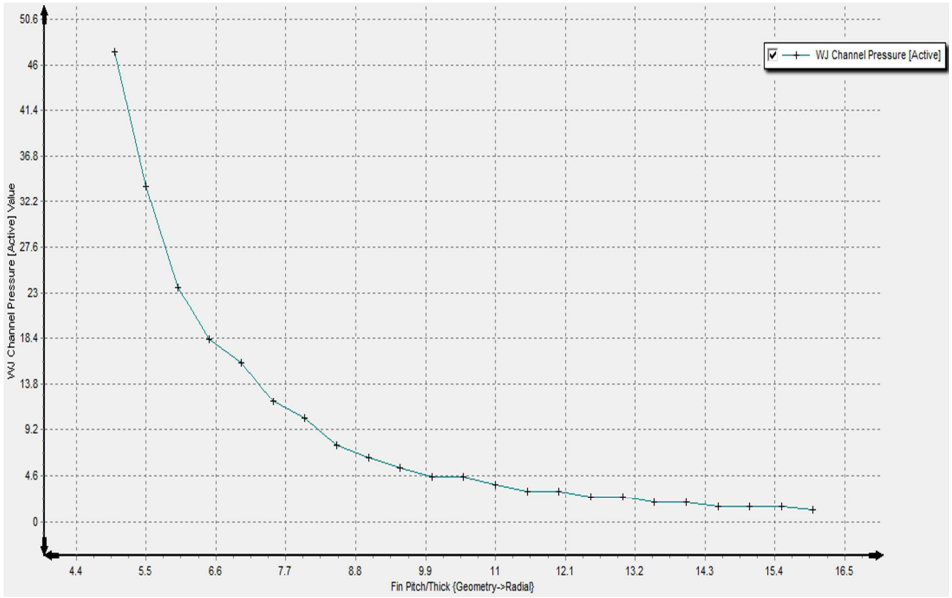

Figure 5.5 – Sensitivity analysis: Ph Vs Fpt.

As analyzed in the previous sections, when the channel width is increasing the pressure drop decreases. When **Fpt** is superior to 10, the variation is less pronounced so is important to check if the same thing happens with **Vf** to establish the best relation between velocity and pressure drop.

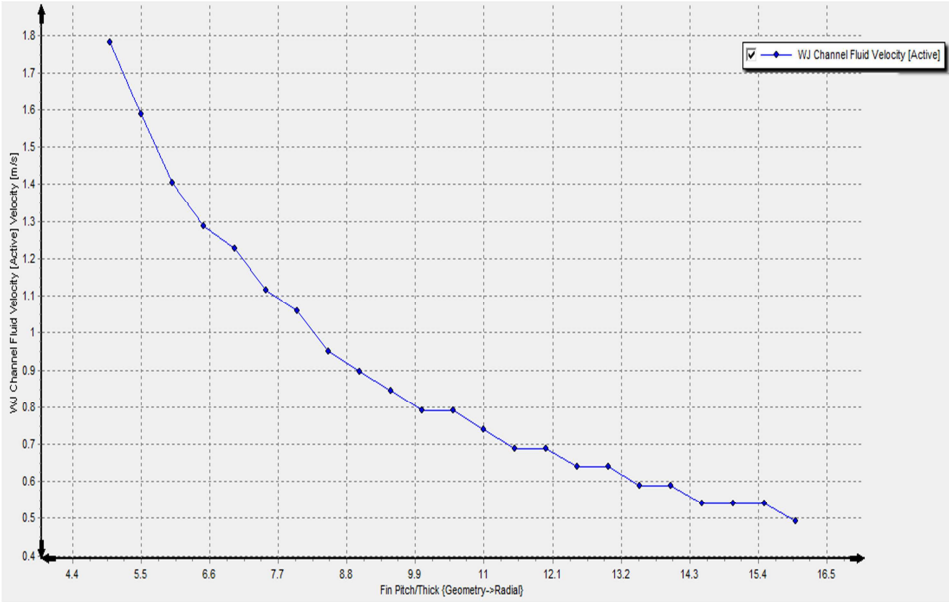

Figure 5.6 – Sensitivity analysis: Vf Vs Fpt.

In the same way, the velocity in the channel decreases with area growth. Is important to have high values of velocity to get a better **h**, however is good practice in construction to keep values around 1 m/s. When **Fpt** is superior to 10 the velocity decrease by steps, which indicate that further reduction don't represent necessary a great improvement in fluid flow. The temperature variation in the critical machine components, winding and magnets, allows for final conclusions.

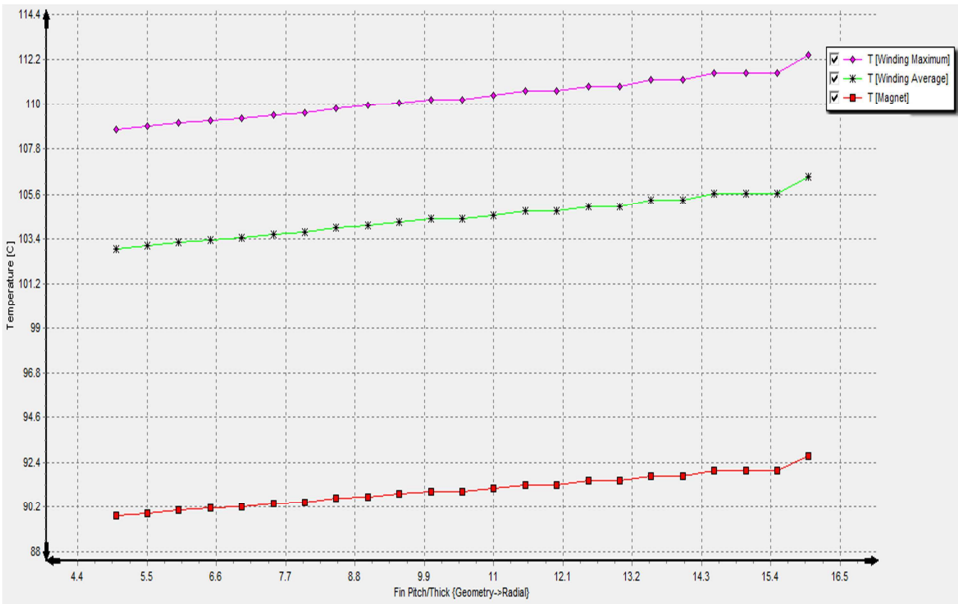

Figure 5.7 – Sensitivity analysis: Temperature Vs Fpt (Pink – Winding hot spot; Green – Winding Average; Red – Magnet).

Magnet temperature is not too sensitive to **Fpt** as the average and hot spot winding temperature. As analyzed before, the minimum temperature is reached when **Vf** is higher due to the high value of **h** attained. When **Fpt** is equal to 11 the temperature attained is in the middle of maximum and minimum for each component. As this value is in the range for the analysis taken in the last two graphs, the channel width can be defined for **Fpt** equal to 11 resulting in a zigzag water jacket with 16 channels.

5.5. Sensitivity Analysis

Sensitivity analysis can be used also to check the magnet and winding temperature dependence to tolerances and manufacturing constrains. The most common critical points in a machine cooled by water jackets will be presented in next topics. The analysis is done for the same working point taking into account the geometry already defined for the housing water jacket.

5.5.1. Housing – Lamination Gap

As discussed in section 5.2.3, a special concern is needed with interface gap between housing and stator lamination to guarantee the better contact with cooled housing and iron. The next graph shows how sensitive the thermal performance is to this variable.

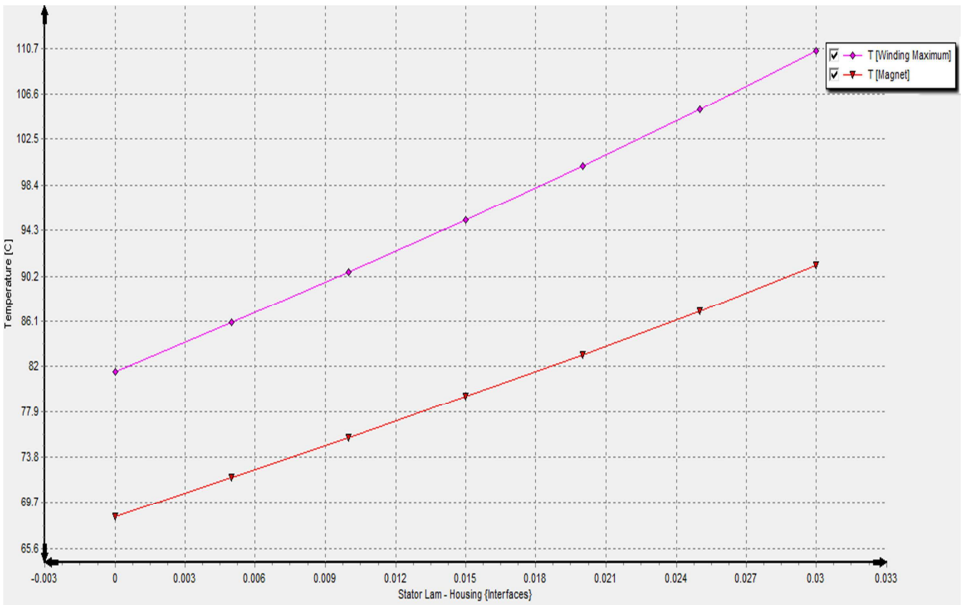

Figure 5.8 – Sensitivity analysis: Temperature Vs IG_sh (Pink – Winding hot spot; Red – Magnet).

The interface gap used in performance calculations considers an average manufacturing process and the value for interface gap between stator and housing (**IG_sh**) is 0.03 mm, as can be consulted in appendix E.6. If a perfect contact is considered, the temperature reduction in winding hot spot and magnet is 30 ºC and 20 ºC respectively. This confirms the great impact already expected. One way to improve the thermal performance and minimize the impact of this contact resistant is using heat paste

sink. That procedure typically reduces the interface gap **IG_sh** from 0.03 mm to 0.01 mm which allows achieving a temperature reduction in winding hot spot and magnet of 18 ºC and 14 ºC respectively.

5.5.2. Liner – Lamination Gap

This interface is more critical when there is no impregnation in the winding. Considering that heat dissipation in this region is done by conduction, if air is present between stator iron and liner the thermal contact resistance will be much higher due to the less thermal conductivity of air when compared with impregnation materials. Next graph illustrates temperature variation for this winding.

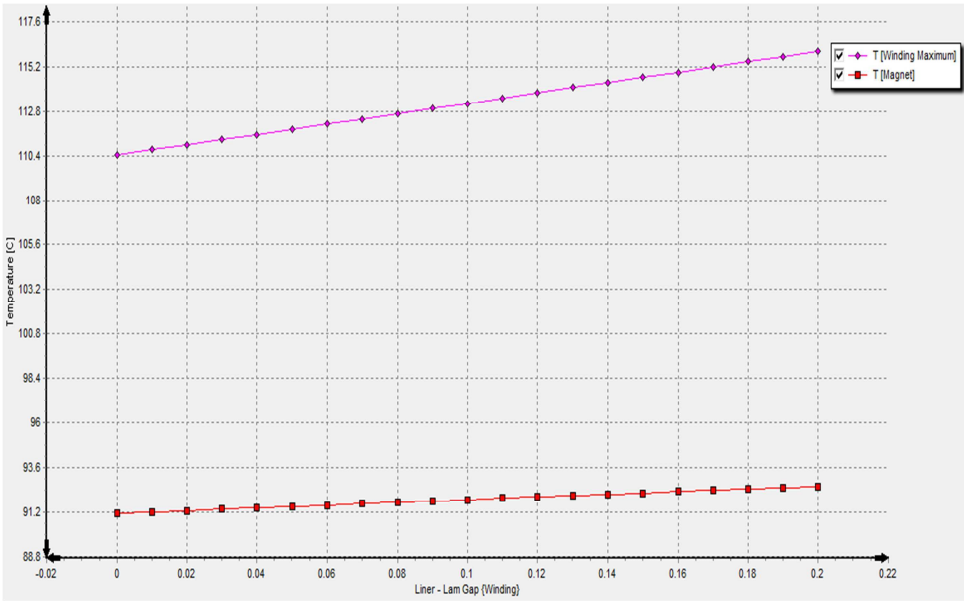

Figure 5.9 – Sensitivity analysis: Temperature Vs IG_ls (Pink – Winding hot spot; Red – Magnet).

Magnet temperature is not so sensitive to this interface gap, as expected. Winding hot spot temperature increase at 6 ºC between perfect contact and interface gap between liner and stator (**IG_ls**) equal to 0.2 mm. The difference is apparently lower due to the impregnation material used, Dobeckan® LE 6500, which has a very good thermal conductivity. The use of Nomex® as slot liner helps to reduce this gap because aramid paper absorbs very well the impregnation material. Both arguments allow defining **IG_ls** as zero without losing rigor in the common practical results.

5.5.3. Water Jacket Inlet Temperature

This variable is only dependent of coolant cooling system. Due to the leakage of information about this value, a sensitivity study is important to verify how much impact it has in steady state performance. It can be stated that a transient operation, defined by different duty cycles, is more appropriate to describe the machine behavior along the different trials in competition. However, steady state operation represents a worst case scenario and an easy way to perform a trend analysis. Next graph shows the temperature variation.

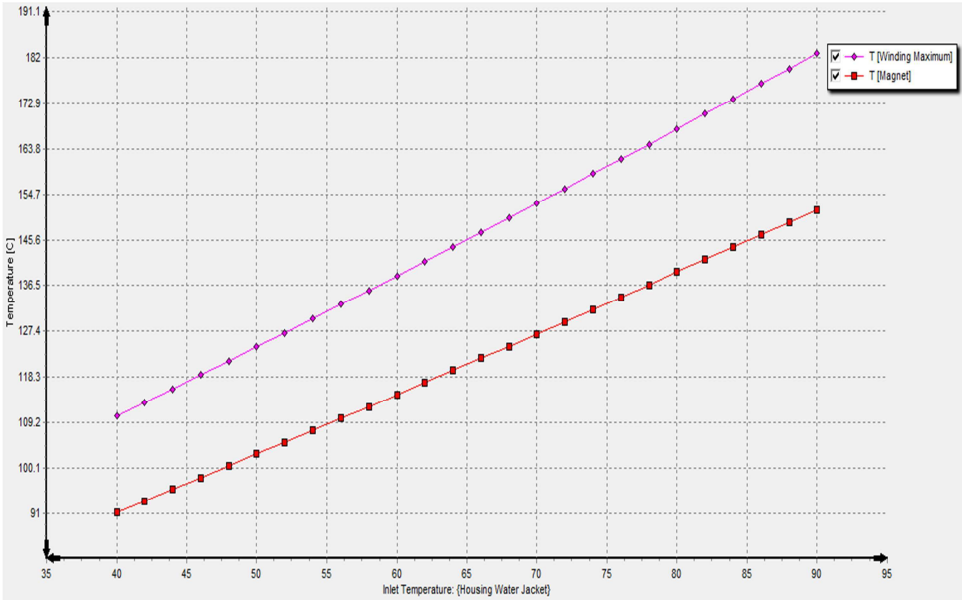

Figure 5.10 – Sensitivity analysis: Temperature Vs TinI (Pink – Winding hot spot; Red - Magnet).

This variation observed states the expected great dependence of cooling system performance related to inlet temperature of coolant. If inlet temperature in steady state is 90 ºC, the winding hot spot attains maximum temperature allowed for class H. Temperature difference comparing with current simulation conditions is around 70 ºC, for winding hot spot, and 60 ºC for magnets. There is no right or wrong value for **TinI**, all are possible. The cooling type available to coolant will determine it. The major influence in terms of transient analysis is in the endurance trial because it has a large duration and coolant can attain a temperature much higher than ambient.

5.6. Construction Details

Prototyping phase is not the aim of this work, however this project has the purpose to construct the machine designed. It's therefore advisable laboratory testing to verify the methods of calculation used in the design by means of measuring certain parameters. Some simple procedures that can be executed in a standard machine lab could be consulted in [4] with the purpose of measuring: machine's inertia, winding resistance, **EMF**, cogging torque and different inductances.

In section 4.2.1.4 this topic was approached to note the main manufacturing solutions that can be used to improve the machine's performance. It's also important to focus construction hypothesis to implement the water jacket cooling and give improvement for winding and impregnation.

5.6.1. Water Jacket Channels

As defined in thermal project, the housing water jacket is based in axial channels all connected in series to perform a zigzag system. The machine's **2D** cross section in appendix B.1 shows the final shape to perform in the aluminum. An extrusion process is the first approach to attain the objective by means of a mold injection with the channel geometry. This is a simple way to obtain the 16 channels

around the aluminum cylinder. The channels connection with “end-knee” can be done in a second finishing process, in weld shop or in other extrusion process by means of a mold with the “end-knee” required. Aluminum’s anodization can be done in the end using the common chemical treatment.

5.6.2. Temperature Sensors

This subject is very important in machine control and monitoring the winding current temperature conditions. This topic is intended to give a placement suggestion, between several hypotheses that can be considered. The simpler and standard is place one sensor for each phase in the winding hot spot, which can be determined using **FEA** like depicted in section 5.3.2. Then one sensor for each end winding is placed in front and rear parts. The mounting is done when the wound of machine is being processed and impregnation is performed with sensors already in place.

5.6.3. Winding & Impregnation

The winding designed in chapter 4 has **Sp** equal to 2 so to manufacture it is planned to use a 3-needle machine. This winding all 3 phases simultaneously, indexing after each coil is completed to the next coil rotation with continuous interconnections of magnet wire. This type of winding machinery can even make automatic terminations. Then end turns are usually formed and tied before varnishing the entire wound, completing stator assembly. The exterior winding connection can be done avoiding a board connector in order to optimize the weight. A single cable with 3 phases grouped can be done.

Impregnation process is necessary to provide a heat conduction path from the inner copper turns to the lamination stack and eliminate movements of adjacent turns as current is switched on and off. Moreover, is necessary to provide a higher dielectric strength than that of the air which would otherwise lie between the turns of insulated magnet wire. Therefore impregnation method has to be selected to ensure adequate penetration of the impregnant and an impermeable construction. The 3 main methods used are: dip or flood impregnation, trickle impregnation and **VPI**. Dip method is frequently used in low voltage machines by simply soaking the motor into the resin and then curing it in an oven. It’s easy and cheap to implement, however is common that impregnating agent gets coated on unwanted parts of the winding so this method it’s not adequate for the high performances required. The trickle impregnation is used also in small machines where a thin jet of impregnating resin is poured on to preheated and rotating winding. The resin penetrates through the winding and gets polymerized in short time. This method attains good quality in impregnation but there is limited amount of liquid and film property data available for trickle and this process don’t guarantee complete impregnation in the difficult areas. For this reasons, **VPI** is the adequate method to use. It’s directed to special machines with purpose designed insulation, such as machines driven by inverter drives and coils requiring high quality impregnation. The pre-dried winding is placed in an impregnant chamber which is then evacuated to very low vacuum. Impregnation agent is fed in till complete submersion of winding. For further penetration dry compressed air or nitrogen pressure is applied after breaking vacuum. In the end of process, finishing varnishes are used to give an enveloping coat over the exposed impregnated winding for additional protection against moisture and dust [74].

6. Results

This chapter presents the results that exhibit machine's performance in different aspects: steady state performance defined with **Psh** equal to 25 kW at **Nc**; duty cycle analyses for all competitions; performance charts, efficiency and thermal maps.

6.1. Steady State

Once defined the best cooling system in last chapter, is possible to have a real idea about motor's performance at steady state using the current cooling strategy. By means of **GoTAR** routine is easy to perform an iterative loop where **PC-BDC** losses are exported to Motor CAD and temperatures exported to **PC-BDC** until convergence is obtained. This is done due to losses dependence on temperature and vice versa. The parameters used to judge convergence are winding and magnet temperatures as well as copper and iron losses. The allowable convergence error defined between calculations was 0.5 %. Next table summarizes the most important **EM** and thermal results.

Variables	Results
WireDia	1.432 mm
Rph20	25.9 mΩ
LDiff	0.047 mH
Ld	0.3288 mH
Lq	0.38 mH
Kw1	0.827
Ks1	0.955
Psh	25 kW
Tsh	39.8 Nm
Nc	6000 RPM
J	14.2 A/mm^2
η	95.45 %
WCu	869 W
WFe	302.3 W
WMag	3.1 W
δ	42.5 º
PF	0.737
Vll1	224.2 V
Dtot	116 mm
Mlgth	212 mm
Wt_Tot	7.72 kg
Mw	10.33 kg
RotJ	8.56 E-4 kg.m^2
Ph	5.22 kPa
Vf	0.74 m/s
ReC	289.1 %
Tlf	283 years
TMag	91.1 ºC
TWav	104.5 ºC
TWhs	110.4 ºC
Twjo	45 ºC

Table 6.1 – Steady state: PC-BDC and Motor CAD results.

Analyzing the results and starting by those related with **EM** project, is clearly seen that **Nsh** defined in section 4.5.4 improve the wire diameter, reducing it. Global diameter is the same but is attained with more strands, so one strand diameter is less that when **Nsh** was equal to 1. Copper losses have a dominant effect over all the others, which is normal in heavily loaded machines. Nevertheless the phase resistance represents a low value for common machines with same size and reflects the advantage of using few slots. This enables to decrease the phase resistance and reducing the highest weight that copper losses have in the overall performance. The effect of using skew is reflected in **Ks1** which decrease **EMF** by 4.5% when compared with unskewed result. This will reduce output torque in same way and maximum power density, however it has to be done to guarantee a sinewound machine. The strategy followed for **Ppth** allows exploring the machine drive in a higher speed range, as depicted in section 4.5.1. To prove it, is seen that **RMS** fundamental line voltage (**Vll1**) is much below of voltage limit established by six step in 180º electrical. The difference gives good margin to explore the machine until the maximum speed of 9000 **RPM**.

Regarding the overall dimensions and weight, it can be seen that main team goals in this topics are achieved. The total diameter is less than 12 cm and total motor length is around 20 cm. It's important to note that end caps are not optimized so the 21 cm exposed can be reduced without great difficult to 20 or even more. The same can be said with total motor weight. It's a little bit higher than 10 kg, however the bearings that will be really applied are lightweight than those simulated and end cap thickness can be less. Moreover, slits can be introduced in the shaft to reduce weight, which is a common practice in the mechanical point of view.

Regarding thermal performance variables it's important to note the high efficiency attained, which demonstrates the importance of an extreme cooling strategy in a high performance machine. Fluid flow parameters as well as critical components temperatures were depicted in section 5.4.3, therefore same conclusions are valid here. It's useful to check in appendix E.3 the diagram that illustrates fluid flow and the pressure drops across the housing.

The high value of insulation life time attained is explained by the winding hot spot temperature and good thermal resistance of class H insulators. In a typical lifetime curve for class H, when the hot spot is 120 ºC the life time corresponds to $1e^6$ hours, which means 114 years. Therefore for 110 ºC the increase is a little bit higher than double. These values are only indicative and reflect the continuous operation of the machine in the working point analyzed. Other interesting result can be seen in the lumped thermal circuit of the machine exposed in appendix E.8. The water jackets dissipate 1.08 kW in housing active part and 50 W in the front and rear parts. This means that water jacket dissipation (**Pwjd**) is 1.18 kW, which represents a great performance of this cooling strategy. Moreover, the temperature increase of coolant relative to **Tinl** is 5 ºC and can be considered a good value at steady state operation. It's also possible to check that radiation process has more influence in heat transfer to ambient that natural convection cooling. This is normal when housing material has good emissivity.

In appendix B.1 and B.2 can be depicted the final dimension of MM03_V3 prototype, with radial and axial **2D** cross sections respectively, obtained with AutoCAD® software.

6.2. Duty Cycle

Thermal analysis for complex duty cycles is increasingly important in a variety of applications. The two main types of transient calculations are: simple transient and duty cycle. While in simple transient losses are fixed, in duty cycle losses inputted are varying as defined for each competition in analyses. To obtain reliable data, a Matlab® simulation program was developed by the team. Such script is intended to simulate with accuracy the car performance for endurance, autocross and acceleration trials. The results obtained are based in a quasi-stationary simulation that accounts with car operation limits. They are determined by its mechanical characteristics, including the electric machine designed, and limits of longitudinal, lateral and combined acceleration. The analytical models used in this Matlab® simulation have basis on mechanic systems dynamics and these results were validated on track with FST04e. The output for each competition is 3 vectors: torque, speed and time. This means that for each time computed, the value of torque and speed obtained represents the behavior that car has to develop to fulfill the team requirements for such trial tested.

As losses depend on temperature and temperature on losses, is advisable to develop a script using Matlab® or Excel® to directly connect **PC-BDC** and Motor CAD, taking advantage of Windows® Active X. For each torque-speed point obtained in simulation algorithm, is necessary to run **PC-BDC** and **PC-FEA** to calibrate the models in case of saturation and calculate all the components losses. Then, these values are passed to Motor CAD by means of **GoTAR**, in order to perform the transient analysis and actualize **PC-BDC** models with the correct temperatures for that time transient. Losses calculated for such period are used to perform the duty cycle analysis, repeating the process until the end of time vector. This is an automated way to deal with such problem, where too many points are involved and implying very laborious execution by “hand”. In industry is also typical performing this procedure by means of cluster computers in order to face the high number of calculations involved. In this project and mainly due to the leakage of time to perform such demanding scripts, some simplifications were assumed for each trial as function of results observed. Team is only interested in final transient temperatures obtained in winding and magnets and not so much in their evolution along the duty cycle. This helps to perform the necessary simplifications in models and check the worst case scenario. To perform duty cycle analysis is considered as initial condition that all machine components are at ambient temperature of 40 ºC and no changes on it are considered.

6.2.1. Acceleration Competition

The program output for this trial consists in 75 points for torque-speed values. The simulation considers that with this machine the competition will be completed in 3.73 seconds. Since the number of points is not too high, a Matlab® script was developed to calculate the average power used in this trial and performing some simplifications to setup duty cycle. The idea was sampling program output and instead of calculates a duty cycle with 75 points, compress the vector and execute the same duty cycle for 15 points. This means that each group of 5 points with torque-speed information is calculated in one by means of torque and speed average. It’s not expected to obtain great error as the time duration is short and the sampling value is low. Using this procedure is possible to input each value in **PC-BDC** and calibrate machine model to saturation using **PC-FEA**. Losses values are passed to

Motor CAD and duty cycle is performed for each time step, giving information for temperatures to be applied in the next simulation using **PC-BDC**. A script could be done to execute this procedure, however 15 points is not too much to perform all calculations by "hand". Next figure shows an example of duty cycle obtained.

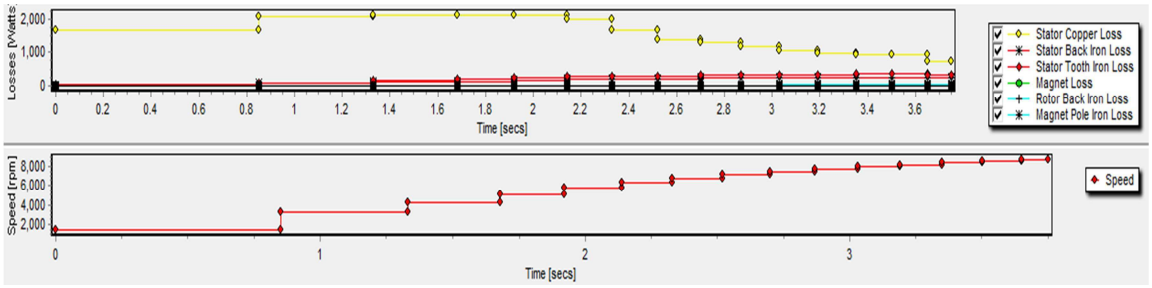

Figure 6.1 – Duty cycle analysis: Duty cycle for acceleration competition.

Next table summarize the important results regarding this simulation. As referred, only the final components temperatures are exposed. The average power in this trial is 36.36 kW.

Variables	Results
TMag	40.1 ºC
TWhs	46.6 ºC
Twjo	45 ºC

Table 6.2 – Duty cycle analysis: Acceleration competition results.

Due to the short competition duration, is observed that values are very close to ambient temperature. However, the average power developed is high and at some points **Tpeak** is attained. This states that cooling system is good enough to team perform this trial with best performance.

6.2.2. Autocross Competition

The program output for this trial consists in 813 points for torque-speed values. The simulation considers that with this machine the competition will be completed in 97.5 seconds regarding the 2 laps involved. Due to high number of points used, the simple approximation depicted in acceleration competition can't be used. The average torque for this case leads to a big error because losses vary with torque square which states that compressing the points using the mean value is not reliable. The procedure adopted was developing a script in Matlab® to check how much time the machine is saturated under this competition. Previous studies with **PC-BDC** and **PC-FEA** were done to check what was the limit torque developed that saturates the machine. Identifying these values in output vector was seen that machine is saturated during 32.8% of total time, which means 32 seconds. As the team is interested in a worst case scenario and the main goal of this test is check if machine handles the competition requirements, during this time was decided to applied the worst case regarding losses. This means that component losses applied correspond to **Ppeak** at **Nc**, which is a upper bound loss during that time. For the following 67.2% is assumed that machine operates with no saturation, therefore **RMS** torque can be computed to compress all torque points and the same is

done with speed that is averaged. The resulting point, 13.74 Nm at 3110 **RPM**, is checked in **PC-BDC** and **PC-FEA** for model adjustment, if necessary, and losses passed to Motor CAD to perform the duty cycle. This procedure is approximate but certainly represents a worst case scenario so the results are on the safe side. Next table summarize the important values regarding this simulation.

Variables	Results
TMag	42 ºC
TWhs	138.1 ºC
Twjo	45.6 ºC

Table 6.3 - Duty cycle analysis: Autocross competition results.

The results exposed confirm that machine equipped with the water jacket cooling system developed handles all requirements needed for this competition, even in a worst case analyses. Magnet segmentation and consequently the low losses developed, as can be depicted in section 6.1, allows low magnet temperature. The good winding impregnation improved with **VPI** allows achieving safe results in temperature, far from thermal limit.

6.2.3. Endurance Competition

The program output for this trial consists in 1138 points for torque-speed values. The simulation considers that with this machine the competition will be completed in 23.4 minutes. Due to high number of points, the same considerations about autocross trial can be taken here. A Matlab® script was developed to check how much time the machine is saturated under this competition. Preliminary results indicate that it occurs during 2.6% of time, which means 36 seconds. Facing this result, is a good approximation scorn the saturation effects and compact all the results in one point, calculated by means of **RMS** torque and speed average. To compensate this approximation and perform a worst case scenario, the mandatory stop depicted in section 1.2 is not applied which means that trial is done continuously. The equivalent point to analyze in duty cycle corresponds to 17.25 Nm at 4068 **RPM** and same analysis with **PC-BDC** and **PC-FEA** was done to calibrate the machine model, passing the losses to Motor CAD. Next table represents the important results for this competition.

Variables	Results
TMag	54.2 ºC
TWhs	58.7 ºC
Twjo	45.6 ºC

Table 6.4 - Duty cycle analysis: Endurance competition results.

The magnet temperature is higher than in other competitions. This is mainly due to the long duration time that allows establishing the thermal time constants associated with this phenomenon. On the other hand, the winding hot spot attained is reduced for a long time competition. This is explained manly by the average power developed during this trial, which corresponds to 5 kW. In fact Matlab® program has also in consideration the fuel economy trial disputed during endurance and gives some optimization to maximize the final points, regarding all competitions. This justifies the low average power. As seen in section 6.1, this motor works at steady state for 25 kW at 6000 **RPM**. As the

average power in long competitions is lower, this means that machine and cooling system handles team requirements.

6.3. Performance Charts

In machine design is important to appraise machine performance across the entire torque-speed envelope that can include a field weakening region. Design optimization over this performance is challenging as all **CAD** tools available, like **PC-BDC**, only provide analysis at individual working points. It's therefore useful a computationally efficient technique that allows for rapid and accurate modeling of entire operational envelope of any **BPM** machine. Such solution was found with Motor LAB software from Motor Design Ltd©, a software package that takes advantage of Windows® Active X to connect **PC-BDC** and Motor CAD. It performs the calculation of torque-speed characteristics, loss and efficiency maps that can be used in an iterative design process. This approach is based on classical *dq* phasor model combined with polynomial expressions for flux linkage and loss. The required parameters for analysis are obtained from reduced set of **2D FEA** field solutions using **PC-FEA** embedded solver. This allows calibrating the analytical modulation done by **PC-BDC** automatically, without need to use visual match of **GoFER** routines. Such functionality is adequate when computational methods and scripts are developed to perform complex solutions. This allows taking into account the non-linearity of **ψd1** and **ψq1**, caused by saturation and cross coupling effects, enabling accurate loss modeling. The torque-speed characteristics and efficiency maps obtained with Motor LAB were validated against data provided for the 2004 Toyota Prius motor and measurements taken from an in-house 35 kW **IPM** traction motor, as can be consulted in [17]. The next flowchart illustrates the operating principle of Motor LAB software.

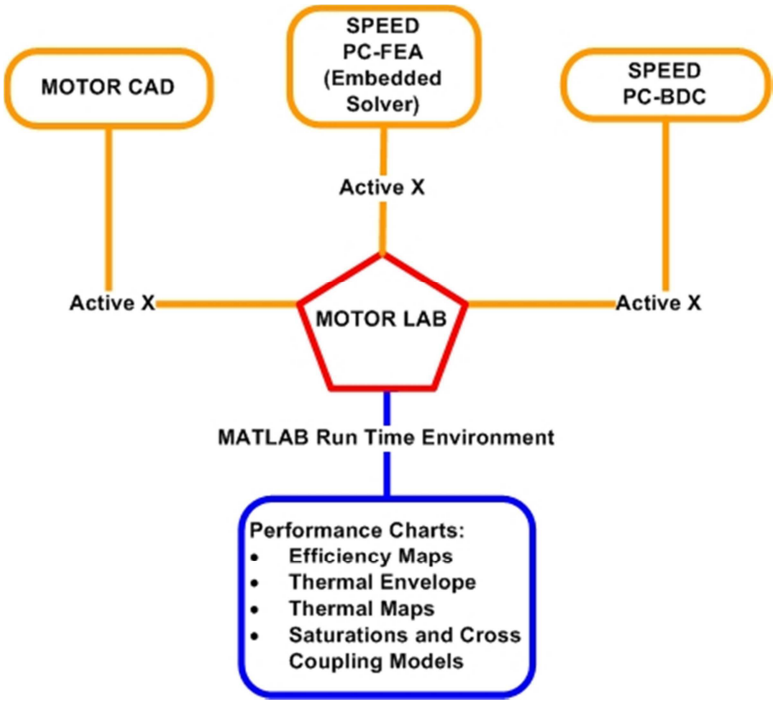

Figure 6.2 – Motor LAB workflow.

6.3.1. Fixed Inductance Model

Based on equations depicted in section 4.1, is possible to calculate the torque-speed characteristic constrained by maximum voltage available from the inverter and considering a linear inductance approximation to describe **ψd1** and **ψq1**. Mechanical, magnet and copper losses are calculated by **PC-BDC**, however iron losses are performed with Wrobel/Mellor iron loss model. It's a computationally efficient calculation that provides accurate iron loss prediction at any operating point from only two time-stepping **FEA** calculations: at short circuit and open circuit. This avoids the typical computationally intensive methods to calculate iron losses at single points, even more when a large number of operating points are needed for entire envelope. This method simplifies that procedure with very good comproved results. More details can be consulted in [17], [18].

Performance graphs obtained are considering a maximum speed of 10000 **RPM**, near from maximum required by the team. Current varies in 4 steps until its maximum of 267 Apk, which is the current that allows machine to develop **Ppeak** at **Nc**. Next graph shows torque-speed result.

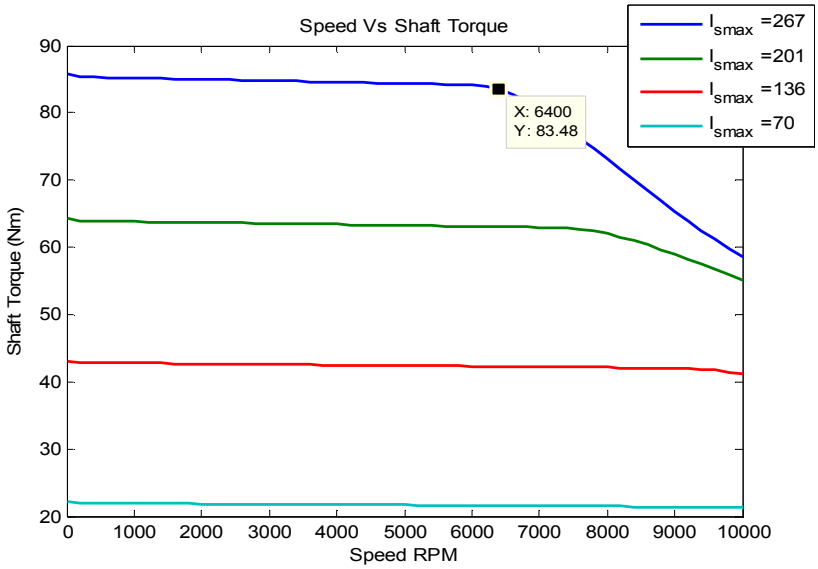

Figure 6.3 – Performance charts: Torque Vs Speed (fixed inductance model).

It´s seen that around of corner speed the maximum torque (**Tmax**) developed with peak current is 83.5 Nm, much higher than expected when compared to **Tpeak** of 67.64 Nm. Neglecting saturation effect, torque obtained is higher because **Xq** has the unsaturated value. Comparing these results with saturation and cross coupling modeling could be useful to understand its viability.

6.3.2. Saturation & Cross Coupling Model

The linear approximation used to describe flux linkage doesn't account for cross coupling and saturation effects. Therefore, this calculation may not be fit for purpose when modeling at high operating currents or in field weakening region. The variation of **ψd1** and **ψq1** with both current components is accurately described by second order polynomial functions as given [17]. A computation comprising 15 **2D FEA** solutions which contain 5 distinct values of **Iq1** and 3 distinct

values of **Id1** provides sufficient data to calculate those polynomial function coefficients, using a least squares fitting method [17]. Results obtained are exposed in next figures.

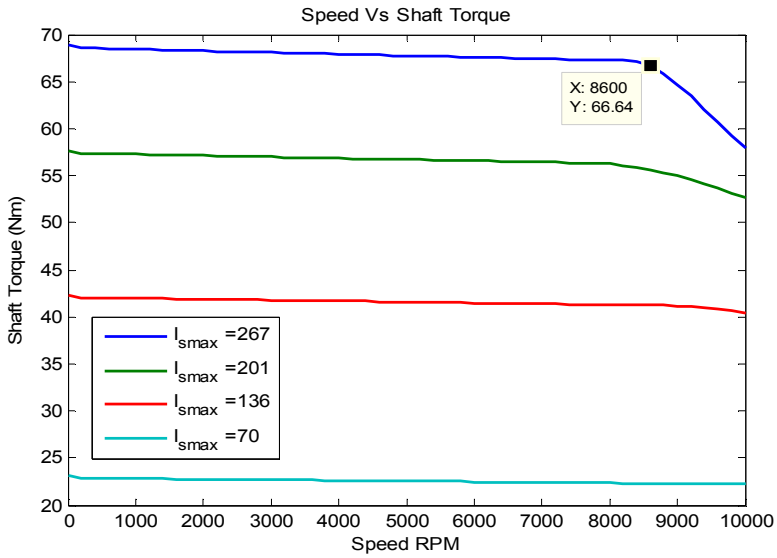

Figure 6.4 – Performance charts: Torque Vs Speed (saturation & cross coupling model).

Comparing the two results is possible to see that **Tmax** is around 66.64 Nm, more close to **Tpeak**. This reveals the importance of considering saturation effects and concerns approached during chapter 3 and 4 to perform good calibration of analytical models by means of efficient ways to compute torque using **FEA**. Constant inductance model is only accurate in absence of saturation, at low values of current or during field weakening. It can be comproved on the graph when **Isp** is 136 Apk. Moreover, due to **Xq** saturation corner speed increase to 8500 **RPM** which confirms that best practice is perform machine design for entire torque-speed envelope and not for a single point. Several effects are occurring at same time and this analysis allows a quick look for machine performance.

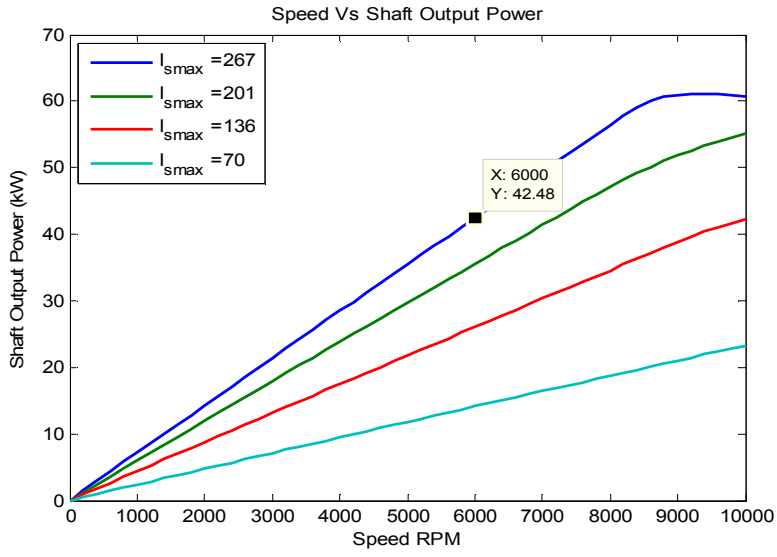

Figure 6.5 – Performance charts: Power Vs Speed (saturation & cross coupling model).

This characteristic confirms that **Ppeak** is attained at 6000 **RPM** like required, independently of corner speed increase due to saturation effect. Considering field weakening is possible to achieve maximum power (**Pmax**) of 62.5 kW at 10000 **RPM**, which is the machine limit, defining a power density of 6.3 kW/kg. Moreover, is possible to check that machine is operating in the current limited region (Mode I) and voltage and current limited region (Mode II) when **Isp** is 267 Apk. In Mode I input voltage rises linearly with speed and is desirable to operate with **γ** that maximizes torque, taking advantage of reluctance. In Mode II when inverter reaches maximum modulation depth at corner speed of 8500 **RPM**, **γ** is further advanced relative to the initial value. The result is a larger magnitude of negative **Id1**, which demagnetize the field and reduces both **ψd1** and **ψq1**, allowing higher rotational speed for same voltage. The torque is reduced and power is constant, however as this machine has reduced saliency it's not possible to explore field weakening beyond 10000 **RPM**.

6.3.2.1. Efficiency Maps

The proposed techniques implemented with Motor LAB software turn also possible to plot the efficiency characteristic over the full torque-speed envelope, performing an efficiency map. This is very useful to understand where the ideal exploration regime of machine designed is.

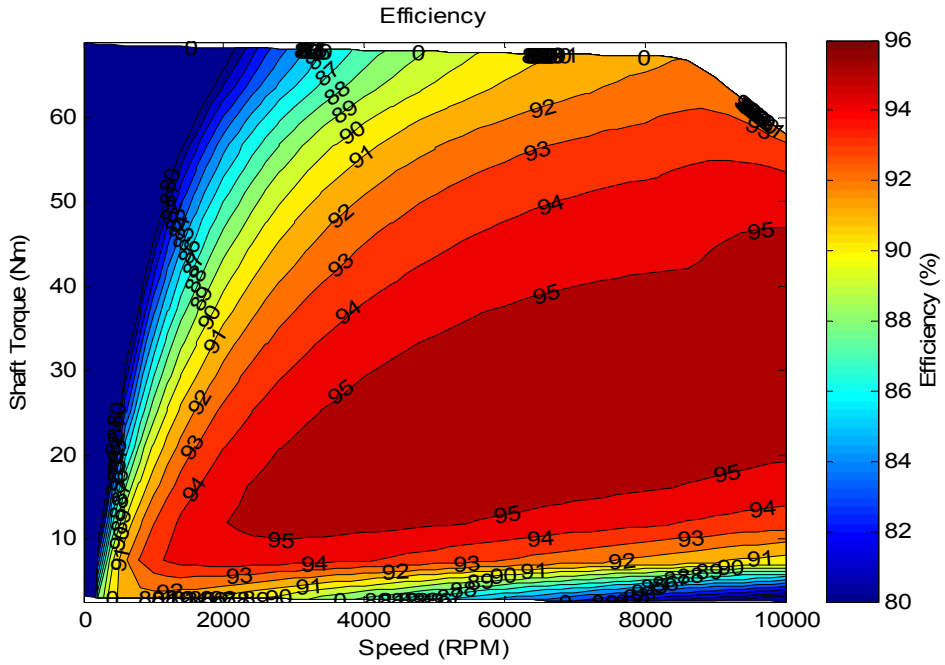

Figure 6.6 – Performance charts: Torque Vs Speed (efficiency map).

At high speeds is possible to achieve a larger spectrum of efficiency in torque-speed characteristic. This is due to the highest weight of copper losses at low speeds because copper losses are constant in Mode I and II. Therefore at high speeds and with more power developed, the relative value of this loss is decreased and efficiency increase. The ideal working point for the machine, corresponding to an efficiency of 95%, can be achieved in a large speed spectrum between 2000 **RPM** and 10000 **RPM**. This represents a good standard for a variable speed drive and gives very

good indications for fuel economy competition. In endurance trial **RMS** torque is 17 Nm and analyzing the efficiency map is possible to see that this value is attained with efficiency above 90% for almost all speed ranges. The same map in power-speed envelope is useful to take more conclusions.

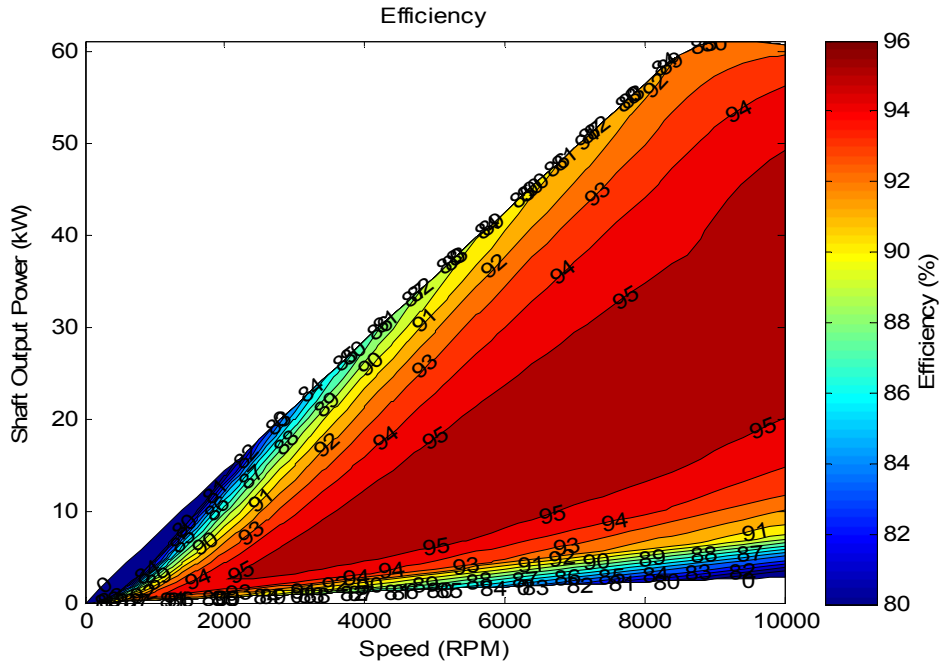

Figure 6.7 – Performance charts: Power Vs Speed (efficiency map).

The contour plot shows a big area between 90 and 95% of efficiency which is a very good result, mainly in **Ppeak** at **Nc** where machine attain approximately 91%. In autocross competition the average power is 16 kW and contour plot shows that is possible to attain such result with efficiency superior to 90% between 3000 **RPM** and 10000 **RPM**. This is a very comfortable margin and gives good perspective for fuel economy competition.

6.3.3. Limit Envelope

This study is directed to understand the machine limits at steady state and transient operation. This issue is dependent on thermal performance and insulation class used, so the procedure was perform calculations with the techniques developed considering that winding hot spot is always fixed in the thermal class H limit, 180 ºC. Then is possible to verify the maximum power-speed envelope developed and efficiency attained.

This is done both for steady state and transient analysis. However the idea of transient limit is to understand how much time machine handles **Ppeak** at **Nc**. Previous studies done on Motor CAD reveal that machine can handle the peak regime required by the team during 80 seconds. This means that in the end of this time, winding hot spot is at 180 ºC. This was performed by means of a duty cycle where all losses calculated by **PC-BDC** were loaded in Motor CAD in steps of 5 seconds. After running the transient, **PC-BDC** model was updated for those temperatures attained. This was repeated until the machine gets the limit temperature in winding.

6.3.3.1. Steady State

The following graphs illustrate the limit envelope.

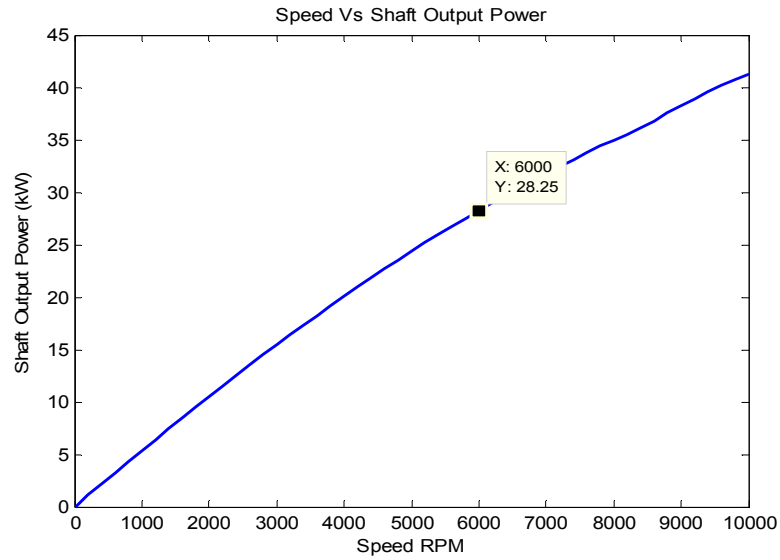

Figure 6.8 – Performance charts: Power Vs Speed (steady state limit).

The steady state limit power achieved at 6000 **RPM** is 28.25 kW, a little bit above from the 25 kW defined. This result is very important because all data obtained using Matlab® scripts developed in duty cycle analyses indicates that average power is much below this limit. This confirms that machine is good enough to support all the performances demands in autocross and endurance competition. For acceleration trial only transient limit envelop can give more conclusions because this kind of competition has the specificity of exploring **Ppeak**. It's also possible to define **Pmax** at steady state limit, which corresponds to 42 kW at 10000 **RPM**.

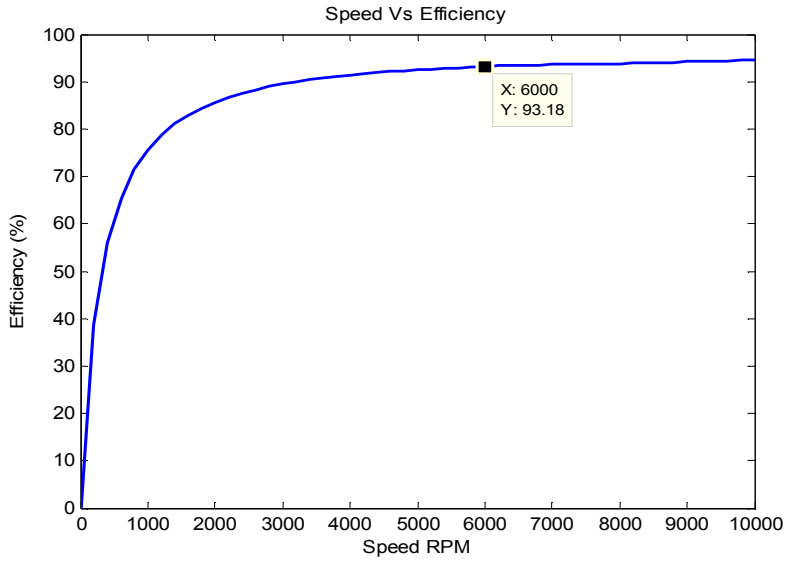

Figure 6.9 – Performance charts: Efficiency Vs Speed (steady state limit).

Machine efficiency within steady state thermal limit for 6000 **RPM** is 93.2%. This is a great result and gives good indications in the battery management point of view, such as analyzed in contour plots section.

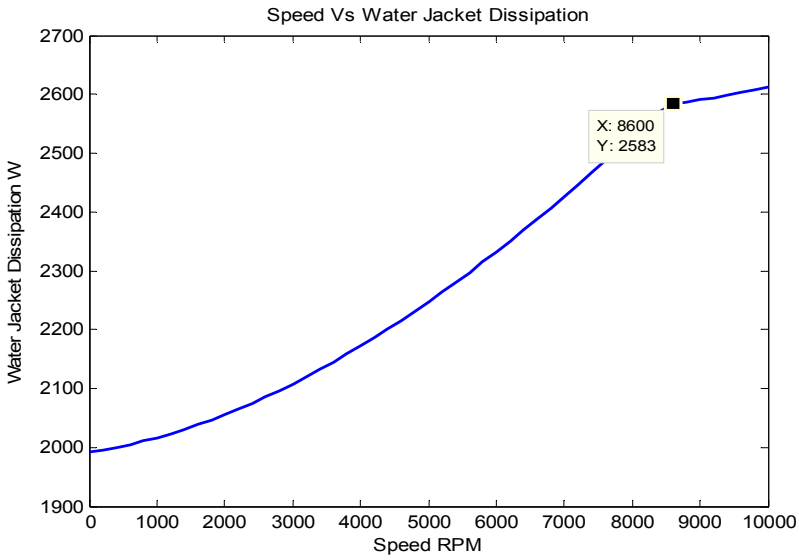

Figure 6.10 – Performance charts: Water jacket dissipation Vs Speed (steady state limit).

This graph depicts very well the cooling system capacity. As this machine is very small, with a length of 21 cm and diameter of 12 cm, approximately, it's fact that has few area to dissipate the heat for such high power densities involved. The extreme cooling solution developed shows that at **Pmax** in steady state, 42 kW at 10000 **RPM**, housing water jackets are dissipating 2.6 kW. This highlights the cooling system performance for such high **TRV** machine.

6.3.3.2. Transient Operation

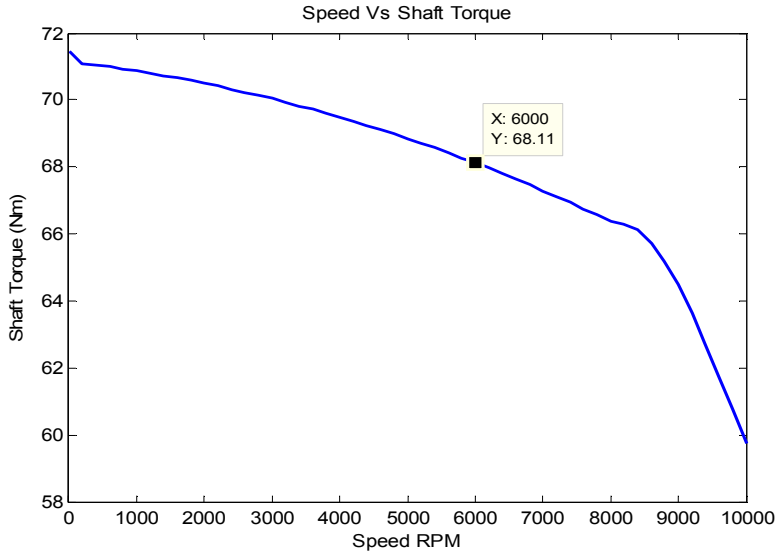

Figure 6.11 – Performance charts: Torque Vs Speed (transient operation limit).

This analysis is necessary to evaluate the capacity of machine to develop **Ppeak** during a certain time. Torque-speed characteristic indicates that the motor develops 68.11 Nm at 6000 **RPM** continuously for 80 seconds. This result is very close from **Tpeak** of 67.64 Nm when a duty cycle analysis was performed in Motor CAD to avail the transient limit capacity of machine during the same time. The results concordance gives good indications for previous calculations made. The machine guarantees a large margin of safety in exploration of **Ppeak**, mainly used in acceleration competition as it has to be concluded before 4 seconds. The 80 seconds obtained are large enough to guarantee good performance and not excessive overheating as concluded in duty cycle analyses. The only limitation is related to mechanical issues like wheel slippage due to excessive torque at low speeds.

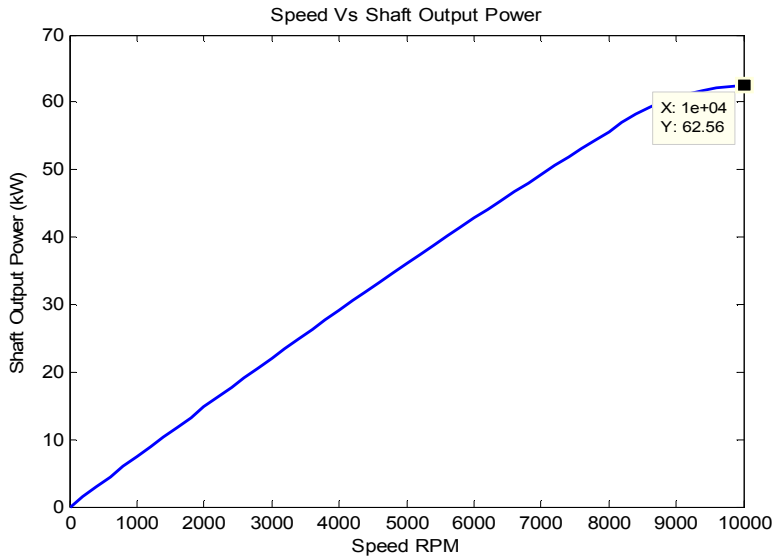

Figure 6.12 – Performance charts: Power Vs Speed (transient operation limit).

The **Pmax** that is possible to achieve and maintain during these 80 seconds is defined at 10000 **RPM** and value is 62.5 kW. It's an interesting result because the same 80 seconds represent the thermal limit to maintain **Ppeak** fixed in 42.5 kW at **Nc** and the maximum power limit at maximum speed.

Following two graphs exhibit the same variations as depicted in steady state. The first relates efficiency with speed, attained for all working points during these 80 seconds transient. It´s possible to check that **Ppeak** at **Nc** is attained with 91.5% of efficiency. As in acceleration competition the time is too much less, is expected to achieve higher efficiency than this. The second relates water jacket dissipation with speed. Dissipation values are not so high because the time involved in transient is less than machine thermal time constant. However is possible to check that peak value of **Pwjd** corresponds to 2 kW, which is very high taking into account the considerations referred in steady state analysis.

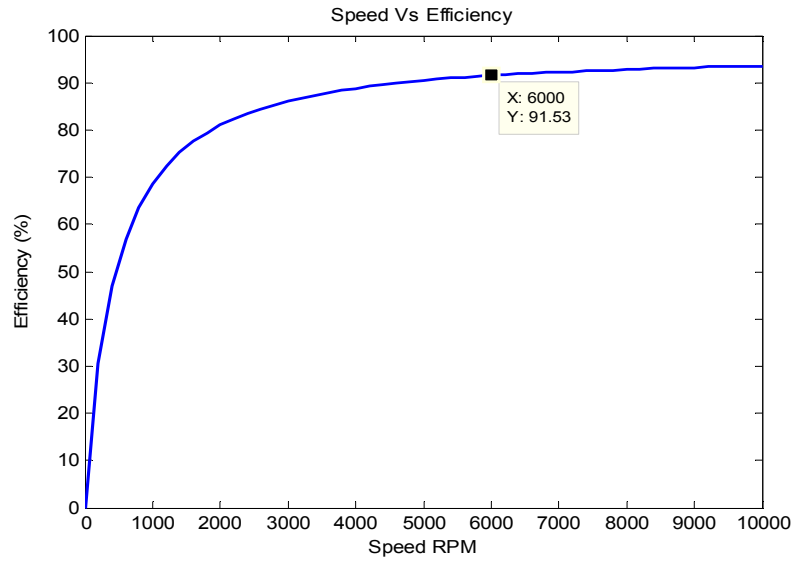

Figure 6.13 – Performance charts: Efficiency Vs Speed (transient operation limit).

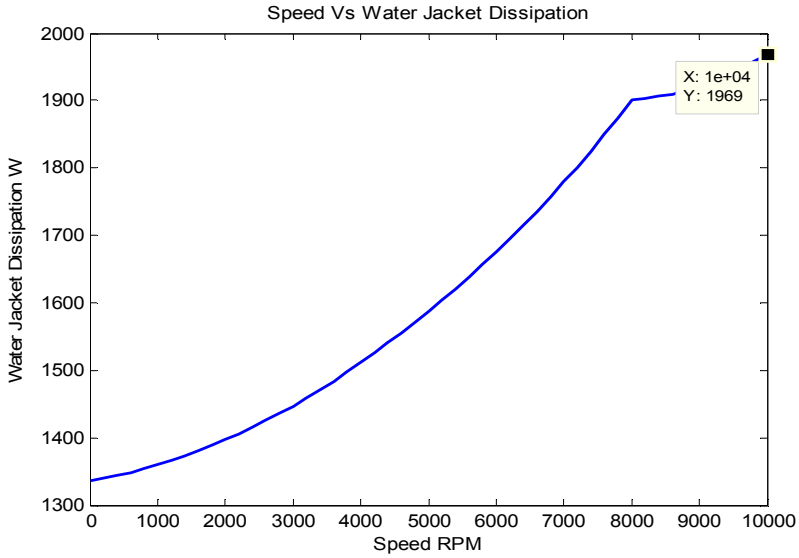

Figure 6.14 – Performance charts: Water jacket dissipation Vs Speed (transient operation limit).

6.3.4. Thermal Maps

When these techniques are coupled with thermal modeling by means of introducing Motor CAD in the chain represented in figure 6.2, is possible to generate thermal maps to define the continuous and transient operating envelope of machine designed. This will be presented for steady state to give illustration of qualitative results. Same conclusions can be taken to transient operation on that ground.

Next picture shows winding hot spot variation depicted in torque-speed characteristic.

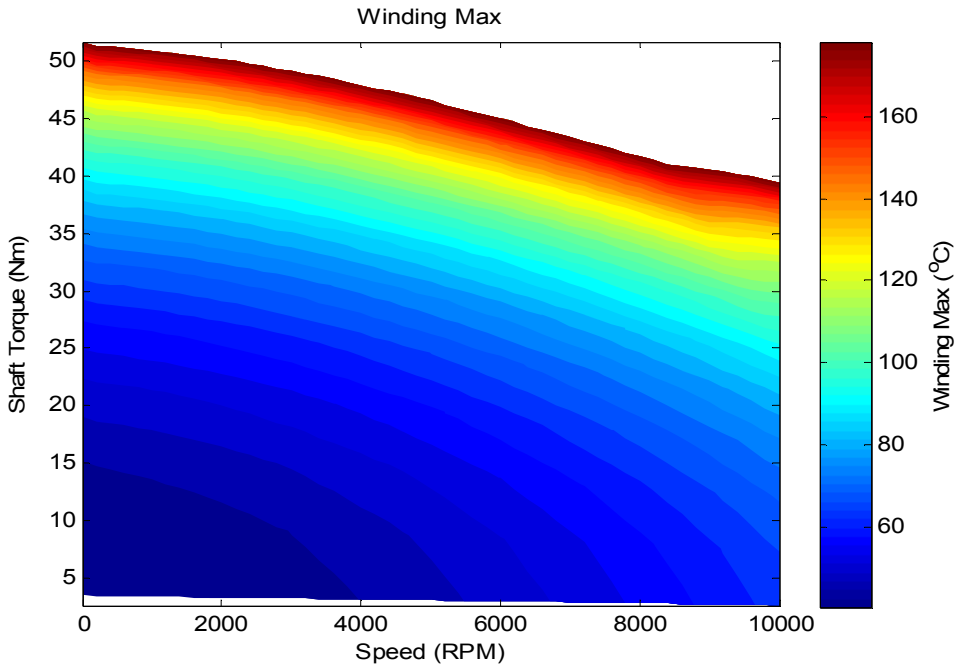

Figure 6.15 – Performance charts: Torque Vs Speed (winding hot spot thermal map).

This thermal map shows that the winding hot spot temperature increase with machine load. This is expectable because torque is proportional to current and temperature increase with current square. So every time that maximum torque is achieved, the maximum hot spot will result independently of speed value. In terms of power-speed chart it results that at **Pmax**, maximum hot spot is verified for all speed range.

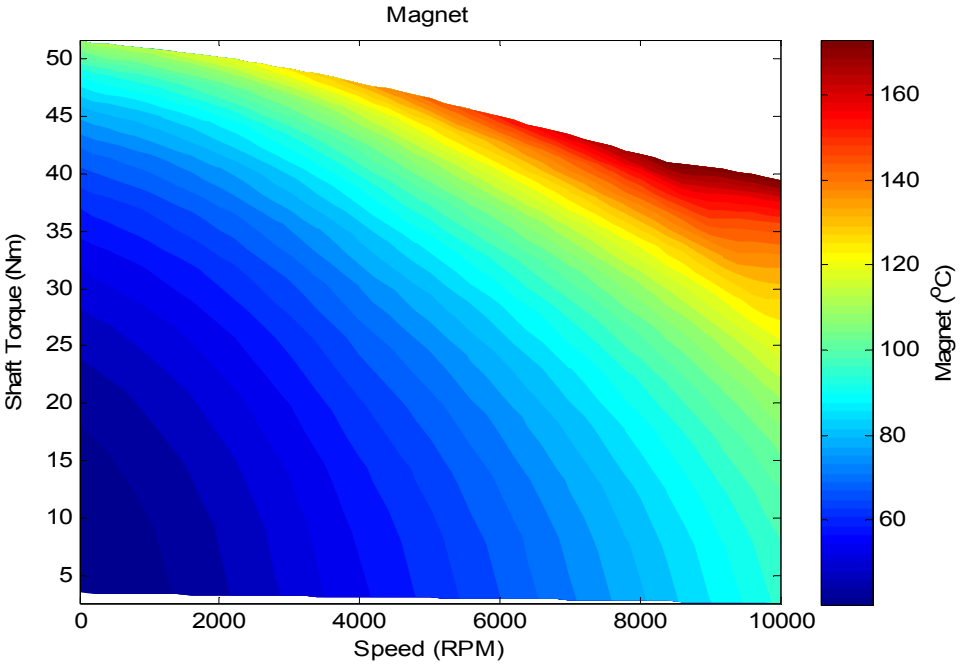

Figure 6.16 – Performance charts: Torque Vs Speed (magnet thermal map).

Highest magnet temperature is verified at high speed and load envelope. This is due to **fsp** effect, which means that higher speed leads to higher **fsp** and consequently high flux pulsation in magnets. As the eddy currents are resistance limited, an increase on them will increase magnet losses and so the temperature.

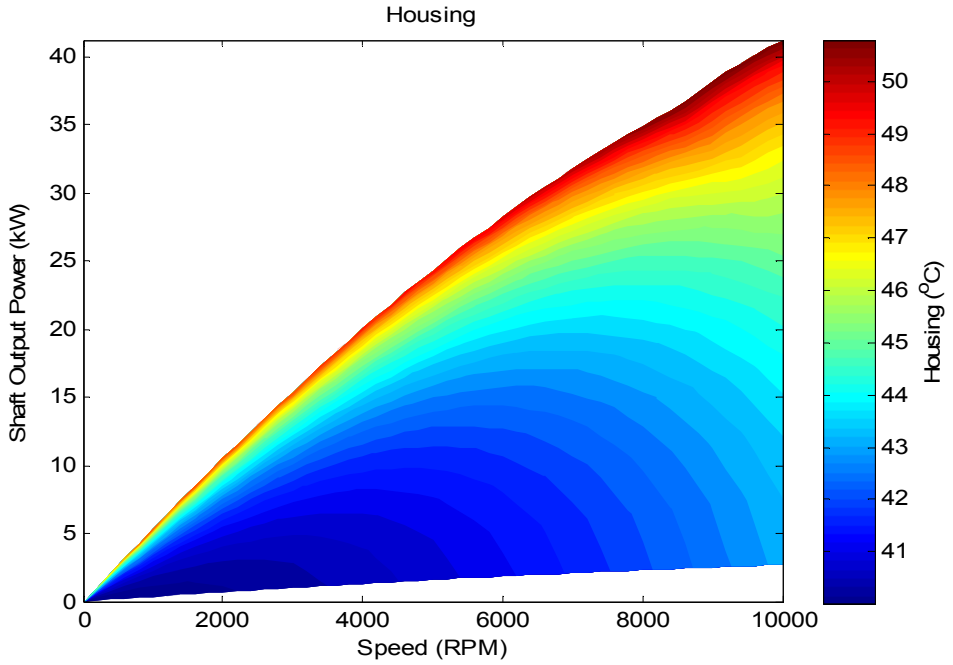

Figure 6.17 – Performance charts: Power Vs Speed (housing thermal map).

The lowest housing temperature is of course limited by water inlet and in this case is 40ºC. Water temperature will attain the maximum at **Pmax**. This is an expected result because at such working point iron losses are high due to great speed and cooper losses are high due to current. The dissipation occurred will increase the housing temperature, until 50 ºC, in **Pmax** at 10000 **RPM**.

6.4. Other teams' machines

This finishing subchapter has the purpose to give an overview about the machines developed in other formula student teams around the world. At the present, the leading teams on this feature are AMZ racing from Switzerland and DUT racing from Netherlands. The first exhibit in 2012 the new "*Umbrail*", a formula student car equipped with 2 **AC BPM** out-runner motors with **Ppeak** of 40 kW. Anyway, changes are planned to an **IPM** machine. The team from TU Delft University has been achieving very good positions in competition. The new DUT 12 is equipped with 4 **BPM** motors cooled with a spiral duct water jacket system developed in partnership with AMK. Each machine develops **Ppeak** of 28 kW and weights 4 kg, which results in a power density of 7 kW/kg. Since the power density of MM03_V3 prototype is 6.3 kW/kg, good indications about **EM** and thermal design process have to be taken. This motor is in the same range of the bests developed, which gives good perspectives for future competitions results to *Projecto FST Novabase*.

7. Conclusions

This work presents the complete virtual prototyping of a brushless **AC** machine with interior magnets. This design was made after an intensive research in the last 6 months in order to achieve the necessary knowledge and tools to fulfill the team requirements in the project, after a first approach not so well succeeded.

This prototype achieves all the specification requirements given, in the peak power and weight, as well as the goals for all the contests involved in the formula student competition. It has also power density very close to the other machines already constructed by another formula student teams.

It was possible to check the advantage of use this spoke rotor type, mostly in terms of weight because with this geometry it's possible to avoid a rotor with a massive iron. Results indicate a reduction relation of 1:3 and much better moment of inertia, 1:28 reduction comparing with Agni 95R.

In the electromagnetic point of view, the torque ripple attained could be considered acceptable for this application, on the grounds that car inertia filters most of those variations. Although electromagnetic noise and vibrations can result, this kind of subject isn't as important as with servo-motors design or other applications where high position precision is required.

To eliminate cogging torque, a skew angle was needed and the results were good not only in the cogging cross off but also in the filtering effect of the harmonic content relative to the air gap field. This enables a sinusoidal flux linkage and a better **EMF** waveform, reducing the initial torque ripple.

Another important issue about the fractional slot winding was the guarantee of an unbalanced magnetic pull in the rotor in order to avoid mechanical problems, which was achieved with Papst design.

In the cooling system, the sensitivity analysis performed let concluded not only about the ideal dimensions of water jackets channels but also to the main constrains in the machine construction. The robust analysis made indicate a great dependence on the winding temperature of interface gap between housing and stator lamination. This effect can be mitigated using heat sink paste to reduce this interface.

In the ducting system, the water velocity and the pressure drops across the housing channels have very good values, according to the average duct wall roughness considered in the aluminum alloy used. So there is no problem with particles in fluid to wear away the surface.

The intensive cooling strategy and the thermal class of the machine, improved with vacuum impregnation, allow the achieving of high power density. A very good behavior in the thermal limits was proven in last chapter by means of thermal maps and thermal envelope limit analysis at steady state and transient operation.

The superior limit peak performance is 62.5kW @ 10000 **RPM** (6.3 kW/kg) during 80 seconds, which is a superb result for a machine with 10 kg. It's important to note that such accomplishment is only possible due to the iron alloy used in the project and sintered **NdFeB** magnets. Such high power densities in small machines require low loss irons as well as high saturation polarization, as achieved in VACODUR® 49. At the same time, big values of **Br** are needed to attain high values of open circuit field in the air gap and with it, higher **Eq1**. The sintered **NdFeB** magnets are the strongest and should be used to attain these goals.

7.1. Improvement Topics

As machine design for such high performance vehicle is a very complex and iterative procedure, at first sight could be said that this machine is oversized for the application, on the grounds that maximum power limit is not used. Taking this into account and due to the leakage of time to present some improvements in the design, this sub-chapter will present some ideas based on the background attained with the project developed. Then, the next step is applying it in a future design to achieve a lightweight motor.

1) The final results in steady state and mainly the transient results, as they are the most important to the team, shows that the final temperature in the magnets is far from the maximum temperature allowed for the grade N35AH, 220ºC. So in the iterative design process could be a good approach to choose a magnet with higher energy product and a maximum working temperature around 180ºC, like UH series [14]. Therefore it is possible to reduce the magnet cost and increase the air gap field at open circuit.

2) Regarding what is required in the last point, it's important to note that the low losses on magnets are due to segmentation, which turns possible the temperature values attained. First of all it's important to better check the magnet losses with a transient solver using **3D FEA** software like FLUX. Applying the **2D** calculation, the assumption is that eddy currents do not run in a circle, because the whole length of the rotor is treated as a **2D** cross section. A first approximation with **2D** is useful but taking into account that magnet loose flux with the temperature increase, this issue has to be studied in more detail. Besides **3D** calculation, some analytical formulations to expand the **2D** magnet losses to **3D** could also be explored. The purpose is achieving the ideal number of segments, if their use is needed, because this particular implementation increases a lot the final price.

3) In the same way, it's also important to check the torque and flux linkage of skewed machine with a **3D FEA** tool. This kind of problem is a classical **3D** analysis as the skew angle is in the axial direction, however **PC-FEA** normally makes a good job with the sliced model. It could be interesting to compare both results.

4) Still regarding the losses, other important issue could be the skin effect. It depends of winding and conductor distribution in the slot, but as they have not been considered in this study it's important to check them using a dedicated **FEA 2D** tool. At high speeds the increase in the resistivity could not be negligible and as last resource *Litz* wire is needed, although it's undesirable as it decreases the slot fill gross. If any problem occurs with this phenomenon, the best is to correct the conductor position in the slot [7].

5) The maximum machine power is not being used by the team. Therefore this indicates that the iron weight can be decreased by reducing the tooth width for instance. This allows not only to consider the machine more saturated but also decrease the overall machine cost. The

maximum corner speed is also above the team requirements, so it is possible to increase the reactance of the machine, increasing the number of turns and with it reducing the necessary current. This procedure will reduce the corner speed and also improves the cooling system due to the current decreasing. Even if the resistance increases by the effect of put more turns to the same slot area, the copper losses varies with current square and this effect is always dominating.

6) About the winding layout in such high **TRV** machine, the best approach is using a non-overlapping end winding with **Sp** equal to 1. In this case the wound is around one single tooth, so is possible to reduce the **MLT** and with it the resistance and the copper weight. At the same time, the copper losses will be small and the improvement in the end space cooling is a natural consequence. Using a precision machine to make the winding is possible to achieve slot fill gross in the order of 60%, even 65%, using Nomex® as solid divider. In this current project, the overlapping type put some limits to achieve higher slot fill due to the mush nature of this winding. Moreover, concentrated winding simplifies the production, reduces the cost and can enable a low torque ripple. The only expense is that has to be made outside Portugal.

7) To increase the power density of machine could be interesting to explore other slots/pole combinations in conjugation with other design variables to avoid stator skew. The Papst design combination with short air gap leads to higher cogging torque and needs always skewing, which reduce the **EMF**. The cogging can be reduced mainly in two ways: adequate slots/pole combination or bifurcated tooth type. Increase the air gap for this application is not a feasible solution. So, maintaining the fractional slot strategy due to the reasons described in 4th chapter, will always be difficult to decrease the cogging with slots/pole combination. The **L.C.M** of slot and pole numbers is a low value which generally increases cogging. Therefore it's interesting to explore this in combination with bifurcated tooth and slot opening values. The main concern in all the trials is maintaining the **G.C.D** of slot and pole number superior to one, otherwise problems with unbalanced magnetic pull will emerge, as occur with 9s/8p combination.

8) Another possibility regarding the last point is skewing the magnets. Basically, stator iron surface faced a magnet has to be independent of magnet position. The ratio of magnet width to pole pitch has to be chosen so that the area of stator tooth tips covered by a magnet is constant, as the rotor rotates. This can be achieved skewing the magnets, cutting it into a certain number of pieces and shifting them. More study on this can be done using **3D FEA**.

9) Regarding mechanical parts, in order to reduce the machine weight, could be interesting consider some changes in the shaft geometry, namely from the solid type to spider type [19].

10) In the cooling system, it's important to have a more appropriate value of water inlet temperature in the channels. As determined in the sensitivity analysis, this value has a great influence in the overall thermal performance, so the higher this value, the greater the

maximum winding temperature. This is due to the increase of housing temperature, which reduces the cooling efficiency. The team could predict a steady state average value to consider in the project, depending of the cooling system of coolant and other variables in the flow system, like the number of radiators.

11) To improve the end space cooling could be considered wafters in the rotor, as sometimes is done with the induction machines, or potting on the end windings cavity. Also some **CFD** studies to calibrate the Schubert correlation could be interesting in the academic point of view. In fact, this is not a critical topic as the end winding temperatures are near the average winding temperature. Besides that, machine thermal class is enough high to give security in the end winding lifetime in such small machine, where the space between them and the end caps is short. These considerations are also in favor to implement a non-overlapping winding.

7.2. Future Work

The presented design was based on simple electromagnetic and thermal assumptions, developed along sophisticated tools and tested with software already used in other motoring applications in the industry. Nevertheless more work can be done in this subject but with a different approach.

Different ways of investigating optimum design are being developed all around. One good example is **BCS** software from SPIN Company at Italy. They use **SPEED** software to achieve the optimum electromagnetic design, based on the definition of design variables, constraints and objectives.

It's possible to avail some of benefits in the software used, mainly with Active X interface, to make some scripting in order to integrate the thermal and electromagnetic design together, working with **SPEED** and MOTOR CAD as a black box using MATLAB® or Microsoft® Excel. The **FEA** calibration could be done using **PC-FEA** embedded solver which permits to calibrate the **SPEED** analytical models in **EM** design, constrained to one or more objective functions. At the same time, MOTOR-CAD updates the **SPEED** thermal model and with this became possible to automate the iterative design described in section 3.4.

Such application could boost the machine project, exploring other solutions to the team in less time. For example, another interior magnet machine like V shaped magnet or the classical **IPM** with slits, used to buried the magnets in rotor slots and protect them better against magnet losses. The goal is to find the best configuration with less weight, given some initial constants, constrains and define the objective function to achieve the goal defined. Comparing the final results it could be interesting to check what the best machine is: the one with non-massive rotor steel like used in this design or other **IPM** with high saliency and slits? In the answer might be the next machine development.

Bibliography

[1] Guedes, M. (2011). *Battery management system for formula student.* Lisboa: IST

[2] Libert, F. (2004). *Design, optimization and comparison of permanent magnet motors for a low-speed direct-driven mixer.* Stockholm: KTH

[3] Institution of Mechanical Engineers. (2012). Formula student. In *Formula Student UK 2012*, Silverstone, 11-15 July, 2012

[4] Hendershot, J.R. & Miller, T. J. E. (2010). *Design of brushless permanent-magnet machines.* Florida: Motor Design Books LLC

[5] Martins, J. & Brito, F. (2011). *Carros eléctricos.* Porto: Publindustria

[6] Pyrhönen, J., Jokinen, T., Hrabovcová, V. (2007). *Design of rotating electrical machines.* Finland: Wiley

[7] Staton, D. & Popescu, M. (2012). *Design of brushless permanent magnet machines – training slides.* Ellesmere: Authors

[8] Miller, T. J. E. (2011). *SPEED's electric machines.* [S.I]:CD-ADAPCO

[9] Strauss, F. (1952, January). Synchronous machines with rotating permanent magnets fields. *Transactions of The American Institute of Electrical: Power Apparatus and Systems, Part III.* Vol. 71. (887-893)

[10] Merrill, F. W. (1954, January). Permanent magnet excited synchronous motors. *Transactions of The American Institute of Electrical: Power Apparatus and Systems, Part III.Vol.73. pp.1754-1760*

[11] Hershberger, D. D. (1953, January) *Design considerations of fractional horsepower size permanent magnet motors and generators. Transactions of The American Institute of Electrical: Power Apparatus and Systems, Part III,* vol. 72, (581-585)

[12] Vacuumschmelze. *Application notes*. CWIEME 2012. [S.I]: Author

[13] Vacuumschmelze.(2012). *VACODUR 49 datasheet*. CWIEME 2012. [S.I]: Author

[14] HPMG. *Magnets catalogue*. CWIEME 2012. [S.I]: Author

[15] Hanselman, D. (2006). *Brushless permanent magnet motor design.* USA: Magna Physics Pub

[16] Agni Motors. 95 series datasheet. *Agni Motors website*. Accessed June 3, 2012, in www.agnimotors.com

[17] Goss, J., Mellor, P. H., Wrobel, R., Staton, D. A., Popescu, M. (2012). The design of AC permanent magnet motors for electric vehicles: a computationally efficient model of the operational envelope. In *6th IET International Conference on Power Electronics, Machines and Drives (PEMD 2012)*, Bristol, 27-29 March, 2012 (1-6).

[18] Mellor, P.H., Wrobel, R., Holliday, D. (2009). A computationally efficient iron loss model for brushless AC machines that caters for rated flux and field weakened operation. In *Electric Machines and Drives Conference, 2009. (IEMDC'09).IEEE 2009*, Bristol, 3-6 May, 2009 (490-494).

[19] Staton, D., Hawkins, D. (2012). *Motor-CAD v7.1 manual.* Ellesmere: Authors

[20] Aerospace Specification Metals. Aluminum alloy 6061 properties. *Aerospace Specification Metals (ASM) Website.* Accessed August 5, 2012, in http://asm.matweb.com/search/SpecificMaterial.asp?bassnum=MA6061t6

[21] Aerospace Specification Metals. Stainless steel 455 properties. *Aerospace Specification Metals (ASM) Website*. Accessed August 5, 2012, in http://asm.matweb.com/search/SpecificMaterial.asp?bassnum=NCAR70

[22] Formula Student. (2012). 2012 Formula student rules. *Formula Student website*. Accessed June 18, 2012, in http://www.formulastudent.com/docs/fs2012-docs/fs2012-rules-final.pdf?sfvrsn=0

[23] Siemens. (2003) *SIMODRIVE: AC motors for main spindle drives*. [S.I.]: Authors

[24] Boglietti, A., Cavagnino, A., Staton, D. A. (2003). Thermal analysis of TEFC induction motors. In *38th IAS Annual Meeting. Conference Record of the Industry Applications Conference. IEEE 2003*, vol.2, 12-16 October, 2003 (849-856).

[25] *AMZ Racing Team website*. Accessed September 13, 2012, in http://www.amzracing.ch/

[26] Li, H. & Chen, Z. (2009, April). Design optimization and site matching of direct-drive permanent magnet wind power generator systems. *Renewable Energy: An International Journal*, vol. 34, (1175-1184)

[27] Polinder, H., van der Pijl, F. F. A., de Vilder, G.-J., Tavner, P. J. (2006, September) Comparison of direct-drive and geared generator concepts for wind turbines. *IEEE Transactions on Energy Conversion,* vol.21, (725-733)

[28] *K & J magnetics Inc website*. Accessed August 5, 2012, in http://www.kjmagnetics.com/

[29] M & M Resources International INC. (2007). *The standard of cold rolled grain oriented electrical steel.* China: Authors

[30] Miller, T. J. E. (2011). *SPEED PC-BDC 9.1: user's manual*. [S. l]: Author

[31] University of Glasgow. Bernard Hague. *University of Glasgow website.* Accessed August 5, 2012, in http://www.universitystory.gla.ac.uk/biography/?id=WH0207&type=P

[32] Miller, T. J. E. (2011). *SPEED PC-BDC GoFER: user's manual.* [S. l]: Author

[33] Miller, T. J. E. (2011). *SPEED PC-FEA 5.5: user's manual.* [S. l]: Author

[34] Miller, T. J. E. (2011). *WinSPEED 2011: user's manual for windows*. [S. l]: Author

[35] Miller, T. J. E. (2011). *SPEED tutorial B08: open-circuit EMF GoFERs in PC-BDC.* [S. l]: Author

[36] Miller, T. J. E. (2011). *SPEED tutorial B13: adjustment factors in PC-BDC.* [S. l]: Author

[37] Miller, T. J. E. (2011). *SPEED tutorial B18: eddy-current losses in magnets and rotor cans in PC-BDC.* [S. l]: Author

[38] Yang, S.-C., Lorenz, R. D., Suzuki, T., Jahns, T. M. (2010). *Surface permanent magnet synchronous machine design for saliency-tracking self-sensing position estimation at zero and low speed.* In *Energy Conversion Congress and Exposition (ECCE), 2010 IEEE*, Atlanta, 12-16 September, 2012 (3493-3500)

[39] Miller, T. J. E. (2009). *SPEED tutorial B23: PC-FEA transient solver.* [S. l]: Author

[40] Holman, J. P. (1997). *Heat transfer.* (2nd edition). New York: McGraw-Hill Companies

[41] Mills, A. F. (1999). *Heat transfer.* (2nd edition). U.S.A: Prentice Hall

[42] Staton, D., Boglietti, A., Cavagnino, A. (2003). Solving the more difficult aspects of electric motor thermal analysis. In *Electric Machines and Drives Conference, 2003. IEMDC'03. IEEE International*, vol. 2, Madison, 1-4 June, 2003 (747-755)

[43] Simonson, J. R. (1988). *Engineering heat transfer* (2nd Edition). [S.I]: Macmillan

[44] Gnielinski, V. (1976) New equations for heat and mass transfer in turbulent pipe and channel flow. *International Chemical Engineering*, vol.16, (359-368)

[45] Miller, D. S. (1990). *Internal flow systems.* [S.l]: BHRA

[46] Taylor, G. I. (1935). *Distribution of velocity and temperature between concentric cylinders.* [S.l]: Proc. Roy Soc

[47] Gazley, C. (1958, January) Heat transfer characteristics of rotating and axial flow between concentric cylinders. *Trans ASME*, (79-89)

[48] Hayase, T., Humphery, J. A. C., Greif, R. (1992, August) Numerical calculation of convective heat transfer between rotating coaxial cylinders with periodically embedded cavities. Trans ASME, (589-597)

[49] Högmark, C., Reinap, A., Frogner, K., Alaküla, M. (2012) Laminated winding with a rapid cooling capability for electrical machines. In *The International Conference for Inductive and Electromagnetic Components, Systems and Devices including Manufacturing and Processing, CWIEME,* Berlin, 26-28 June, 2012

[50] Vacuumschmelze. VACODUR 49 static virgin curve. *Vacuumschmelze website.* Accessed August 5, 2012, in http://www.vacuumschmelze.com/fileadmin/Medienbiliothek_2010/Downloads/HT/VACODUR_49_.pdf

[51] Loctite. Loctite 392 technical data sheet. *Loctite website*. Accessed August 5, 2012, in https://tds.us.henkel.com/NA/UT/HNAUTTDS.nsf/web/3B75570F803B272A882571870000D747/$File/392-EN.pdf

[52] Sumereder, C., Muhr, M., Körbler, B. (2003, May). Life time management of power transformers. In *e & i Elektrotechnik und Informationstechnik,* vol.120, (420-423)

[53] Miller, T. J. E. (2011). *SPEED tutorial B04: windings, EMF waveforms and harmonics.* [S. l]: Author

[54] Miller, T. J. E. (2011). *SPEED tutorial B05: slot fill factors in PC-BDC.* [S. l]: Author

[55] Zimmermann, O. (2012). ANOFOL, coils from anodized aluminum – the alternative to copper. In *The International Conference for Inductive and Electromagnetic Components, Systems and Devices including Manufacturing and Processing,* CWIEME, Berlin, 26-28 June, 2012

[56] Tremel, J. (2012). Flexible semi-automated - workplace for placing permanent magnets. In *The International Conference for Inductive and Electromagnetic Components, Systems and Devices including Manufacturing and Processing,* CWIEME, Berlin, 26-28 June, 2012

[57] Vandenbossche, L., Jacobs, S., Attrazic, E. (2012). New magnetic materials for rotating machines: an innovative approach of evaluation of the iron losses in magnetic laminations, applied to the optimization of highly saturated electric motors. In *The International Conference for Inductive and Electromagnetic Components, Systems and Devices including Manufacturing and Processing,* CWIEME, Berlin, 26-28 June, 2012

[58] Herget, F. (2012). New challenges for electrical steel. In *The International Conference for Inductive and Electromagnetic Components, Systems and Devices including Manufacturing and Processing,* CWIEME, Berlin, 26-28 June, 2012

[59] Volbers, N., Gerster, J. (2012). High saturation, high strength iron-cobalt alloy for electrical machines. In *The International Conference for Inductive and Electromagnetic Components, Systems and Devices including Manufacturing and Processing,* CWIEME, Berlin, 26-28 June, 2012

[60] Staton, D., Hawkins, D., Popescu, M. (2012) Practical strategies for improved cooling of electrical motors and generators. In *The International Conference for Inductive and Electromagnetic Components, Systems and Devices including Manufacturing and Processing,* CWIEME, Berlin, 26-28 June, 2012

[61] Holst, S., Anders, M. (2012). STAR-CCM+ and SPEED for electric machine cooling analysis. In *The International Conference for Inductive and Electromagnetic Components, Systems and Devices including Manufacturing and Processing,* CWIEME, Berlin, 26-28 June, 2012

[62] Lombard, P., Vayrette, J., Marion, F. (2012). Using analytical approach with finite element analysis for coupling magnetic and thermal analysis for motors. In *The International Conference for Inductive and Electromagnetic Components, Systems and Devices including Manufacturing and Processing,* CWIEME, Berlin, 26-28 June, 2012

[63] SKF. *Squeezing more efficiency from anti friction bearings.* Energy Efficiency & Technology website. Accessed August 5, 2012 in http://eetweb.com/mechanical-systems/squeezing-efficiency-anti-friction-201005/index1.html

[64] Miller, T. J. E. (2011). *SPEED tutorial B03: sinewave drive in PC-BDC.* [S. l]: Author

[65] Miller, T. J. E. (2011). *SPEED tutorial B14: IPM: Calculating torque and saturation using i-psi GoFER.* [S. l]: Author

[66] Miller, T. J. E. (2011). *SPEED tutorial B17: demagnetization calculations in PC-BDC/PC-FEA.* [S. l]: Author

[67] Miller, T. J. E. (2011). *SPEED tutorial B21: voltage in PC-BDC*. [S. l]: Author

[68] Constantinides, S., Gulick, D. (2004) NdFeB for high temperature motor applications. In *SMMA Fall Technical Conference,* 3-5 November, 2004. Accessed August 5, 2012 in http://www.arnoldmagnetics.com/WorkArea/DownloadAsset.aspx?id=4434

[69] Dupont. Teonex® PEN film. *Pleo website*. Accessed August 5, 2012, in http://www.pleo.com/dupont/pen1446.htm

[70] Elantas. Dobeckan® LE 6500. *Elantas website*. Accessed August 5, 2012, in http://www.elantas.com/elantas-italia/products/impregnating-varnishes-secondary-insulation/upr-low-voc-resins.html

[71] Dupont. Nomex® aramid paper. *Pleo website*. Accessed August 5, 2012, in http://www.pleo.com/dupont/nomex_spec.htm

[72] SPIndustries. SPInduwedge epoxy. *SPIndustries website*. Accessed August 5, 2012, in http://www.spi-at.com/img/Spinduwedge%20epoxy%20Klasse%20H%201.0.pdf

[73] AST. Technical information: bearing materials. *AST website*. Accessed August 5, 2012, in http://www.astbearings.com/assets/files/Bearing-Materials-Technical-Information-Sheet_ENB-04-0553.pdf

[74] Elantas. Impregnating Resins. Accessed August 5, 2012, in http://www.elantas.com/beck-india/products-services/secondary-insulation-si/impregnating-resins.html

Appendix A

PC-BDC Definitions

This appendix shows all the important figures defining the design variables and others auxiliaries.

A.1 Machine and Power Converter [30]

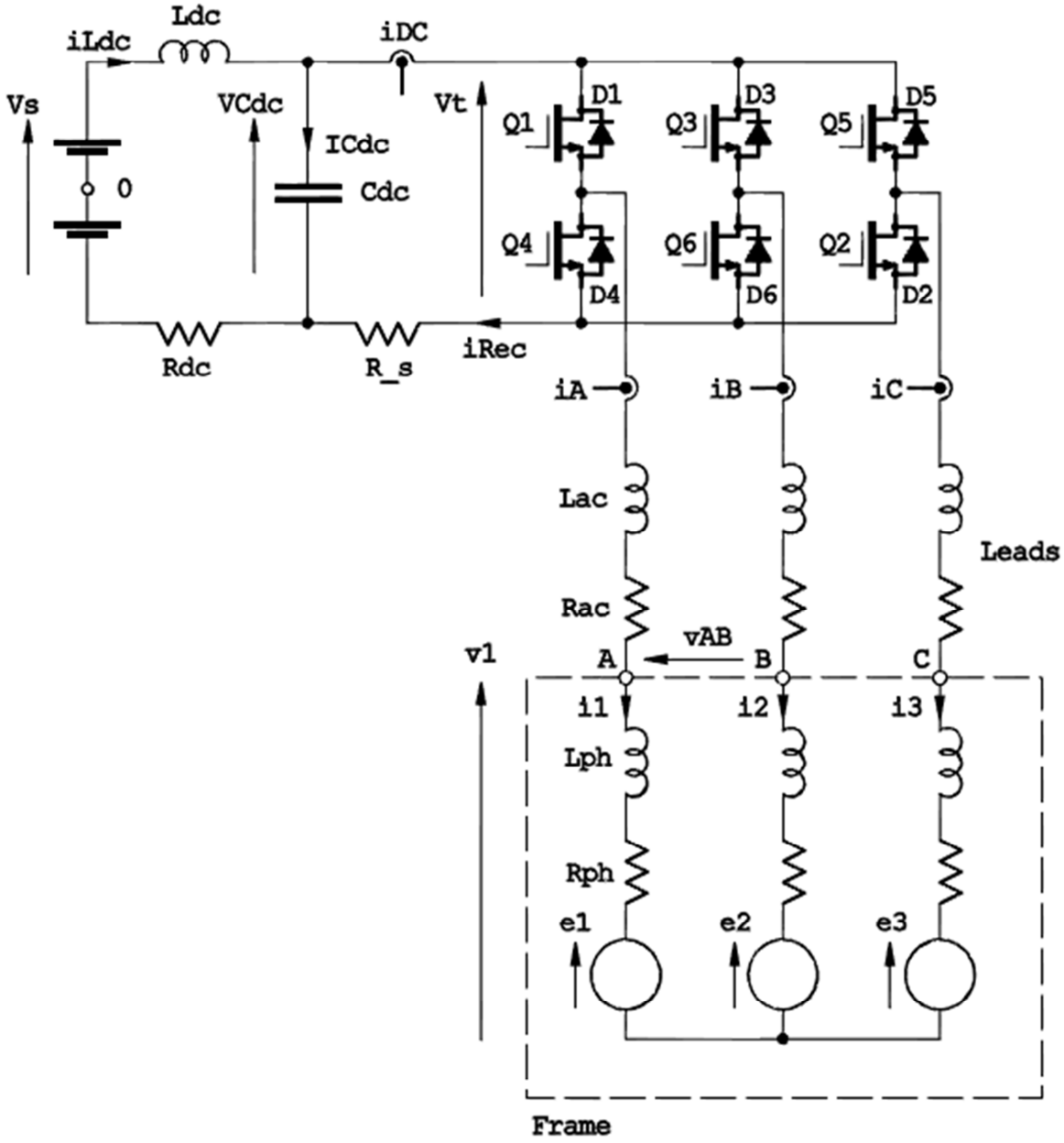

A.2 Slot & Tooth Geometry [30]

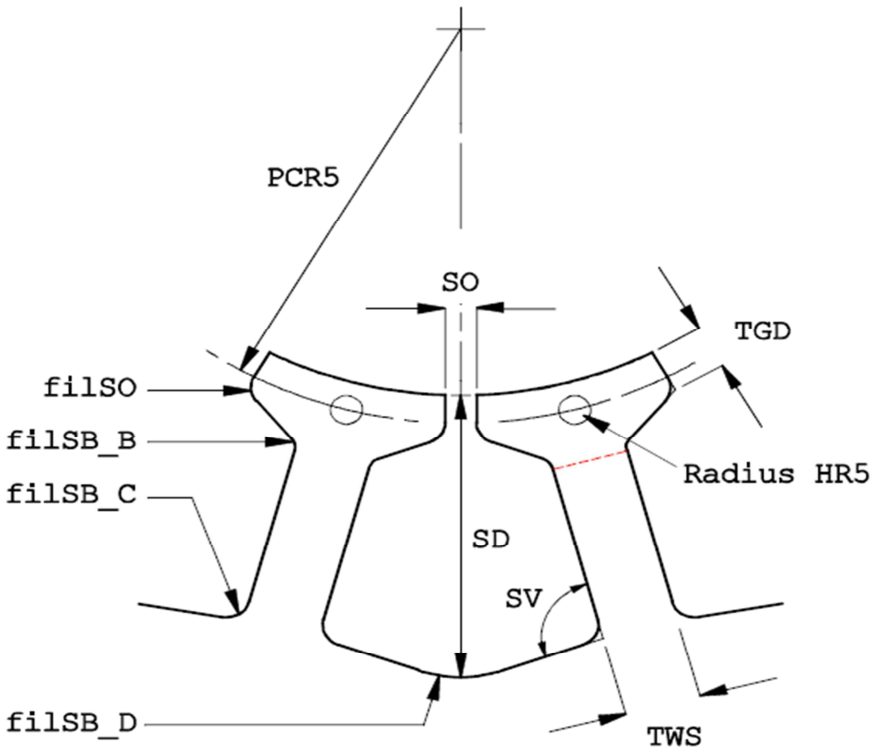

A.3 Double Layer Winding [30]

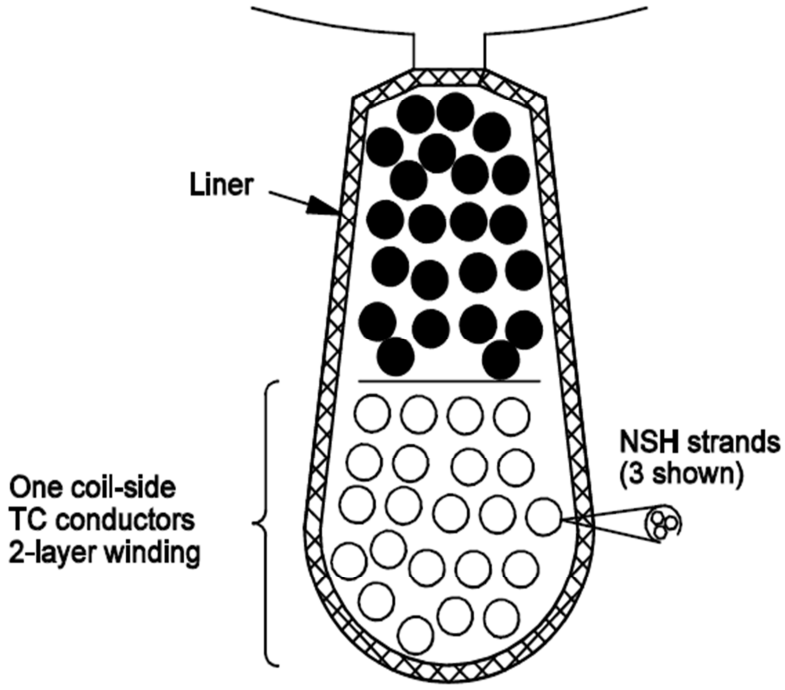

A.4 Axial Cross Section Geometry [30]

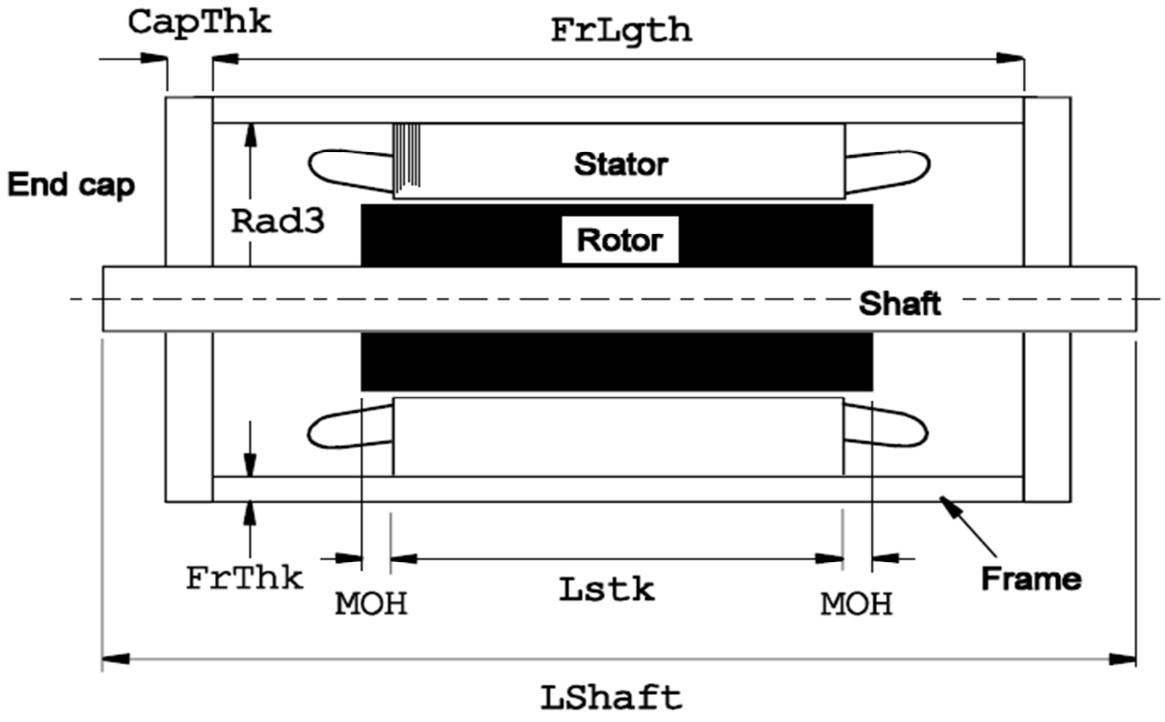

A.5 End Winding Geometry [30]

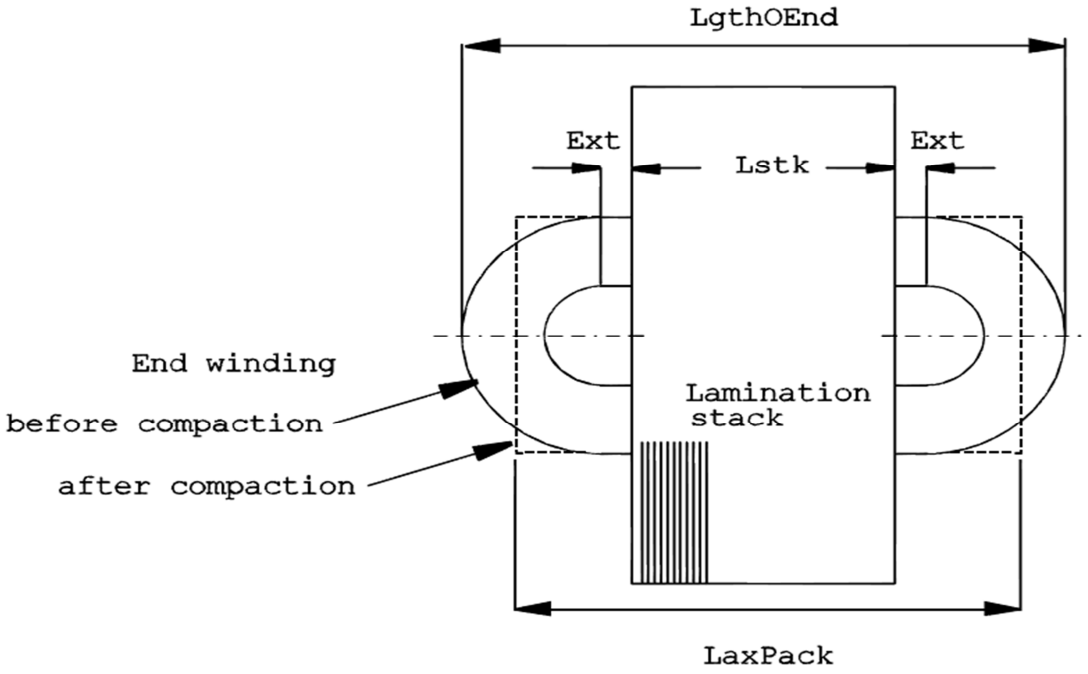

A.6 Radial Cross Section Geometry [30]

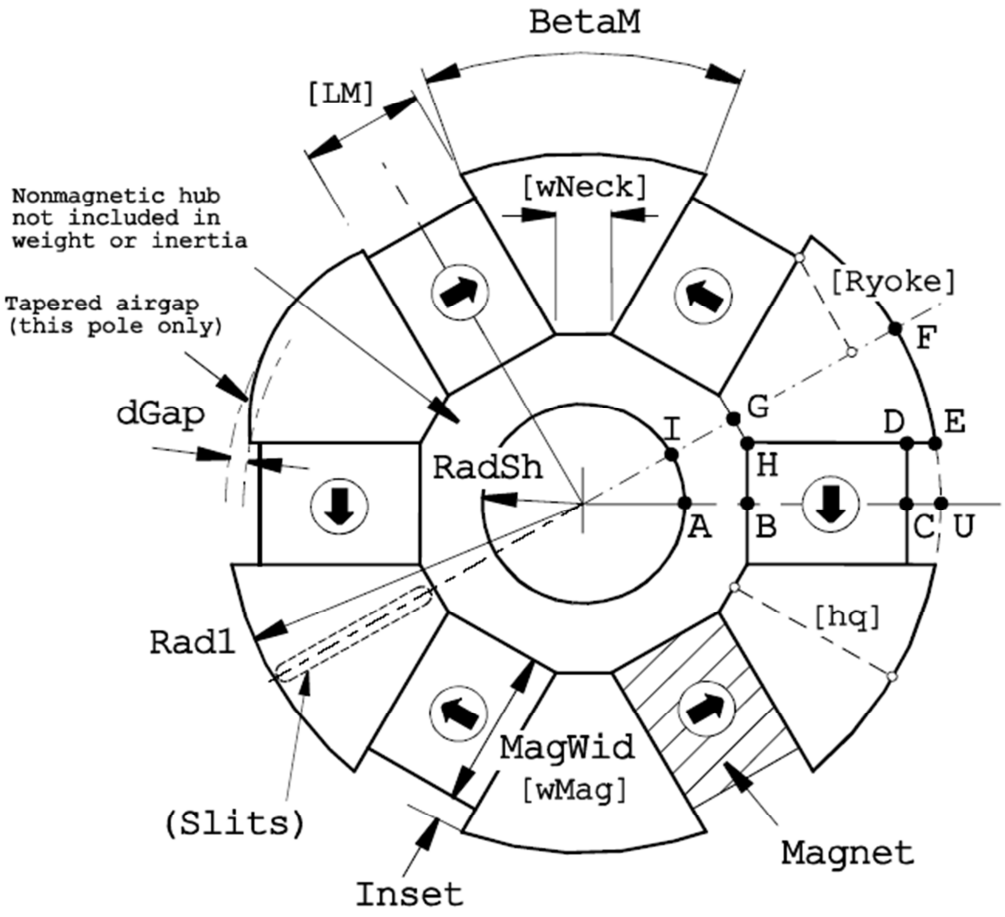

A.7 Glue Line Clearance [30]

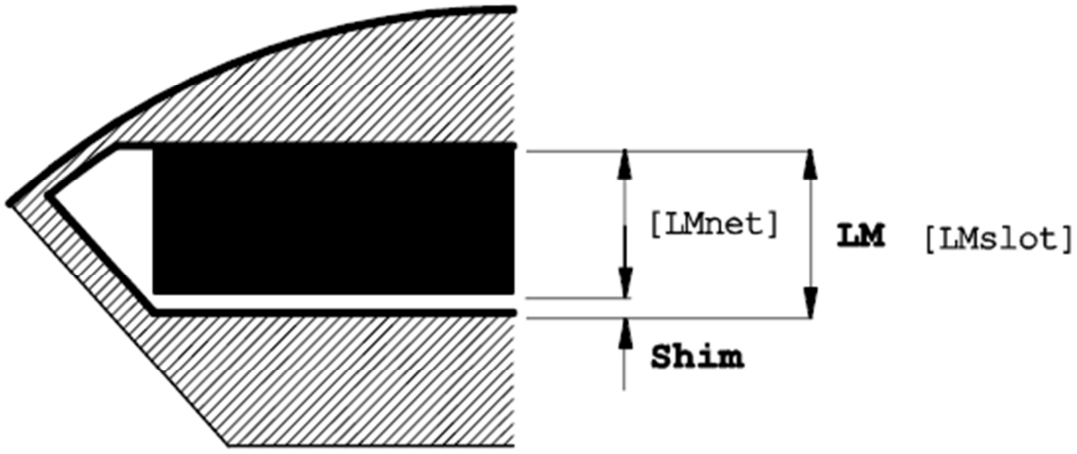

A.8 Top Stick & Phase Separator [30]

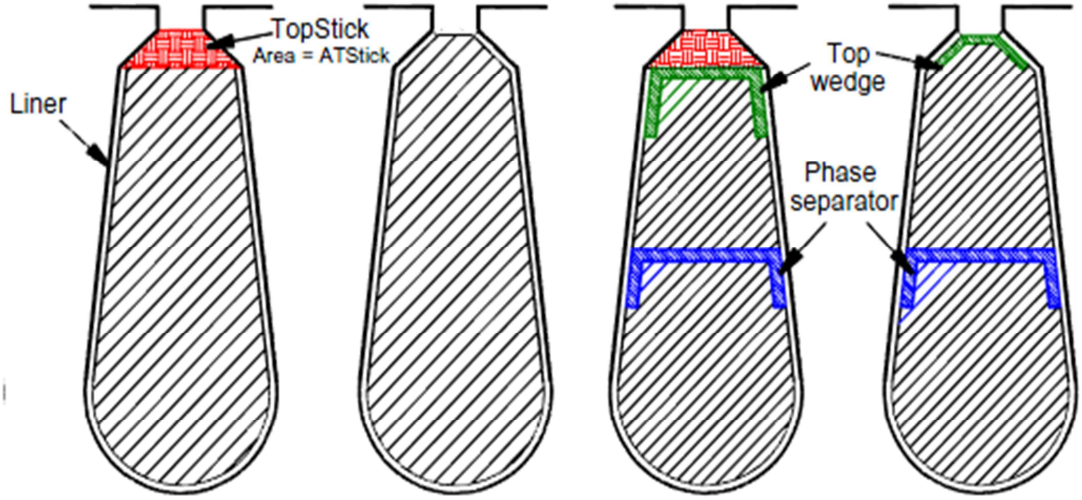

A.9 Winding Connection: 2 Parallel Paths [8]

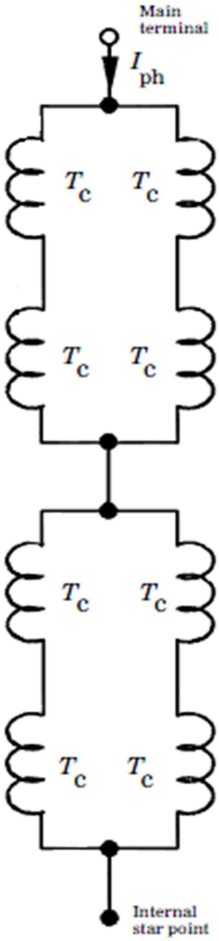

Appendix B

MM03_V3 CAD Drawing

This appendix shows **2D** cross sections of MM03_V3 prototype obtained with AutoCAD® software.

B.1 MM03_V3 Radial Cross Section

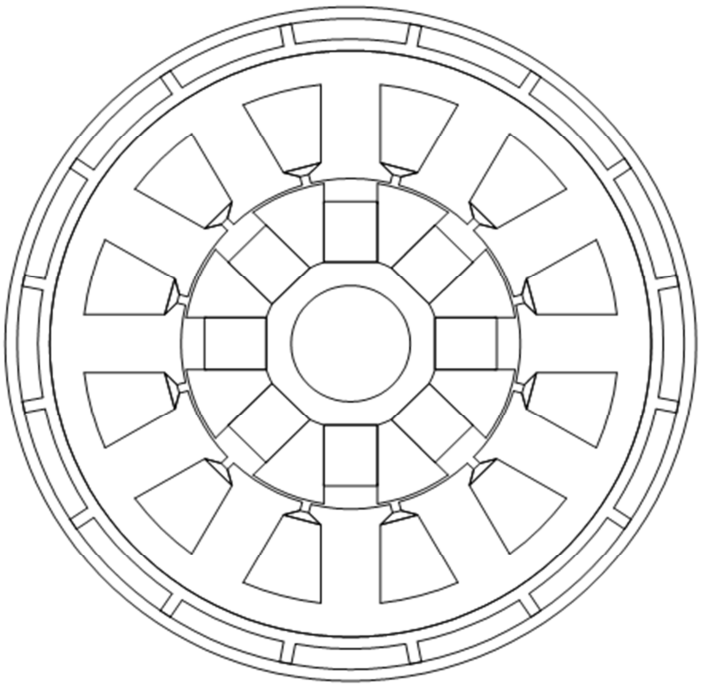

B.2 MM03_V3 Axial Cross Section

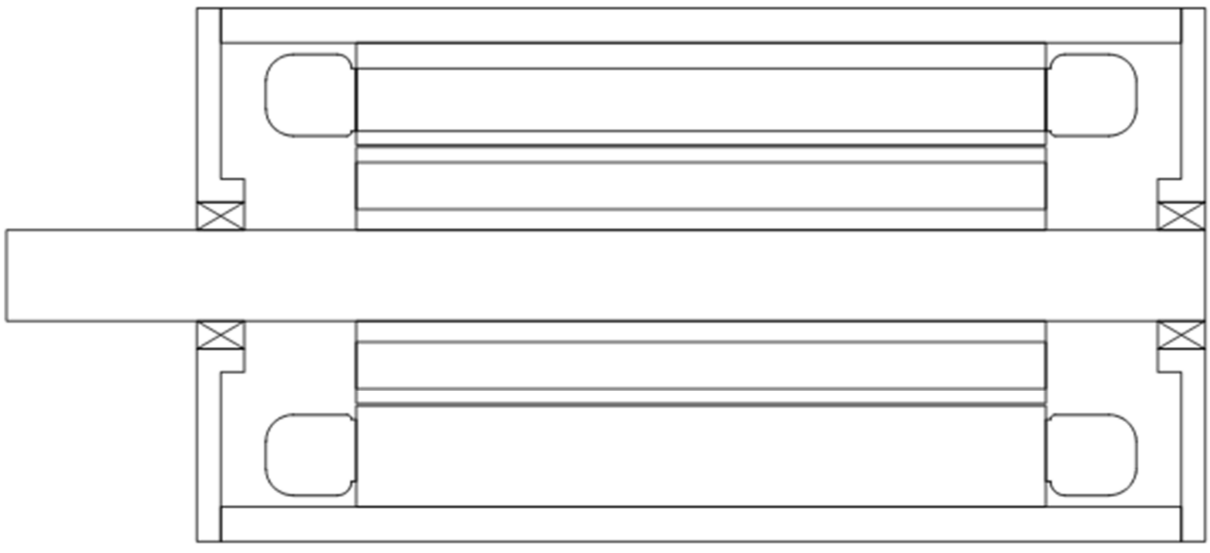

Appendix C

MM03_V3 Electromagnetic Project

This appendix shows auxiliary figures related to chapter 4.

C.1 Cogging Unskewed Harmonics

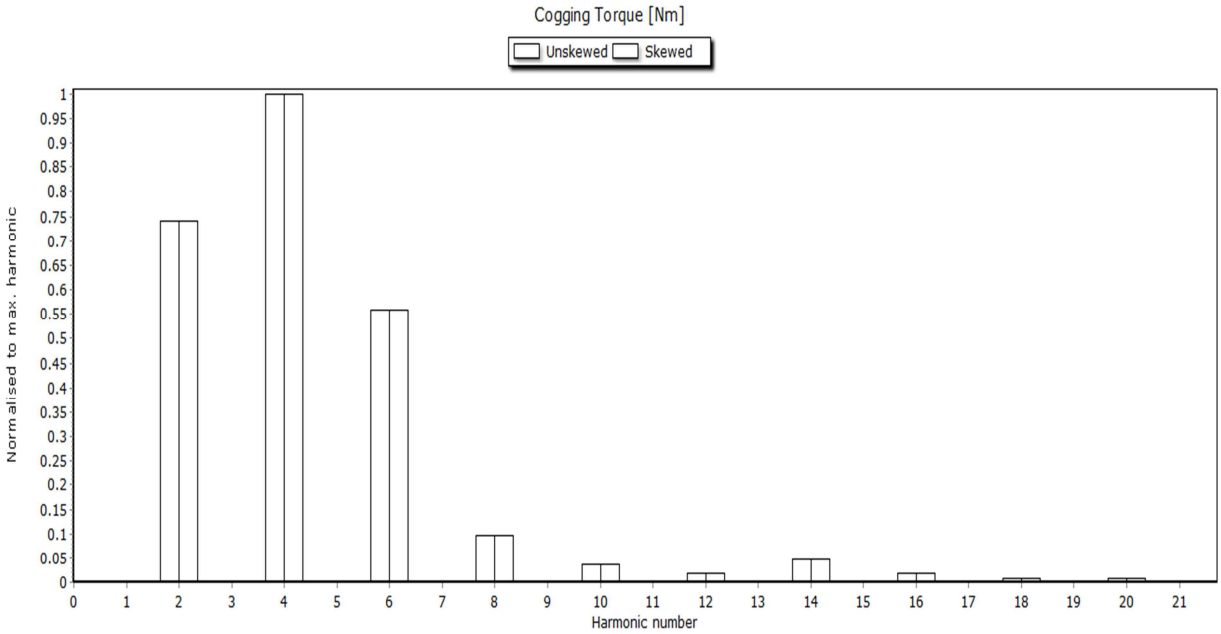

C.2 Cogging Skewed Harmonics

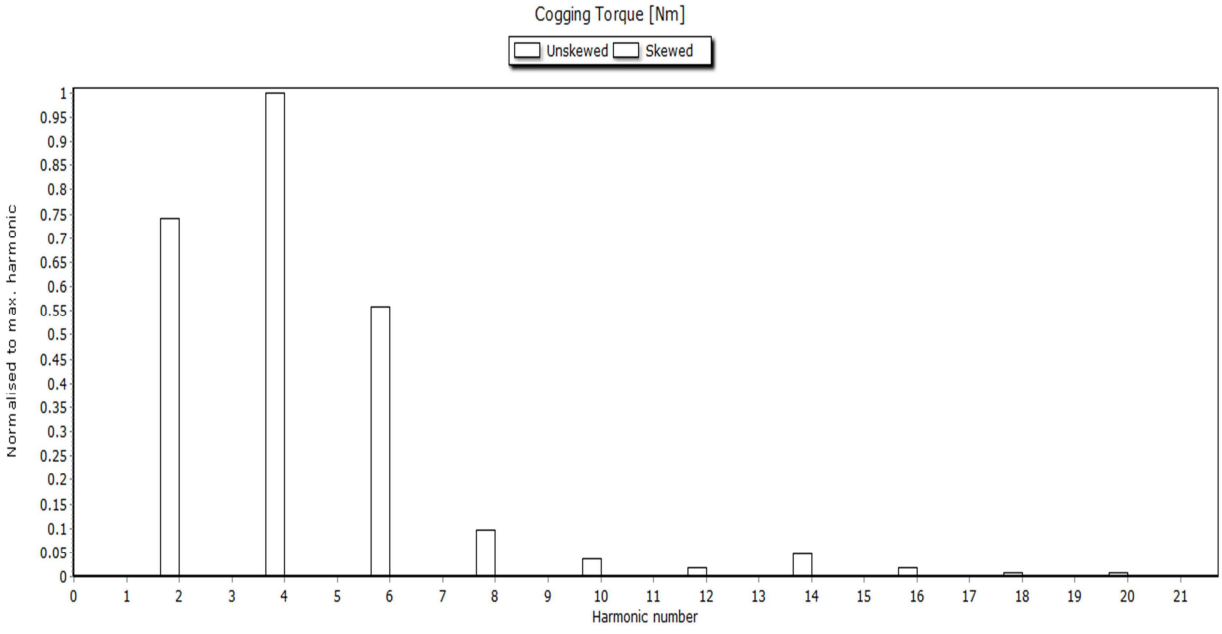

C.3 Boundary Nodes Distribution

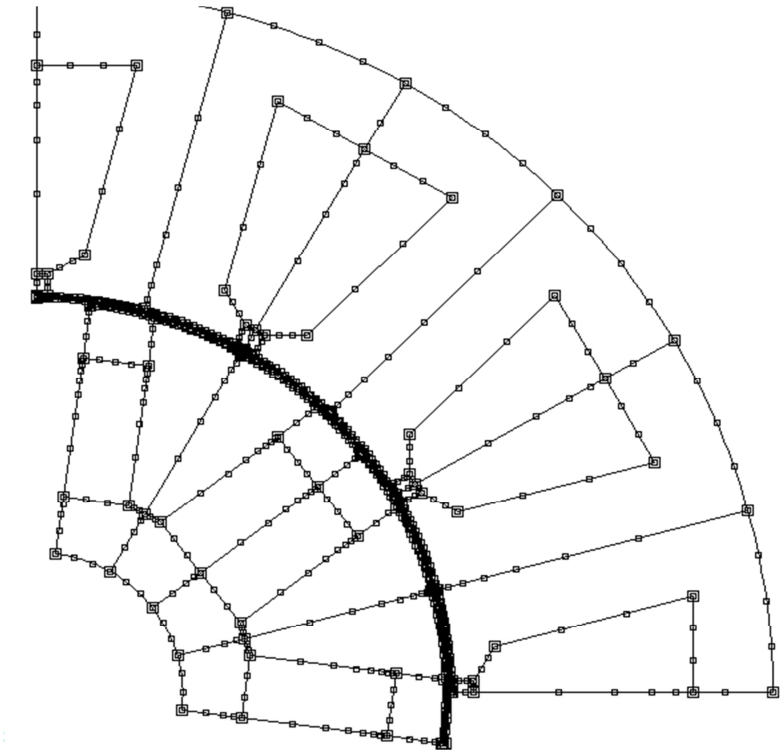

C.4 Optimized Mesh

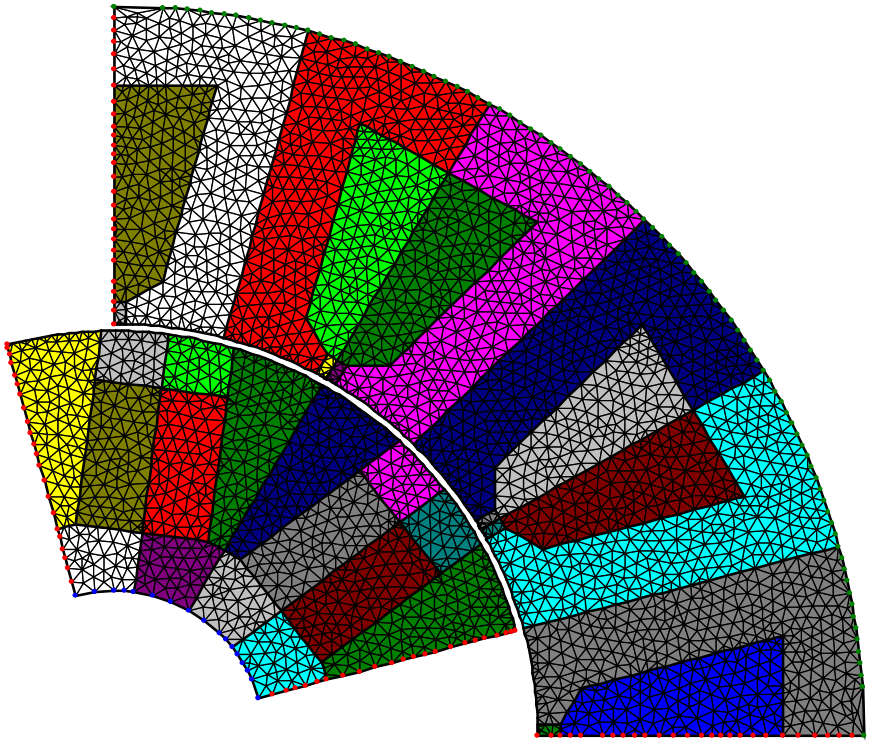

C.5 Rotating Mesh

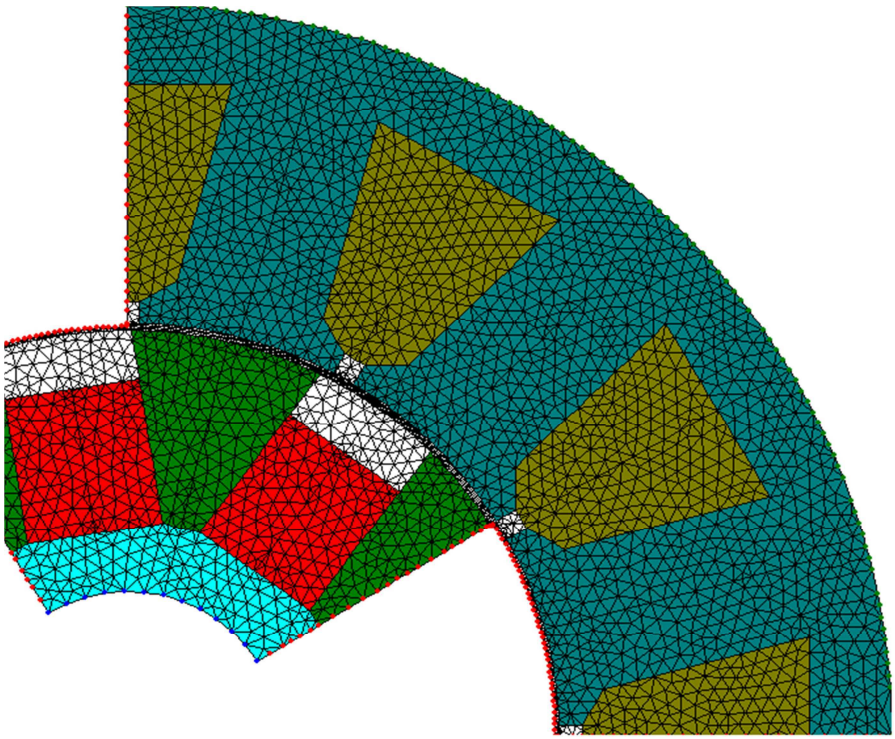

C.6 FEA Iron Losses

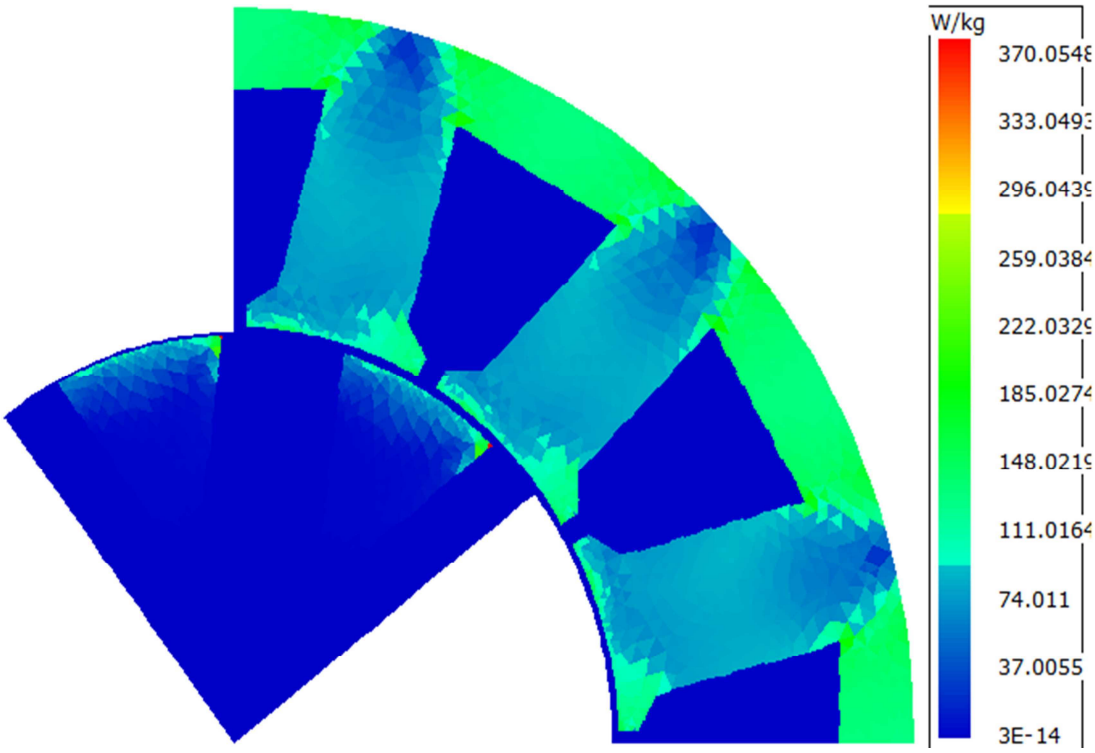

Appendix D

Materials

This appendix shows the properties of main materials as well as the important characteristic curves for **EM** project.

D.1 Housing & End Caps [20]

Aluminum Alloy 6061	
Manufacturer	**Aluminum Distributing Inc**
Density	**2.7 g/cm^3**
Tensile Strength	**310 MPa**
Yield Strength	**276 MPa**
Young Modulus	**68.9 GPa**

D.2 Magnet [14]

N35AH	
Manufacturer	**HPMG**
Br	**1.21 T**
Hc	**2.79E6 A/m**
Recoil Permeability	**1.05**
Br Temperature Coefficient	**-0.11%/ºC**
Hc Temperature Coefficient	**-0.52%/ºC**
Maximum Temperature	**220ºC**
Density	**7400 kg/m^3**

D.3 Shaft [21]

Stainless Steel 455	
Manufacturer	Michlin Metals Inc
Shaft Conductivity	2% (Cu)
Density	7.76 g/cm^3
Tensile Strength	1 GPa
Yield Strength	710 MPa
Young Modulus	200 GPa

D.4 Stator (S) & Rotor Iron (R) [13]

VACODUR® 49	
Manufacturer	VACUUMSCHMELZE
Composition	49%Co/2%V/Fe
H	50 (S)/110 (R) A/m
Saturation Polarization	2.35 T
Maximum Permeability	7000 (S)/15000 (R)
Curie Temperature	950ºC
Specific Loss (1.5T/400Hz)	31 (S)/43 (R) W/Kg
Lamination Thickness	0.1 mm
Stacking Factor	0.98
Density	8.12 g/cm^3
Tensile Strength	400 (S)/720 (R) MPa
Yield Strength	210 (S)/390 (R) MPa
Young Modulus	200 (S)/250 (R) GPa

D.5 Iron BH Curve

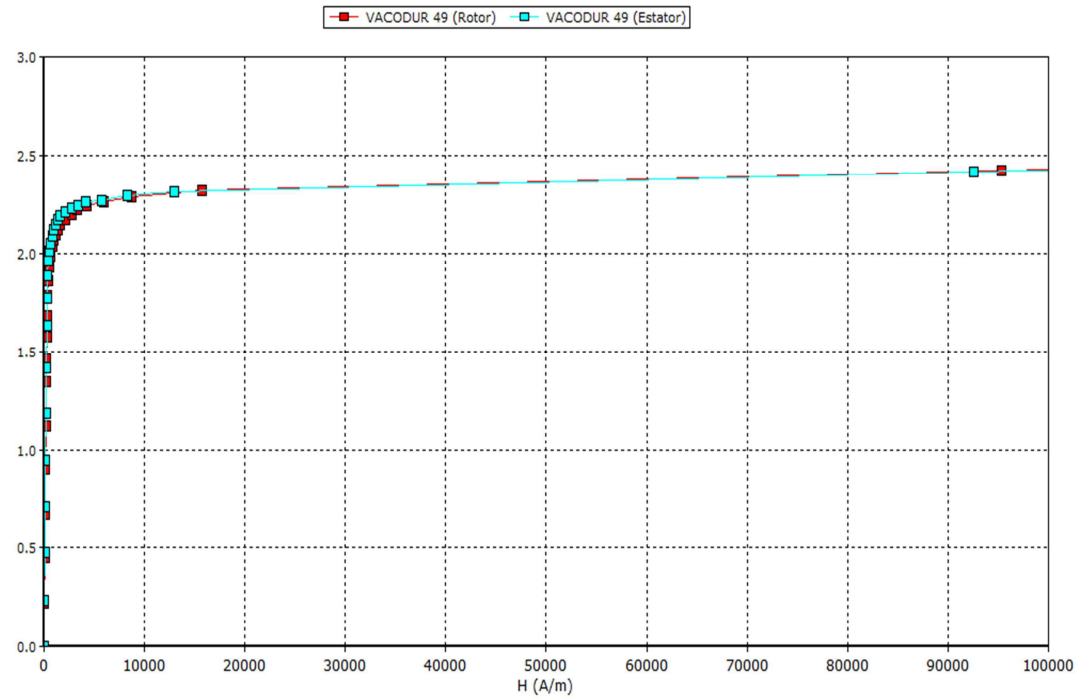

D.6 Iron Incremental μ Vs B Curve

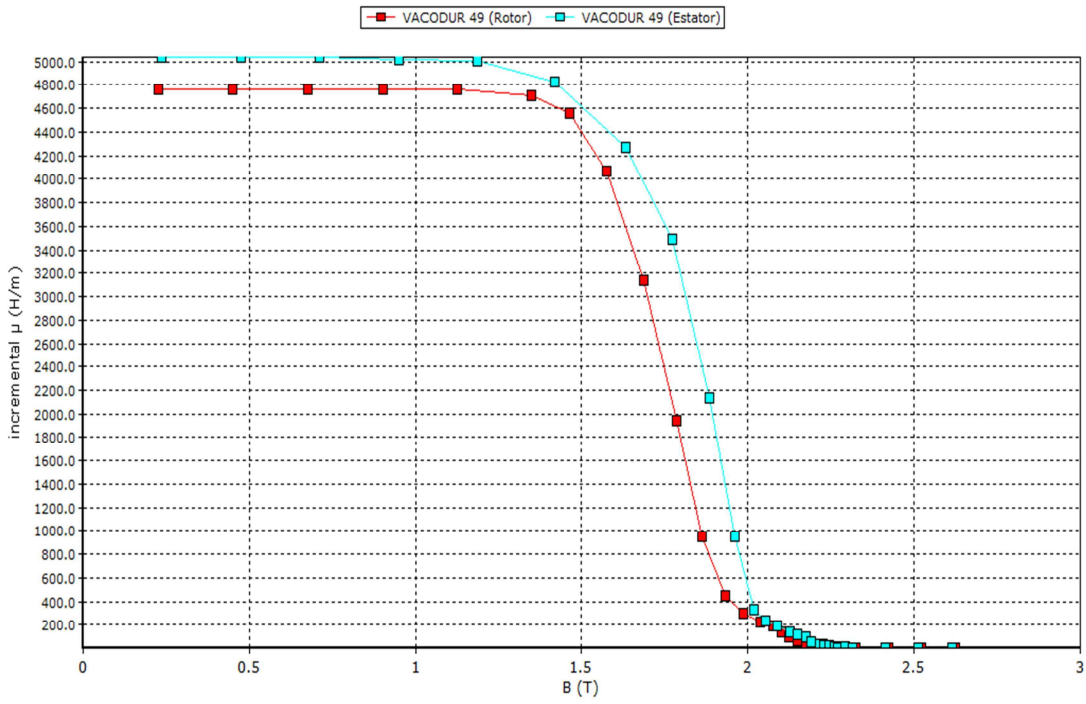

D.7 Iron Relative μ Vs B Curve

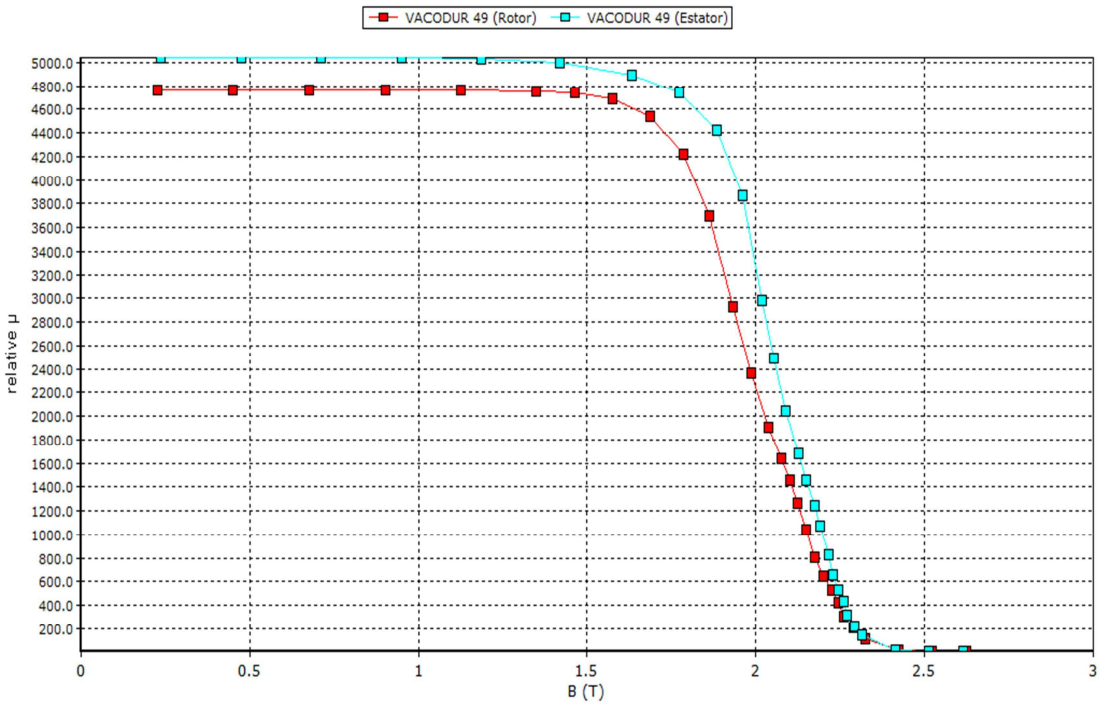

D.8 Iron Loss Vs B @ 400 Hz

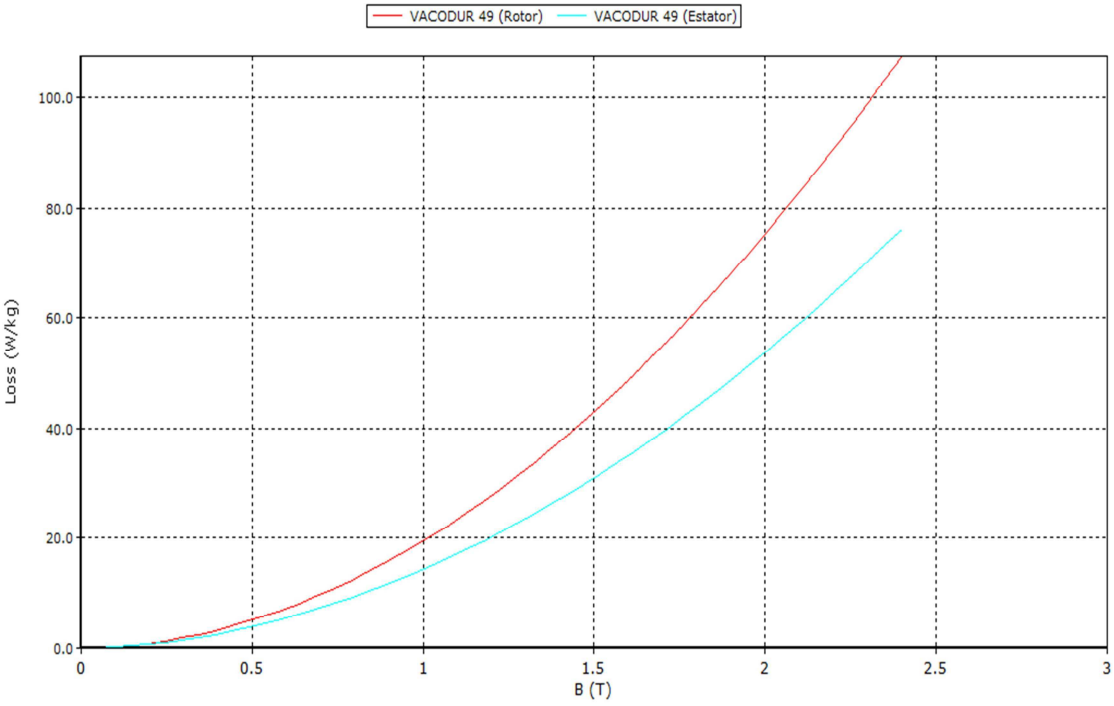

D.9 Magnets Recoil Lines

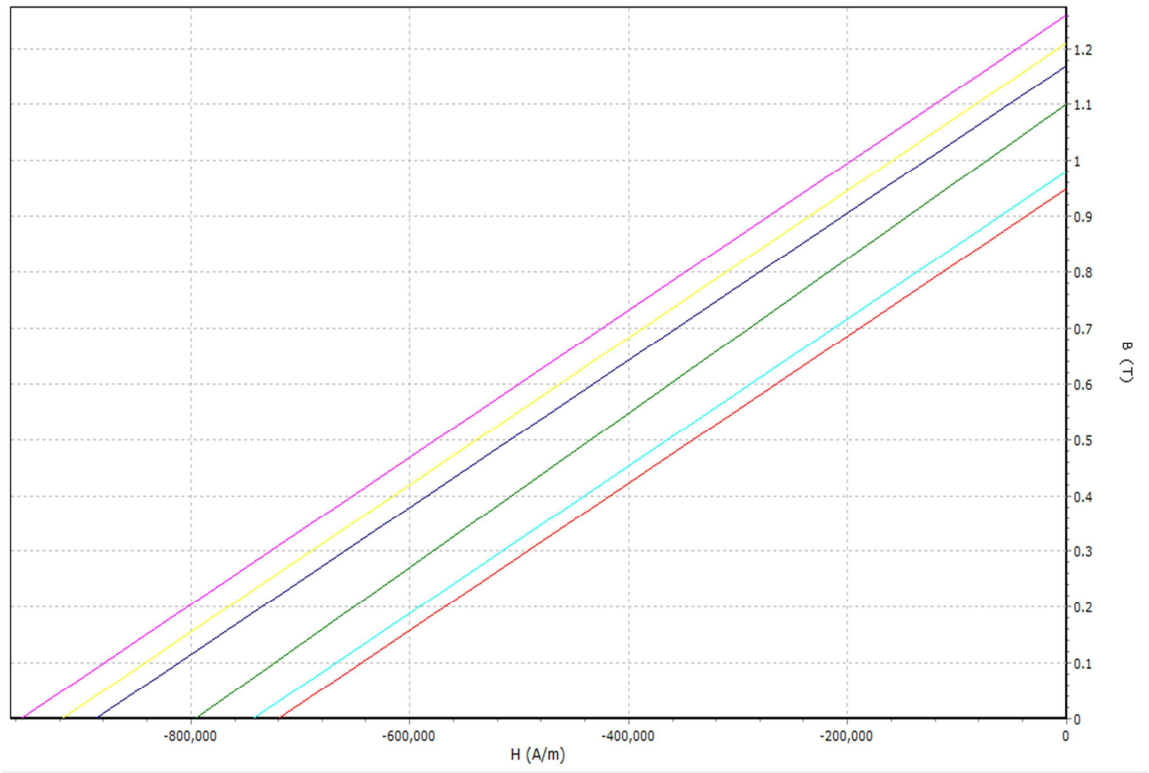

Purple – **NdFeB** N38EH

Yellow – **NdFeB** N35AH

Dark Blue **– NdFeB** N33AH

Green – **Sm-Co** RE2Co17 222/199

Light Blue – **Sm-Co** RE(Sm)Co5 175/119

Red – **Sm-Co** RE(Sm)Co5 159/159

Appendix E

MM03_V3 Thermal Project

This appendix shows the relevant materials properties to perform the thermal analysis as well as complementary results of chapter 5.

E.1 Materials Thermal Properties

Materials	k (W/m/ºC)	Sph (J/kg/ºC)	ρ (kg/m^3)
Aluminum Alloy 6061	167	896	2700
VACODUR® 49	25	420	8120
Copper	394	385	8890
Teonex® (PEN)	0.28	1200	1360
Dobeckan® LE 6500	0.6	1700	1000
Thermoset Epoxy (EP)	0.17	1100	1150
Nomex® 410	0.143	1256	950
Sintered NdFeB	9	420	7400
Stainless Steel 455	20	460	7760
Chrome Steel (SAE 52100)	46.6	475	7810

E.2 PEN Chemical Structure

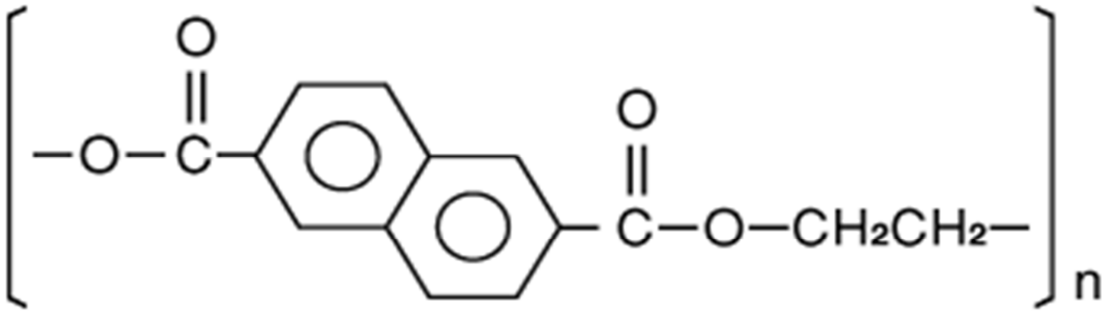

E.3 Channel Pressure Drop

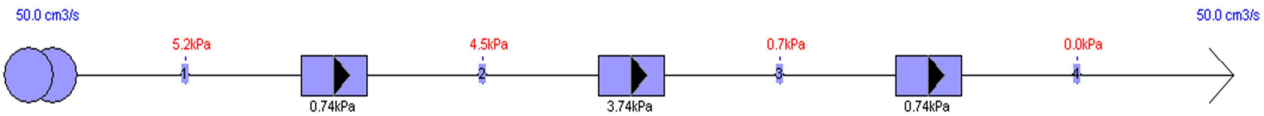

E.4 Materials Roughness [19]

Material	Roughness [mm]
Glass, Plastic, Perspex, Fibreglass	0.0025
PVC	0.005
Steel	0.005
Cast Iron	0.15 - 0.4
New steel pipe	0.025
Light rust	0.25
Heavy rust	1.0
Sheet metal ducts	0.0025
Galvanized metals (normal finish)	0.15
Galvanized metals (smooth finish)	0.025
Aluminium, Copper, Drawn Brass	0.0025

E.5 Materials Emissivity [19]

Material	Emissivity	Material	Emissivity
Aluminium		Iron	
• black anodised	0.86	• polished	0.07 – 0.38
• polished	0.03 – 0.1	• oxidised	0.31 – 0.61
• heavily oxidised	0.20 – 0.30	Nickel	0.21
• sandblasted	0.41	Paints	
Alumina	0.20 – 0.50	• white	0.80 – 0.95
Asbestos	0.96	• gray	0.84 – 0.91
Carbon	0.77 – 0.84	• black lacquer	0.96 – 0.98
Ceramic	0.58	Quartz, fused	0.93
Copper		Rubber	0.94
• polished	0.02	Silver, polished	0.02 – 0.03
• heavily oxidised	0.78	Stainless Steel	0.07
Glass	0.95	Tin, bright	0.04

E.6 Interface Gaps

Component	Gap	Details	Resistance	Conductance
Units	mm		m2.C/W	W/m2/C
Stator Lam - Housing	0.03	Lamination-Metal - Average surface Contact (0.03)	0.001154	866.7
Housing - OHang [F]	0	No Gap - Perfect surface Contact (0)	0	1E09
Housing - OHang [R]	0	No Gap - Perfect surface Contact (0)	0	1E09
Housing - Endcap [F]	0.0017	Aluminium-Aluminium - Medium surface Contact (0.0017)	6.538E-05	1.529E04
Housing - Endcap [R]	0.0017	Aluminium-Aluminium - Medium surface Contact (0.0017)	6.538E-05	1.529E04
Magnet - Rotor Lam	0.005	Metal-Metal - Average surface Contact (0.005)	0.0001923	5200
Rotor Lam - Shaft	0.03	Lamination-Metal - Average surface Contact (0.03)	0.001154	866.7
Bearing Effective Gap [F]	0.4	High Effective Gap [Torino Testing] (0.4)	0.01538	65
Bearing Effective Gap [R]	0.4	High Effective Gap [Torino Testing] (0.4)	0.01538	65
Bearing - Endcap [F]	0.0073	Stainless-Aluminium - Medium surface Contact (0.0073)	0.0002808	3562
Bearing - Endcap [R]	0.0073	Stainless-Aluminium - Medium surface Contact (0.0073)	0.0002808	3562
Bearing - Shaft [F]	0.0112	Stainless-Stainless - Medium surface Contact (0.0112)	0.0004308	2321
Bearing - Shaft [R]	0.0112	Stainless-Stainless - Medium surface Contact (0.0112)	0.0004308	2321

E.7 Slot & Conductors

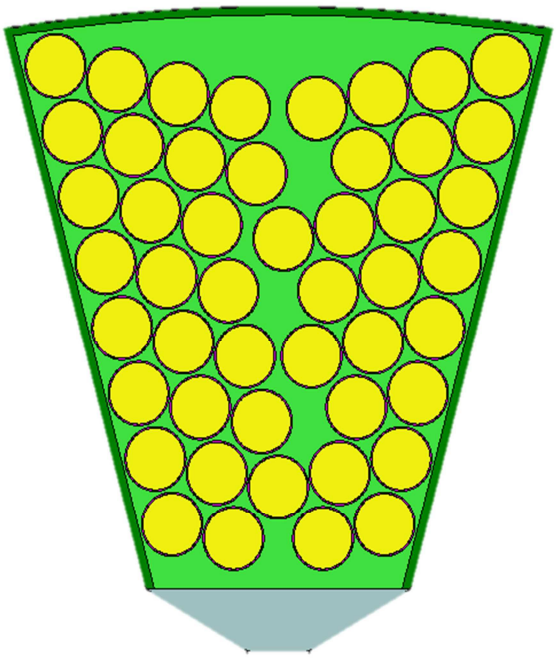

E.8 MM03_V3 Lumped Thermal Circuit